Hanne Tiesler

Identification of Material Parameters from Temperature Measurements in Radio Frequency Ablation
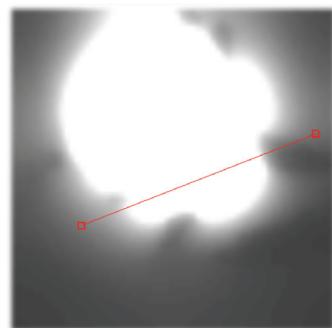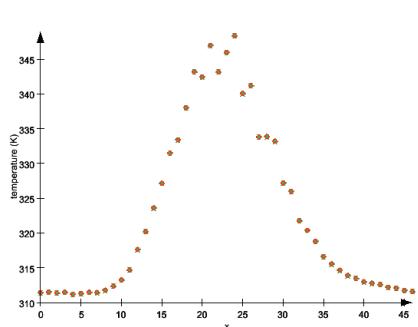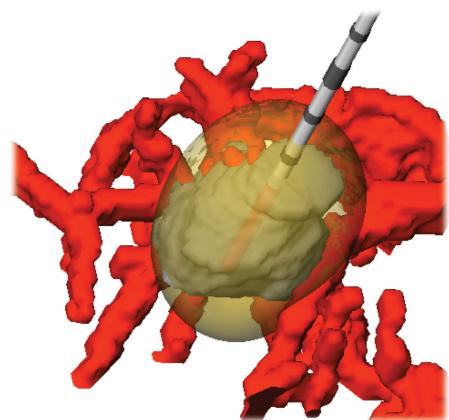
The pictures at the title page show the results for the identification of the electrical conductivity from an exactly known heat source. The figure at the top displays the setting with tumor (grey), vascular structures (red), applicator and the 60 °C iso-surface of the final temperature distribution (transparent yellow). The figure at the bottom left displays the given temperature distribution (red circles) compared with the temperature distribution (green asterisks) according to the identified electrical conductivity. The data are depicted along the red line illustrated in the picture at the bottom right.

Identification of Material Parameters from Temperature Measurements in Radio Frequency Ablation

von

Hanne Tiesler

Dissertation

zur Erlangung des Grades eines Doktors der Naturwissenschaften
- Dr. rer. nat. -

Datum des Promotionskolloquiums: 01.11.2011

Gutachter: Prof. Dr. Tobias Preusser, Jacobs University, Bremen
          Prof. Dr. Christof Büskens, Universität Bremen
          Prof. Dr. Heinz-Otto Peitgen, Universität Bremen

Abstract

The mathematical simulation of the method of radio frequency ablation (RFA) offers an opportunity to improve the success of the RFA. The results of the RFA depend highly on the experience of the radiologist. A simulation will offer a prediction of the results which can be used to adapt the setting and enable a complete destruction of the tumor, e.g. by adapting the probe's position. A good simulation needs as much information of the reality as possible. Especially the material properties pose a challenge since they vary from patient to patient, they can not be measured in vivo and they additionally change during the ablation.

The aim of this thesis is to develop a mathematical model for the identification of the material parameters from temperature measurements and apply it to appropriate data sets. At first a minimization problem is formulated, where the difference between the measured temperature and the calculated temperature is minimized with respect to the material parameters. The temperature distribution is calculated with a coupled system of partial differential equations. Different approaches are considered which depend on the diverse modeling of the material parameters. The parameters are modeled as constant values as well as temperature dependent, tissue dependent and also spatially distributed. The advantages and disadvantages of the diverse models are illustrated by the numerical results for the identification with artificial temperature distributions as well as real temperature measurements.

Zusammenfassung

Die mathematische Simulation der Radiofrequenz Ablation (RFA) in der Leber bietet eine Möglichkeit, den Erfolg der RFA zu verbessern. Die Ergebnisse der RFA hängen stark von der Erfahrung der ausführenden Radiologen ab. Die Vorhersage der Ergebnisse mittels einer Simulation ermöglicht es, vorab Korrekturen vorzunehmen, um eine vollständige Zerstörung des Tumors zu gewährleisten, z.B. durch die Anpassung der Applikatorpositionierung. Für eine gute Simulation ist es nötig, die Realität so genau wie möglich abzubilden, wobei insbesondere die Gewebeeigenschaften eine Herausforderung darstellen, da sie von Patient zu Patient variieren, nicht in vivo messbar sind und sich zudem während der Ablation verändern.

Das Ziel dieser Arbeit ist es, ein mathematisches Modell zur Identifikation der Gewebeparameter aus gemessenen Temperaturdaten aufzustellen und an

geeigneten Daten zu testen. Dafür wird zunächst ein Minimierungsproblem mit den Leitfähigkeiten als Optimierungsvariablen aufgestellt, in dem die Differenz zwischen den gemessenen Temperaturdaten und der berechneten Temperaturverteilung minimiert werden soll. Für die Berechnung der Temperaturverteilung im Gewebe wird ein gekoppeltes System aus partiellen Differentialgleichungen verwendet. Es werden unterschiedliche Ansätze für die Identifikation verfolgt, die in den verschiedenen Modellierungen der Parameter begründet sind. Neben konstanten Parametern werden temperatur- und gewebeabhängige sowie örtlich verteilte Parameter betrachtet. Die numerischen Ergebnisse der Identifikation zeigen die Vor- und Nachteile der unterschiedlichen Ansätze sowohl für künstlich erzeugte Daten als auch für echte Temperaturmessungen.

Acknowledgement

Contents

Contents

List of Figures

IV

List of Tables

Notations

σ	electrical conductivity, S m^{-1}	$L^p(\Omega)$	Lebesgue space, $1 \le p \le \infty$
λ	thermal conductivity, W K^{-1}m^{-1}	$W^{k,p}(\Omega)$	Sobolev space, $1 \le p \le \infty$
		$H^k(\Omega)$	Sobolev space for $p = 2$
ρ	density of the tissue, kg m^{-3}	$L^p(a,b;X)$	Bochner space, $1 \le p \le \infty$
c	specific heat capacity, J kg^{-1}K^{-1}	Z^*	dual space of Z
$\nu(x)$	blood perfusion coefficient,	$(\cdot,\cdot)_X$	inner product on X
Ω	computational domain, $\Omega \subset \mathbb{R}^N$	$\langle\cdot,\cdot\rangle_{V^*,V}$	dual pairing on V
$\partial\Omega$	outer boundary of Ω	$\|\cdot\|_V$	norm on V
Γ_+	positive electrode	$\partial^\alpha y$	weak derivative of y
Γ_-	negative electrode	$a(\cdot,\cdot)$	bilinear form
Γ	positive and negative electrode $\Gamma := \Gamma_+ \cup \Gamma_-$	$l(\cdot)$	linear form
		∂_t	time derivative
Ω_v	vascular system, $\Omega_v \subset \Omega$	$y(t,x)$	state of a general PDE, with $y \in Y$
Q	space-time cylinder $Q := [0, t_{\text{fin}}] \times \Omega$	$u(t,x)$	(general) control, $u \in U$
$\phi(t,x)$	electric potential	$F(y,u)$	general objective functional
$T(t,x)$	temperature distribution	$h(y,u)$	general constraints, $h : Y \times U \to Z$
T_{body}	body temperature	$D_y F(y,u)$	partial Fréchet derivative of F with respect to y
$T_g(x)$	measured temperature distribution at time t_{fin}	$\mu(t,x)$	adjoint state
Q_{rf}	heat source	$\mathcal{L}(y,u,\mu)$	general Lagrange functional
$u_g(x)$	measured or given heat source		
Q_{perf}	heat sink	$T_\alpha(x)$	Tikhonov functional
P_{eff}	effective power in the tissue	d	descent direction
P_{set}	power set up at the generator	∇	gradient
R	resistance of the tissue	∇^2	Hessian matrix
R_I	resistance of the generator	$\alpha,\beta,\gamma,\theta$	regularization coefficients
P_Ω	whole power	U_{ad}	admissible set for the control

1 Introduction

"Those diseases which medicines do not cure, iron cures; those which iron cannot cure, fire cures; and those which fire cannot cure, are to be reckoned wholly incurable"

Hippocrates, 400 BC - 377 BC

1.1 Motivation

The liver is the largest blood filtering organ in the human body which is conductive to the transportation of malignant cells into the liver. Therefore, between all patients with malignant cancer diseases approximately 50 % will develop liver metastases which lead to a high mortality [65]. The major cause of death by cancer disease is lung cancer (19.9 %), followed by colorectal cancer (12.3 %) and breast cancer (7.5 %), whereas colorectal cancer is the most common cancer [19]. Without any treatment of colorectal liver metastases the median survival rate is between 9 and 12 months [65, 84].

The gold standard for colorectal metastases in the liver is surgical resection whereas only 10-20 % of the liver metastases are resectable [18]. The reasons for these limitations are given by the location of the tumor, the patient's condition, the absence warranty for the later operating capability of the liver or extra-hepatic metastases which deteriorate the overall prognosis. The minimally invasive method of radio frequency ablation (RFA) provides an alternative treatment for liver metastases and primary hepatic tumors. During the treatment the tumorous cells are destroyed by targeted heating. A probe with one or more electrodes is percutaneously placed in the tumor and the electric current leads to a heating of the tissue such that the proteins of the cells coagulate and the tissue is destroyed. Different studies substantiate this promising approach though RFA is also limited. In their study, Feliberti and Wagman [18] investigate the advantages of RFA especially in comparison with the alternative chemotherapy, which is often used in those cases where a resection is not possible. Their results prove that RFA has a better survival rate than chemotherapy. Nevertheless they also realized that the RFA is limited to small lesions (≤ 3 cm). Also Suppiah et al. [84] affirm a higher survival rate with RFA, the median survival increases in their study to 12.9 months. However, although the RFA is an advantageous and promising method to achieve really good results (i.e. the whole destruction of the malignant tissue) a lot of experience is needed for a successful treatment [18]. This problem is corroborated by the study of Mulier et al. [61], where the method of RFA is compared with the surgical resection for resectable colorectal liver metastases. Beside the inexperience of the radiologists another limitation

is stated by the vascular system. In the vicinity of larger blood vessels the RFA fails in many cases, probably due to the cooling effect of the blood flow. If this effect is not considered in advance, the outcome of the RFA is quite different from the suspected result. Whereas Paulet et al. [63] assert that the proximity to vascular structures is not such a limitation if the radiologists are aware of it and treat the tumor more intensively. The main limitations they specify for recurrence or residual tumors are the size of the lesion ($> 3\,\text{cm}$) and the difference in the electrical conductivity in tumorous and surrounding tissue. The heat sink effect caused by the vascular structure is also named as limitation if it is not considered carefully by the radiologists.

These findings encourage further improvements for the patient individual modeling and the simulation of the RFA since a realistic modeling could be implemented in a training and planning software for the radiologists. Such a tool could compensate at least partially the inexperience of the radiologists and improve the planning by a better prediction and optimization of the result of the RFA. For example, if there are vascular structures in the vicinity of the tumor the cooling effect of the blood vessels may lead to a coagulated area which does not correspond to the expected one, given by the manufacturer's information. As result the tumor is not completely destroyed. A good simulation of the treatment in advance could have provided these informations and the radiologist could have thought through the placement more carefully. Moreover, an additional optimization of the probe placement can provide an optimized placement which facilitates a complete ablation of the tumor. Therefore a detailed simulation in advance is of great avail since the major priority of the RFA is to assure a completely destructed tumor including a safety boundary.

1.2 The aim of the work

Altogether, the treatment with RFA and especially the success rate can be significantly improved by a realistic numerical simulation. Such a simulation needs a good modeling, based on physical and biological facts. The numerical calculations can be as good as possible but if the basic information are inaccurate or incorrect the prediction for the RFA will not match the reality. Some of these basic physical facts are well known, as for example the modeling of the heat transfer. Whereas the tissue properties, which enter the equations as parameters, e.g. the thermal conductivity, the heat capacity, the density or the electrical conductivity, constitute a major challenge for the modeling. These parameters are important for a realistic modeling since they describe the properties of the material. As described by Paulet et al. [63] the electrical conductivity has a wide influence on the success of the RFA and needs to be considered carefully. The difficulty lies in the fact that the parameters are subject to different physical and biological conditions and in particular they are not known exactly. However, all studies concerning the parameters are limited by the fact that the measurements are done only ex vivo for humans and hence the results are not reliable for the modeling of the RFA.

To improve the simulation individually by using the specific material parameters for each

patient, we will formulate an inverse problem with the aim of identifying the material parameters for RFA. Nevertheless there exist some good approximations for the thermal conductivity, the model could be improved and adapted individually if we were able to determine the material parameters for each patient individually. A measurement of the parameters is not possible in vivo, therefore we will need another possibility to identify the individual parameters. Additionally the material parameters change during the therapy which necessitates an identification and adjustment during the treatment. This can be achieved by a parameter identification from temperature measurements during the ablation.

The prediction for the success of the treatment is based on the temperature distribution which can not only be calculated by the numerical model but also measured by magnetic resonance imaging (MRI) during the treatment. Therefore we will formulate an identification problem for the material properties which aims at fitting the calculated temperature to the measured data from MRI, i.e. we obtain an inverse problem which will be solved by minimizing an optimal control problem with a tracking type functional and the mathematical model for the RFA as constraints. The identified parameters can be utilized to improve the numerical model for the RFA and therewith ameliorate the prediction of the outcome of the treatment. If the simulation with identified parameters shows that the current setting will not lead to a successful RFA the setting can be adapted accordingly. Altogether we may have two different feedbacks, one from the MR temperature measurements to identify the material parameters and therewith improve the mathematical model and the forward simulation. The other feedback between the predicted result from the forward calculations for the current RFA setting and the real ablation, which can be adapted accordingly to increase the success of the treatment. A schematic description is shown in figure 1.1.

The method for the identification of the material parameters as described in this thesis is not restricted to the treatment with RFA in the human liver, it can be transferred also to other thermal treatments if we adapt the model in an appropriate way.
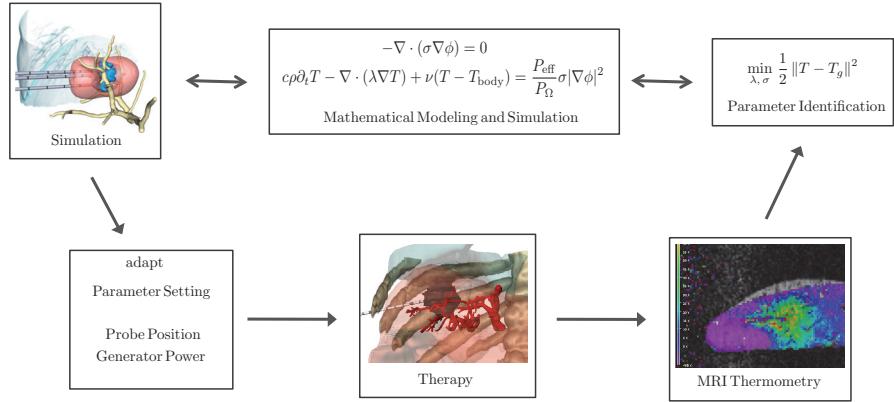
Figure 1.1: Schematic figure to illustrate the correlation between the therapy of RFA, the parameter identification, the adaption of mathematical model and simulation and the adjustment of the RFA setting, e.g. the probe's position, to improve the treatment. The picture for the simulation is taken from [67] and the thermometry figure is provided by H. Rempp (Eberhard Karls University Tübingen, Germany).

1.3 Organization of the thesis

The thesis is organized as follows:

In **Chapter 2** an overview of related work and state of the art in the field of the numerical modeling and simulation of RFA as well as the work in the field of parameter identification problems is given.

In **Chapter 3** the mathematical model of the RFA consisting of partial differential equations is described. In particular we will consider the impact of the material parameters on the whole system and an appropriate modeling. Furthermore a short introduction to the method of finite elements (FEM) is given which is used for the spatial discretization of the RFA model.

In **Chapter 4** the basic mathematical theory for identification problems is presented. Different optimization methods will be described and a short introduction to inverse problems and Tikhonov regularization is given.

In **Chapter 5** the identification problem for the thermal conductivity and the electrical conductivity is formulated. At first the existence of solutions for the different optimal control problems is considered. Afterwards different aspects and modifications of the problems are discussed. Due to the physical effects in the method of RFA we will need some simplifications or particular scaling in the modeling to obtain a numerical solution for the identification problem.

In **Chapter 6** the numerical results of the parameter identification problems derived in Chapter 5 are shown. The above identification problems are applied to different settings. At first an artificial setting is used where the parameters are known and the identified results can be compared with the original ones. Second, temperature measurements

from an experiment in an Agar-gel are used to identify the parameters.

In **Chapter 7** an outlook to further applications of the identification problem is presented. The developed methods are extended to the identification of the density and the heat capacity and in a first approach to the method of high-intensity focused ultrasound. First results for the optimization of the pressure from MR measurements are presented. Final conclusions are drawn in **Chapter 8**.

2 Related work and state of the art

In this chapter we will consider at first the related work and state of the art in the field of the mathematical modeling and simulation of RFA. Second, different approaches in the field of identification problems are described and investigated in terms of their practicability to the present problem of identifying the material properties for the RFA.

2.1 State of the art to the modeling of radio frequency ablation

As described in the introduction, the method of RFA is limited by several factors and a realistic modeling could improve the success and provide a prediction of the results. Various authors have investigated the modeling and simulation of the RFA, motivated by different aspects and aiming at diverse applications. Most of the investigations are rather in the range of academic or ground research than really applicable, since for a real application a lot of aspects need to be regarded, which make the model complex and potentially hard to solve numerically. An overview of the state of the art and future challenges in the modeling of RFA is given by Berjano [10]. The mathematical models are basically the same in literature. The heat distribution is calculated via the so called bio-heat transfer equation, where the energy is given by a source term which is mostly calculated from the electrostatic equation. Most of the models also take a heat sink into account to describe the blood perfusion in the tissue or to incorporate the cooling effect from the vascular system.

For real applications the destroyed part of the tissue is of major interest. This tissue damage is either modeled by the Arrhenius formalism [8] or it is assumed that the tissue can be considered as destroyed if the temperature reaches a certain threshold (commonly 60 °C). Furthermore several special aspects of the modeling are considered and all are aiming at improving the modeling and the simulation, whereas the improvement can be considered under different aspects. On the one hand we have the improvement of the model itself, i.e. the model becomes more realistic, on the other hand we have the improving of the performance to get a real time application, since the calculations for a realistic model are expensive. The improvement of the model can be reached by a better understanding of the physical effects and an appropriate transfer to the mathematical model.

For a better understanding of the physical behavior of the model and an appropriate improvement Chang [15] investigated the influence of the electrical conductivity and the blood perfusion on the system. Whereas Watanabe et al. [92] looked at the effects of the thermal conductivity on the temperature distribution, calculated from different thermophysical models.

Beside the material parameters the influence of the modeled vascular system is subject to some investigations, e.g. from Tungjitkusolmun et al. [89]. They modeled the RFA with finite elements for a four-tine RF probe and simulate the heat distribution for different placements of the probe in the vicinity of a vascular structure. Their results demonstrate that incorporating the effects of the vascular system is important for a realistic prediction of the RFA.

With regard to the improvement of the numerical performance Johnson et al. [42] avoid to solve the electrostatic equation by replacing the heat source by a function which depends on the distance to the probe. Another kind of acceleration is performed by Kröger et al. [51] using a look-up table with coagulation areas calculated in advance by a non-individual reference configuration.

Investiagtions concerning the trajectory planning for a percutaneous needle insertion is described in the works of Schumann et al. [71] and Seitel et al. [75]. Different methods are used to find the best path for the needle placement under consideration of various risk structures. Furthermore, an overview of relevant computer assisted methods for the support of thermal ablations in the liver is given by the paper of Schumann et al. [72].

Another important aspect is the optimization of the probe placement. To assure a successful RFA the probe has to be placed in a good position such that the whole tumor is destroyed and as much healthy tissue as possible is preserved. Amongst others such optimization is performed by Altrogge [5] and Villard et al. [91]. The used approaches are quite different, Villard et al. use ellipsoids in consideration of the cooling effects due to the vessels, to describe the coagulated area whereas Altrogge calculates the coagulation by a coupled system of partial differential equations, the electrostatic equation and the bio-heat transport equation. Both use standard optimization techniques to find an optimal position for the probe placement.

Moreover, Altrogge [5] investigated the dependence of the whole system on the material parameters by modeling the thermal conductivity and the electrical conductivity as stochastically distributed. The resulting system of stochastic partial differential equations is used for a stochastic optimization and a sensitivity analysis of the optimal probe placement with respect to changes in the parameters.

Altogether, the modeling and simulation of RFA involves problems of different kinds. One major problem is based on the numerical performance and another is closely interrelated to the physical parameters in the model. Without a realistic modeling of the material parameters the simulation of the RFA will not be realistic either.

2.2 State of the art in the field of identification problems

This work aims at the patient individually identification of the material parameters during the treatment with RFA to improve the mathematical model and therewith the simulation. In the following an overview of relevant work in the field of identification problems of different kinds and in different areas is given. The state of the art to the modeling of the parameters for the treatment with RFA will be presented in the section

of the modeling 3.3.3.

During the last 20 years the parameter identification in connection with elliptic or parabolic PDEs has been subject to various investigations. On the one hand we have the more theoretical papers as for example [9, 17, 31, 58] and on the other hand some which focus more on the numerical aspects and which use different approaches to solve the identification problem. In the following we will take a closer look into some of these approaches.

The approach which is set apart from all others is the idea to use a Kirchhoff transformation for the parameter identification. The Kirchhoff transformation is a linearization technique to transform a nonlinear PDE into a PDE which can be solved by using standard linear techniques [26]. For example the steady state heat equation

$$\text{div}(\lambda(T)\nabla T) = 0, \qquad\qquad x \in [0,1],$$

$$-\lambda(T)\frac{\partial T}{\partial x} = q = \text{const}, \qquad\qquad x \in [0,1],$$

$$T_L = T(x = 0) \quad \text{or} \quad T_R = T(x = 1)$$

with temperature dependent thermal conductivity λ and known values T_L and T_R transforms with the substitution $\psi := \int_{T_0}^{T} \lambda(\xi)d\xi$ into the following Laplace equation in ψ

$$\nabla^2 \psi = 0, \qquad\qquad x \in [0,1], \qquad (2.1a)$$

$$-\frac{\partial \psi}{\partial x} = q = \text{const}, \qquad\qquad x \in [0,1], \qquad (2.1b)$$

$$\psi(x = 0) = \int_0^{T_L} \lambda(\xi)\,d\xi \qquad \text{or} \quad \psi(x = 1) = \int_0^{T_R} \lambda(\xi)\,d\xi. \qquad (2.1c)$$

The solution of the Laplace equation (2.1) is given as

$$\psi(x) = -qx + \int_0^{T_L} \lambda(\xi)d\xi = \int_0^{T(x)} \lambda(\xi)d\xi \qquad (2.2)$$

or

$$\psi(x) = -q(x - 1) + \int_0^{T_R} \lambda(\xi)d\xi = \int_0^{T(x)} \lambda(\xi)d\xi. \qquad (2.3)$$

For a given thermal conductivity, the temperature distribution can be calculated from these two equations. The intention by Kim [46] is to determine the temperature dependent thermal conductivity λ. Therefore, he approximates the thermal conductivity as a linear combination

$$\lambda(T) \approx \sum_{n=0}^{N} \lambda_n \Phi_n(T), \qquad (2.4)$$

with unknown coefficients λ_n and known functions $\Phi_n(T)$. He assumes a known type of function for $\lambda(T)$, e.g. a polynomial which means the known functions are given by

$\Phi_n(T) = T^n$. The aim is then to identify the unknown coefficients λ_n from the known data (q, T_L, T_R). Between the known data (q, T_L, T_R) and the unknown coefficients λ_n a relation is established by equalizing equation (2.1c) and (2.2) or (2.3) respectively

$$
\begin{aligned}
\int_0^{T_L} \lambda(\xi)\, d\xi &= q + \int_0^{T_R} \lambda(\xi)\, d\xi \\
\int_{T_L}^{T_R} \lambda(\xi)\, d\xi &= -q
\end{aligned}
\tag{2.5}
$$

and the insertion of (2.4) in the resulting equation (2.5)

$$
-q = \sum_{n=0}^{N} \lambda_n \int_{T_L}^{T_R} \Phi_n(\xi)\, d\xi.
\tag{2.6}
$$

The final linear equation (2.6) can be solved with respect to the coefficients λ_n.
The problem can be extended to a non-steady state problem and the solution works as well as for the steady-state problem, see Kim et al. [47]. However, to solve this problem for the thermal properties either the thermal diffusivity, i.e. the relation between the thermal conductivity $\lambda(T)$ and the heat capacity $c(T)$, has to be known or two different data measurements are needed, see also [47]. The more complex the equation in the beginning the less applicable is this method. Therefore the method is not applicable for the problem presented in this thesis. But for simple problems this will offer an alternative solution. However, the solution depends on the approximation (2.4) of the thermal conductivity $\lambda(T)$.
Another approach to calculate the material parameters from given temperature measurements can be found in the paper of Sumi and Kuwabara [81] and also in the paper of Sumi and Yanagimura [83]. They focus on the identification of the thermal conductivity for the steady state and the non-steady state heat equation respectively, by comparing different measured temperature distributions. In their calculations they neglect the Helmholtz-term and the heat source and heat sink term. The conductivity distribution, capacity distribution and diffusivity distribution can be determined from six independent measured sets of temperature distributions if either a reference conductivity or a reference capacity is given as initial condition. Using two independent sets of sequential temperature distributions T_1 and T_2, an equation for the unknown gradient of the logarithm of the conductivity can be derived

$$
\left(\nabla T_1 \frac{dT_2}{dt} - \nabla T_2 \frac{dT_1}{dt} \right) \cdot \nabla \ln k + \left(\nabla^2 T_1 \frac{dT_2}{dt} - \nabla^2 T_2 \frac{dT_1}{dt} \right) = 0.
$$

A drawback of this approach for the problem discussed in this work is the missing heat source and heat sink as well as the requirement of six independent sets of temperature distributions. Furthermore the problem can not be transferred to the identification of the electrical conductivity via a coupled system of PDEs.
In an earlier work, Sumi et al. [82], determine the electrical conductivity via the given

potential or the given current density. But this works only under the condition that there is no heat source within the region of interest. A heat source in the domain would lead to additional conditions which do not match the idea of the approach. Therefore it is not applicable to the problem of the present work.

Another early attempt to identify the parameters in a parabolic problem was made by Keung and Zou [44] in 1997. They formulate a fitting type minimization problem whereas they consider the gradient of the difference weighted with the parameter, they wanted to identify. That means they use a weighted H^1-semi-norm and obtain the following objective functional

$$J(\lambda) = \tfrac{1}{2} \int_{T_{\text{fin}} - \epsilon}^{T_{\text{fin}}} \int_{\Omega} \lambda(x) |\nabla(T(\lambda, t) - z)|^2 dx dt + \gamma N(\lambda)$$

with the solution of the parabolic PDE constraints $T(\lambda; t)$, measurements z and the parameter $\lambda(x)$ to be identified and the regularization term

$$N(\lambda) = \int_{\Omega} |\nabla \lambda|^2 dx \quad \text{or} \quad N(\lambda) = \int_{\Omega} |D\lambda|^2.$$

That means they use either the H^1-semi-norm or the semi-norm in the space of bounded variations (BV)
$$BV(\Omega) := \{\lambda \in L^1(\Omega) | \, \|\lambda\|_{BV(\Omega)} < \infty\}$$
with $\|\lambda\|_{BV(\Omega)} = \|\lambda\|_{L^1(\Omega)} + \int_{\Omega} |D\lambda|$, where $\int_{\Omega} |D\lambda|$ defines a set and not an integral

$$\int_{\Omega} |D\lambda| := \sup \left\{ \int_{\Omega} \lambda \operatorname{div} g \, dx | \, g \in (C_0^1(\Omega))^d \text{ and } |g(x)| \leq 1 \text{ in } \Omega \right\}.$$

The weight in the objective function requires more accuracy in the fitting for large parameter values. However, in the problem discussed in the present thesis the main problems for the fitting are located at those positions where the parameter is not notably large. Here the problems are rather caused by the values of the temperature. Furthermore, Keung and Zou use in their numerical examples the L^2-norm for noisy input data instead of the H^1-semi-norm and omit the weighting parameter too. In the present thesis the objective will be formulated in most cases with the H^1-norm, which enables to account for both, the difference between the values and the difference between the gradients.
A similar formulation for the objective can be found in [49]. Engl and Zou [17] investigate the stability and convergence rates of the above least squares method with Tikhonov regularization. Whereas the motivation for the paper of Keung and Zou [44] is the numerical identification of physical parameters in parabolic initial boundary value problems.
Further similarities to the present work can be found in the paper of Gänzler et al. [21]. They work on the parameter identification in hyperthermia, i.e. on the identification of the individual perfusion. They use the bio-heat transfer equation to describe the temperature distribution in the body. Additionally, they augment their equation by a

Helmholtz term to model the cooling of the tissue by blood perfusion. For the optimal control problem they use the following fitting type cost functional

$$
\begin{aligned}
J(T, w) =& \tfrac{1}{2}\|a(T - T_{\text{bas}}) + b(w - w_{\text{bas}}) - m\|^2_{L^2(\Omega)} + \tfrac{1}{2}\|w - w_{\text{ref}}\|^2_W \\
& - \theta\alpha \int_\Omega \left(\ln w - \frac{w}{w_{\text{ref}}} \right) dx,
\end{aligned}
\tag{2.7}
$$

with respect to the temperature u and the perfusion w. Here W is defined as

$$
W := \{w \in L^2(\Omega)|\, w|_{\Omega_i} \in H^1(\Omega_i)\, \text{for}\, i = 1, \ldots, n_\Omega\}, \quad \text{with}\, \Omega = \bigcup_{i=1}^{n_\Omega} \Omega_i,
$$

where n_Ω denotes the total number of different tissue types. The different domains for the diverse tissue types are denoted by Ω_i.

The measured data for the temperature and the perfusion are denoted by $m \approx a(T - T_{\text{bas}}) + b(w - w_{\text{bas}})$ where T_{bas} and w_{bas} are known offsets. These offsets are needed for the modeling since the MRI can measure only changes in the material and no absolute values. That means the difference between a known value and the present value has to be modeled. The problem is solved with a sequential quadratic programming (SQP) method which is tested on a two dimensional test setting from hyperthermia.

The main differences to the problem in the present thesis are based on the PDE system itself and the intention of Gänzler et al.. In the present model we will use a system of PDEs which are coupled via the right hand side, whereas Gänzler et al. [21] model the heat equation with the specific absorption rate (SAR) as heat source on the right hand side. Moreover, Gänzler et al. are interested in the perfusion and the intention of the present work is the identification of the material parameters as e.g. the thermal conductivity or the electrical conductivity.

However, the most analogy to the identification problem in RFA with regard to the application and the mathematical modeling is stated in the paper of Hömberg et al. [38]. They focus on the state-constrained optimal control of the two-dimensional thermistor problem. This includes a quasi-linear coupled system of a parabolic PDE and an elliptic PDE with different types of boundary conditions. The work distinguishes from other studies mainly by the mixed boundary conditions and the non-smooth domains. The difference to the present study is given by the optimization variable. Hömberg et al. optimize with respect to the temperature and the heat source or more precisely the induced current on the outer boundary, whereas the conductivities are given functions. Their paper focusses on the existence of an optimal solution and the discussion and analysis of the state system as well as the adjoint system and the linearized system. It ends up with the application to a two-dimensional real problem from the automotive industry.

Altogether, in the literature there can be found a lot of works considering the modeling of RFA as well as identification problems with PDEs. But to the author's knowledge there exists no work which investigates the identification of the parameters in the main

part of the PDEs by using a coupled system of PDEs with a coupling term on the right hand side as complex as in the present work. Moreover even most of the existing models for the RFA simplifies or neglect the scaling term needed for the heat source, further details will follow in chapter 3. The identification problem together with the complex model of the RFA implies a lot of difficulties and challenges we will contemplate in the following.

3 Modeling of radio frequency ablation

In this chapter we will derive the mathematical model for the method of RFA. Therefore at first a short description of the treatment with RFA is given. Afterwards we will model the resulting physical effects with the help of partial differential equations (PDEs).

3.1 The method of RFA

The main principle of the treatment is based on heating the malignant tissue by applying electric current to the tissue. The name *radio frequency ablation* is based on the fact that the introduced current is in the range of high frequency, the so called radio frequencies. The used frequency for RFA is typically about $500\,\mathrm{kHz}$.
For the treatment of hepatic metastases or hepatic tumors a probe with one or more electrodes, which is connected to an electric generator, is placed in the tumor, cf. figure 3.1. The current leads to a heating of the cells around the probe due to the resistance of the tissue. Above a temperature of $60\,^\circ\mathrm{C}$ the cells can be considered as destroyed since the proteins of the cells are coagulated and the cells will not regenerate. The aim of the RFA is the destruction of the tumor together with a safety margin to ensure that all malignant tissue is destroyed.
The advantage of the RFA over the resection is that the RFA is minimally invasive and that healthy tissue is preserved. Furthermore tumors placed in the middle of the liver can be destroyed without resection of larger parts of the liver. However, the success of RFA is limited by several factors. The major limitation is that the outcome of the therapy depends highly on the experience of the executing radiologist. An experienced radiologist has the ability to account for example for the cooling effects of the vascular system rather than a radiologist without any or with less experience.

3.2 Modeling of heat propagation

For the mathematical modeling of the method of RFA we need at first a description of the electric potential. Since the wavelength of the electromagnetic waves is large compared with the dimensions of the electrodes and their arrangement the time rate of change for the electrical field can be neglected. Further, the magnetic field which is generated by the changing electrical field can be neglected too, because the magnetic field does not appreciable influence the electrical field. Both is caused by the material properties of the liver and the frequency of about $500\,\mathrm{kHz}$ used for RFA [78]. Therefore, we can consider the alternating current as direct current and use the electrostatic laws to formulate the following partial differential equation for the electric potential $\phi : \Omega \rightarrow \mathbb{R}$
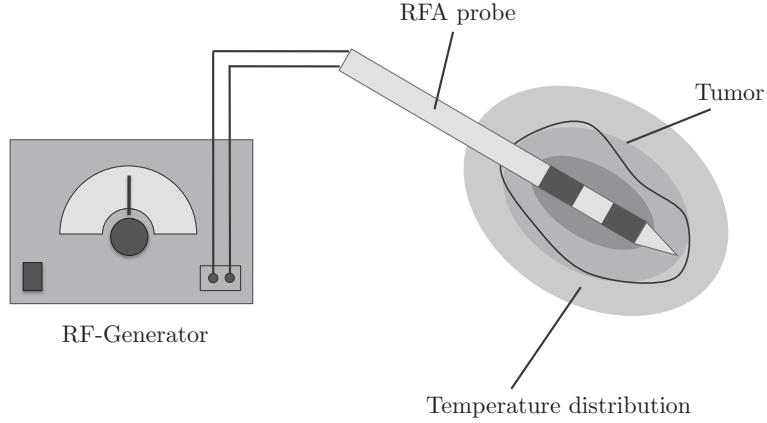
Figure 3.1: Schematic figure of the method of RFA with a bipolar probe. On the left the RF generator is depicted and on the right we see the probe, placed in the tumor. Furthermore the temperature distribution, generated by the electric current, is shown.

$$-\mathrm{div}\left(\sigma(T)\nabla\phi(x)\right) = 0 \quad \text{in } \Omega \setminus \overline{\Gamma},$$

with $\Gamma = \Gamma_+ \cup \Gamma_-$. Here, $\sigma(T)$ denotes the electrical conductivity, depending on the temperature $T(t, x)$. The computational domain is described by Ω, whereas the positive and negative electrodes are denoted by Γ_+ and Γ_- respectively. For a more detailed derivation see e.g. [78]. In figure 3.2 a scheme of the domains is depicted.

If we assume an infinite electrical conductivity σ on the electrodes Γ, the potential ϕ becomes constant on the electrodes and the gradient of the potential $\nabla\phi$ becomes zero on the electrodes accordingly. The potential ϕ is set to 1 and -1 on the positive and the negative electrode respectively. Since these are arbitrarily chosen values we have to scale the potential afterwards. For the outer boundary $\partial\Omega$, the boundary of the computational domain Ω, another condition is needed. There exist different possibilities to formulate the conditions. Three customarily used conditions are the following

- Homogeneous Neumann boundary conditions $\nabla\phi \cdot n = 0$, with the outer normal vector n. This means we assume that there exists no electrical flow at the boundary. This leads to difficulties if we use a monopolar probe, where the second electrode is placed somewhere on the body outside of the computational domain. Therefore, for a monopolar probe we have to choose another boundary condition.

- Homogeneous Dirichlet boundary conditions $\phi = 0$.
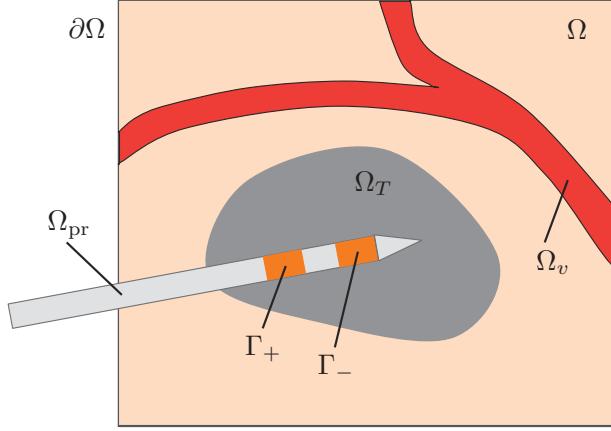
Figure 3.2: Schematic figure of the domains for the model of the RFA. The tumor is denoted by Ω_T, the vascular system by Ω_v, the probe by Ω_{pr} and the whole computational domain by Ω. The positive and negative electrodes on the probe are denoted as Γ_+ and Γ_- respectively.

- Robin boundary conditions

$$\nabla\phi \cdot n = \frac{n \cdot (s - x)}{|s - x|^2}\phi.$$

Here, s denotes the barycenter of the probe and n the outer normal vector. The underlying assumption is that the potential on the outer boundary $\partial\Omega$, i.e. distant from the probe, behaves approximately as the potential ϕ_s induced by a point load at the barycenter s. The potential ϕ_s can be calculated as

$$\phi_s = C \cdot \frac{1}{|s - x|}$$

with a constant $C \in \mathbb{R}$.

The best choice would be the Robin boundary conditions, because of their flexibility regarding the polarity of the probe. However, for the numerical calculations described in the subsequent sections the homogenous Dirichlet conditions will be used. Since all numerical examples are performed with a monopolar probe we do not need the flexibility of the Robin boundary conditions. Altogether, by using the Robin boundary conditions

we obtain the following elliptic boundary value problem

$$
\begin{aligned}
-\operatorname{div}\left(\sigma(T)\nabla\phi(x)\right) &= 0 & &\text{in } \Omega \setminus \overline{\Gamma} \\
\phi(x) &= \pm 1 & &\text{on } \Gamma := \Gamma_+ \cup \Gamma_- \\
\nabla\phi(x)\cdot n &= \frac{n\cdot(s-x)}{|s-x|^2}\phi(x) & &\text{on } \partial\Omega,
\end{aligned}
\tag{3.1}
$$

with the outer normal vector n on $\partial\Omega$. If we use Dirichlet conditions the last row changes accordingly.

For the modeling of the temporal and spatial heat distribution we use the so called *Bioheat-Transfer-Equation*, a parabolic, quasi-linear and inhomogeneous partial differential equation

$$
\rho(T)c(T)\partial_t T(t,x) - \operatorname{div}\left(\lambda(T)\nabla T(t,x)\right) = Q(t,x) \quad \text{in } \mathbb{R}\times\Omega.
\tag{3.2}
$$

Again a detailed derivation can be found amongst others in [78]. The thermal parameters $\rho(T), c(T)$ and $\lambda(T)$ describe the density, the heat capacity and the thermal conductivity respectively. According to the temporal and spatial distribution of the temperature the thermal parameters can be considered as temporally and spatially distributed as well. The right hand side $Q(t,x)$ consists of two different terms, a heat source $Q_{\text{rf}}(x)$ and a heat sink $Q_{\text{perf}}(t,x)$. In some other works, as e.g. [89] or [15], there is an additional term Q_{m} that describes the metabolic heat source. Since this term influences the temperature distribution only marginally, it can be neglected for the calculations.
The heat source $Q_{\text{rf}}(x)$ is induced by the electric potential ϕ. The electrical resistance of the tissue leads to a heating of the tissue up to a value of $100\,^\circ\text{C}$ and higher. The electrical power density P can be calculated by the magnitude of the electrical field times the electrical conductivity σ

$$
P = \sigma|\nabla\phi|^2.
$$

Since we use arbitrary boundary values for ϕ on the electrodes we need a scaling factor for ϕ and thus also for the power density P. The power P_{set} set up at the generator is not the same as the effective power P_{eff} in the tissue, due to the impedance matching of electrical appliance. The impedance matches, i.e. the inner and outer resistance is equal, if the efficiency is $50\,\%$. In other words the maximal power is achieved if both resistors have the same value. In figure 3.3 the impedance matching and the efficiency for the RFA model are depicted.
For the RFA this impedance matching means that the effective power in the tissue depends on the resistance R_I of the generator and on the resistance R of the tissue. In fact we would have to assume various of infinitesimal resistors in the tissue. However, we are not able to model all these resistors and in particular we do not know the circuitry. But we can consider all these infinitesimal resistors as one resistor for the whole domain, since for the series connection as well as for the parallel connection the total amount of resistors $R = \sum_{k=1}^{N} R_k$ add up to an overall resistance R. For the series connection it is the sum of all resistors $R = \sum_{k=1}^{N} R_k$ and for the parallel connection the reciprocal of the overall resistance is the sum of the reciprocals of all resistors $\frac{1}{R} = \sum_{k=1}^{N} \frac{1}{R_k}$. Therefore,
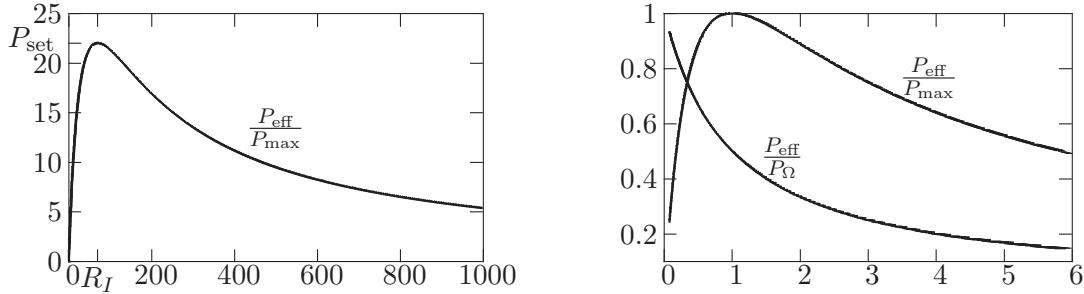
Figure 3.3: In the left figure the process of the effective power in relation to the maximal power is depicted, depending on the resistance of the tissue R. The efficiency is illustrated in the right figure, together with the effective power in relation to the ratio $\frac{R_I}{R}$. The setup power is set to $P_{\text{set}} = 22 \, \text{kg} \, \text{m}^2 \, \text{s}^{-3}$ and the resistance to $R_I = 70 \, \Omega$.
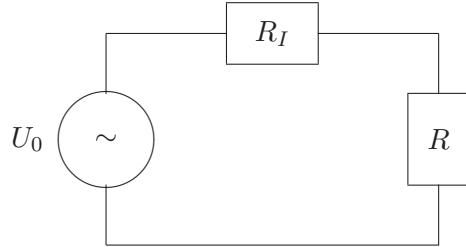
Figure 3.4: Equivalent circuit diagram for the generator and the tissue. The voltage U_0 is preset at the generator. The inner resistance of the generator and the resistance of the tissue are denoted by R_I and R respectively.

we do not have to distinguish between series connection and parallel connection and can assume an overall resistance R for the whole tissue.

For the modeling we assume that for a constant setting the generator can be described as a constant voltage source U_0 with an inner resistance R_I, see equivalent circuit diagram in figure 3.4. Accordingly, we can describe the current flow I by means of the laws for series circuits as $I = \frac{U_0}{R+R_I}$. The resulting effective voltage is

$$U = RI = \frac{RU_0}{R_I + R}.$$

The corresponding effective power P_{eff} is the product of the current flow I and the electrical voltage U between the electrodes, i.e.

$$P_{\text{eff}} = UI = \frac{RU_0}{R + R_I} I = \frac{RU_0^2}{(R + R_I)^2}. \tag{3.3}$$

19

However, to calculate P_{eff} we need the constant voltage U_0, which is induced by the generator for the power P_{set}. Therefore, we assume that P_{set} is the maximal achievable power, i.e. the maximal value of P_{eff}. From the scheme of the impedance matching above we know that the maximum of P_{eff} is reached if the inner resistor R_I equals the outer resistance R and hence we obtain

$$P_{\text{set}} = \frac{U_0^2}{4R_I}.$$

Therewith we can substitute U_0 in (3.3) and the effective power is given by

$$P_{\text{eff}} = \frac{4RR_I P_{\text{set}}}{(R + R_I)^2}.$$

Finally, the effective power needs to be normalized by the whole power $P_\Omega = \int_\Omega \sigma |\nabla\phi|^2 \, dx$ to achieve the efficiency as scaling factor for the electrical power

$$Q_{\text{rf}}(t, x) = \frac{P_{\text{eff}}}{P_\Omega} \sigma(T) |\nabla\phi(x)|^2. \tag{3.4}$$

The resistance R of the tissue has to be calculated accordingly to the assumed potential on the electrodes. For the case where the potential is set to $\phi = \pm 1$ on the electrodes, which add up to a voltage of $U = 2\,\text{V}$ between the two electrodes, and $P = P_\Omega$, we obtain a resistance $R = \frac{4\,\text{V}^2}{P_\Omega}$. If a monopolar probe is modeled instead, we obtain a voltage of $U = 1\,\text{V}$ at the electrode. When the RFA is performed with a monopolar probe, a second electrode is placed somewhere on the body, usually at the patient's leg. By substituting R in (3.3) and reformulating the equation we obtain for the scaling term

$$\frac{P_{\text{eff}}}{P_\Omega} = \frac{4R_I P_{\text{set}}}{(1 + R_I P_\Omega)^2} \qquad (3.5) \qquad\qquad \frac{P_{\text{eff}}}{P_\Omega} = \frac{16 R_I P_{\text{set}}}{(4 + R_I P_\Omega)^2} \qquad (3.6)$$

for the monopolar probe (3.5) and the bipolar probe (3.6) respectively. This notation is used also in section 5.2.2.

Other groups are dealing in different ways with the modeling of the heat source and the associated scaling problem. Chang [15] does not use any scaling and Watanabe et al. [92] assume a constant value of $35\,\text{V}$ on the electrodes. Whereas Chen et al. [16] and Humphries et al. [39] use a simplified scaling term. Another ansatz is pursued by Johnson et al. [42] who calculate the heat source from the electrical current and the probe's position by using the conservation of charge. This ansatz is performed without solving a PDE for the heat source.

Back to the present model (3.2) and the components of the right hand side, the heat sink $Q_{\text{perf}}(t, x)$ describes the cooling effect of the vascular system and the blood perfusion due to the capillaries. One possibility to model $Q_{\text{perf}}(t, x)$ is the approach of Pennes [64] with an additional weighting for the vascular system

$$Q_{\text{perf}}(t, x) = -\nu(x)\left(T(t, x) - T_{\text{body}}\right), \tag{3.7}$$

with

$$\nu(x) = \begin{cases} \nu_\mathrm{v}\,\rho_\mathrm{blood}\,c_\mathrm{blood}, & \text{for } x \in \Omega_v, \\ \nu_\mathrm{c}\,\rho_\mathrm{blood}\,c_\mathrm{blood}, & \text{for } x \notin \Omega_v, \\ 0, & \text{for completely coagulated tissue,} \end{cases}$$

where the blood vessels are denoted by Ω_v. The perfusion coefficient ν is set to zero if the tissue is completely coagulated, since there is no blood perfusion possible any longer. For the non-coagulated tissue the coefficient depends on the blood density ρ_blood and on the heat capacity of blood c_blood as well as on the relative blood circulation rate ν_v for the vessels and ν_c for the capillaries respectively.

Beside this model there exist various other possibilities to model the blood perfusion, see e.g. Arkin et al. [7], where different models are compared. Furthermore there exist other physiological phenomena which can be considered as well, as for example the heat transfer between venous and arterial blood that are close to each other, see e.g. Bowman et al. [13]. In general the more physical and biological effects are included in the model, the outcome maybe more realistic but the more complex and expensive will be the calculations. Thus we will use the above model which accounts for the most important effects without being too complex to solve.

To solve the *Bioheat-Transfer-Equation* (3.2) we need additional initial values and boundary conditions. As initial condition for the temperature we choose a constant value. For real applications it will be the body temperature T_body. On the outer boundary we choose Neumann boundary conditions, assuming that there will be no heat flow across the boundary. Another possibility is to use Dirichlet boundary conditions instead of Neumann conditions, assuming a constant temperature T_body on the outer boundary $\partial\Omega$. The inner boundary, i.e. the probe Ω_pr, is set to a constant temperature T_probe too, due to the fact that most probes are cooled internally. If we want to model a non-cooled probe we neglect these boundary conditions and add the probe to the domain Ω. Altogether for the modeling of the temperature T during the RFA we achieve the following initial value and boundary value problem:

$$\rho c \partial_t T(t,x) - \mathrm{div}\left(\lambda \nabla T(t,x)\right) = Q_\mathrm{rf}(t,x) + Q_\mathrm{perf}(t,x) \qquad \text{in } \mathbb{R}^+ \times \Omega \setminus \Omega_\mathrm{pr}, \qquad (3.8\mathrm{a})$$

$$\begin{aligned} T(0,x) &= T_\mathrm{body} & \text{in } \Omega, \\ T(t,x) &= T_\mathrm{probe} & \text{on } \mathbb{R}^+ \times \Omega_\mathrm{pr}, \\ \nabla T(t,x) \cdot n(x) &= 0 & \text{on } \mathbb{R}^+ \times \partial\Omega. \end{aligned} \qquad (3.8\mathrm{b})$$

Here, Ω_pr denotes the subset of the domain Ω which is covered by the probe and n denotes the outer normal vector on $\partial\Omega$. The terms Q_rf and Q_perf are chosen as in (3.4) and (3.7) respectively.

Considering the whole model, first we have to solve the potential (3.1) and then calculate the heat source (3.4). Afterwards we are able to solve the non-stationary heat equation (3.8) for the temperature T.

3.3 Material properties

In the previous section we derived the mathematical model for the RFA. However, without the knowledge of the material parameters the model will be of no real avail. In this case, material parameters include the electrical conductivity σ, the thermal conductivity λ, the heat density ρ, the heat capacity c and the perfusion coefficient ν.

The problem for the dielectric properties and the thermal properties is the lacking knowledge of the exact values and the exact behavior during the ablation. There exist various experiments and studies concerning these properties but they are all limited. The limitations are caused by different problems. The first one is that most experiments are done in vitro and therefore are non-transferable to in vivo, since we have destructions and changes in the materials. Another limitation is that most experiments are conducted with animal tissue, which may differ considerably from human tissue. In the next sections we will take a closer look at these parameters and their impact on the whole system as well as their behavior during time and heating.

3.3.1 Electrical conductivity

The electrical conductivity, generally named σ, describes a material's ability to conduct electrical current and is the proportional between the current density $\vec{j}$ and the electrical field strength $\vec{E}$ such that

$$\vec{j} = \sigma \vec{E}.$$

The electrical conductivity is the reciprocal of the electrical resistivity and has the SI units $\mathrm{S\,m^{-1}}$. For different materials a distinction is drawn between metallic materials with high conductivity, larger than $10^2\,\mathrm{S\,m^{-1}}$, so called conductors, and materials with low conductivity, smaller than $10^{-8}\,\mathrm{S\,m^{-1}}$, and high resistivity, so called insulators. For example, silver has the highest conductivity $(62.5 \cdot 10^6\,\mathrm{S\,m^{-1}})$ of any known metal. On the other side, amber has a conductivity smaller than $10^{-16}\,\mathrm{S\,m^{-1}}$ and the conductivity of river water lies in the range of $[0.01, \ldots, 0.1]\,\mathrm{S\,m^{-1}}$. The third group of classification consists of the so called semiconductors which are materials that are insulators at the absolute zero $(0\,\mathrm{K})$ but the conductivity increases with increasing temperature. This temperature dependency of the resistivity is an important disparity between metallic conductors and semiconductors. The resistivity of conductors increases with increasing temperature, whereas the resistivity of semiconductors decreases substantial with increasing temperature. These effects are reflected contra wise in the thermal conductivity according to the definition. For some metals the resistivity declines to almost zero for a temperature close to $0\,\mathrm{K}$. Such conductors are called superconductors. The human tissue is a semiconductor with a conductivity somewhere in the range of 0.1 to $0.9\,\mathrm{S\,m^{-1}}$, based on the results of [33, 56, 89, 74]. The conductivity depends on different factors as specific frequencies of light and particularly temperature. The basic facts about the electrical conductivity are taken from [54].

There have been several studies concerning the electrical conductivity since the second part of the 19th century, see e.g. [36]. An overview of the results during the last century

	tumorous tissue	surrounding tissue
$1\,\mathrm{kHz}$	$0.14 \pm 0.06\,\mathrm{Sm}^{-1}$	$0.03 \pm 0.01\,\mathrm{Sm}^{-1}$
$400\,\mathrm{kHz}$	$0.25 \pm 0.06\,\mathrm{Sm}^{-1}$	$0.15 \pm 0.03\,\mathrm{Sm}^{-1}$

Table 3.1: The values for the electric conductivity with standard deviation, measured ex vivo in human hepatic tumors and surrounding tissue. The values are taken from the paper of Laufer et al. [56].

can be found in [20]. However, the temperature dependency for the dielectrical properties has not been under consideration until the last decades. Most prior studies focus on the frequency dependency and the diverse behavior in different organs and various animals and humans [74, 73]. One of the earlier papers regarding the temperature dependency is the work of Stogryn [80], in the context of remote sensing of the ocean by microwave radiometers. Amongst others, in the medical context the temperature dependency becomes more and more important because of the enhancements in hyperthermia and RFA.

But not only the temperature dependency of the electrical conductivity, as studied e.g. by Kubisz and Marzec [53], Chang [15] and Watanabe et al. [92], but also other aspects concerning the conductivity have been investigated by several authors, as for example the change in the dielectric properties after death, see Surowiec et al. [85]. Another important aspect beside the temperature dependency is, especially in medical treatment, the dependency of the conductivity on the tissue type. Different tissue types do not mean only the distinction between tumorous and healthy tissue but also the age of the tissue, fibrosis of the tissue and the arising necrosis during the ablation or in fact different organs. Appropriate research has been done e.g. by Haemmerich et al. [33] and Pop et al. [66]. Especially the differences in the conductivity for tumorous tissue and for native tissue are significant, see also the work of Laufer et al. [56] and their results depicted in table 3.1. Solazzo et al. [77] investigate not only ex vivo samples but instead consider a model with different types of Agar gel (different types mean different sodium chloride (NaCl) concentration) and the properties of the conductivity especially at the intersections.

Altogether, there exist various influences on the behavior of the electrical conductivity, which are not yet entirely investigated. Nevertheless, we know some influences as the temperature dependency and the tissue dependency, which we should keep in mind if we want to model and to identify the electrical conductivity. Another kind of investigations concerning the electrical conductivity has been done by Chang [15], who compared the effects of the modeling of the electrical conductivity with or without temperature dependence on the simulation of the RFA (cf. section 3.3.3).

3.3.2 Thermal conductivity

A material's ability to conduct heat is called thermal conductivity. It describes the carriage of thermal energy by heat conduction. The following facts to the thermal

conductivity are taken from [78] and [54]. The thermal conductivity λ is measured in Watt per Kelvin times meters ($\mathrm{W\,K^{-1}\,m^{-1}}$). The thermal diffusivity α measures the rate for the heat diffusion and is defined as the ratio between the thermal conductivity and the product of the specific heat capacity c and the density ρ

$$\alpha = \frac{\lambda}{\rho c}.$$

The density ρ has the SI units kilogram per cubic meters ($\mathrm{kg\,m^{-3}}$) and the specific heat capacity c the SI units Joule per kilogram per Kelvin ($\mathrm{J\,kg^{-1}\,K^{-1}}$).
The thermal conductivity varies for different materials, for example the conductivity for steel is in the range of $45\,\mathrm{W\,K^{-1}\,m^{-1}}$ and for wool it is only $0.04\,\mathrm{W\,K^{-1}\,m^{-1}}$, both at a temperature of $20\,^\circ\mathrm{C}$. For human tissue we have a thermal conductivity between 0.4 to $0.8\,\mathrm{W\,K^{-1}\,m^{-1}}$ [13]. The thermal conductivity λ depends on the temperature as well as the electrical conductivity. However, the temperature dependency of λ for human tissue can be approximated linearly [78]. In contrast, the heat capacity c can be assumed as constant, at least for temperatures between $0\,^\circ\mathrm{C}$ and $100\,^\circ\mathrm{C}$. Whereas the density ρ depends linearly on the temperature. Valvano et al. [90] describe great differences of the values between the species and also for different organs of one species. Their result for the thermal conductivity in the human lung was $\lambda = 0.4071\,\mathrm{W\,m^{-1}\,K^{-1}}$. For the human liver they measured values of $\lambda = 0.4692\,\mathrm{W\,m^{-1}\,K^{-1}}$ and for colon cancer at $19\,^\circ\mathrm{C}$ they specify a thermal conductivity of $\lambda = 0.545\,\mathrm{W\,m^{-1}\,K^{-1}}$. Here the difference between native and tumorous tissue becomes apparent. Also in the work of Bowman et al. [13] plenty of different experimental results are found for the measurement of the thermal conductivity. It comprises in vivo and ex vivo measurements for various animals and human organs as well as measurements in fresh and also frozen tissue. Subsequent results from Bowman [12] are also shown in the book of Stein [78] we comply with in the section for the modeling of the RFA. Altogether, the experiments give us an idea and a direction for the modeling but they can not tell us the truth about the material properties.

3.3.3 Modeling of the material parameters

To provide an RFA-model as realistic as possible we need a mathematical description of the material properties which particularly implies the temperature dependency and the different tissue types. There exist several studies concerning the temperature dependencies of conductivities but only few concerning the influence on the whole system. Furthermore some studies also incorporate the dependence on frequency, as e.g. Haemmerich et al. [33] and Laufer et al. [56], or account additionally for the degree of coagulation, as in the work of Stein [78]. In the following we will focus on the temperature dependency. Chang [15] investigates the behavior of the potential ϕ and the power density $\sigma|\nabla\phi|^2$ as well as the behavior of the temperature T subject to the modeling of the electrical conductivity σ. He compares four different settings, constant electrical conductivity without tissue perfusion, temperature-dependent electrical conductivity without tissue perfusion,

constant electrical conductivity with tissue perfusion and temperature-dependent electrical conductivity with tissue perfusion. His model for the electrical conductivity is based on the work of Stogryn [80], which represents the electrical conductivity of saline water as a polynomial of fourth degree in the temperature. Despite the fact that the RFA model in the work of Chang [15] is simplified, the results approve a significant influence of the modeling of the electrical conductivity on the outcome of the simulation. Solazzo et al. [77] use a simple linear model with 2 % increase of the electrical conductivity per degree celsius. They focus mainly on the effect of different tissue types of the electrical conductivity in a two-compartment Agar-model as well as in the numerical simulation. The model for the electrical conductivity in the work of Pop et al. [66] is more complex than in the previous described models. The conductivity is represented by a polynomial with an exponential term and an integral-term. These terms are needed to account for the heating as well as for the cooling. Stein [78] distinguishes also between the various states of heating and the influence on the material properties. Between $20\,°C$ and $43\,°C$ we have no irreversible changes. Whereas temperatures above $50\,°C$ lead to protein denaturation and therefore to irreversible changes in the material properties.

Moreover, the temperature dependency of the thermal conductivity $\lambda(T)$ does not need a modeling as complicated as for the electrical conductivity $\sigma(T)$, it can be modeled as a linear function, as e.g. in [78] or [92]. Watanabe et al. [92] compare three different methods of measuring the thermal conductivity and investigated numerically how the differences in the thermal conductivity affect the temperature distribution T. Due to the kind of the measurements, for two methods Watanabe et al. obtain a linear model for the thermal conductivity and for one method, the unsteady hot wire method, the resulting model for the thermal conductivity consists of a linear term for temperatures about $70\,°C$ and an exponential term for $0 \leq T \leq 70\,°C$.

In the following we will use a linear model (3.9) for the thermal conductivity $\lambda(T)$ and a polynomial of fourth degree (3.10) to describe the electrical conductivity $\sigma(T)$. Later on, we will use a spatially distributed electrical conductivity to avoid the imprecise modeling and at the same time allow for temperature dependency. The description of the thermal conductivity is given by

$$\lambda(T) = \lambda_{\text{ref}}(1 + \alpha_\lambda(T - T_{\text{ref}}), \tag{3.9}$$

with a reference thermal conductivity $\lambda_{\text{ref}} \in \mathbb{R}$, for a reference temperature T_{ref}, and a coefficient $\alpha_\lambda \in \mathbb{R}$, based on the investigations of Stein [78]. Whereas the polynomial, used to model the electrical conductivity

$$\sigma(T) = \sigma_0(1 + \sigma_1 T(1 + \sigma_2 T(1 + \sigma_3 T(1 + \sigma_4 T)))), \tag{3.10}$$

with real valued coefficients $\sigma_0, \dots, \sigma_4 \in \mathbb{R}$ is based on the examinations of Zurbuchen et al. [95]. The coefficients are calculated by fitting a polynomial of fourth degree to measurements of the electrical conductivity from porcine liver, cf. figure 3.5.

Due to different problems in the identification process the temperature dependent electrical conductivity $\sigma(T)$ will be reduced subsequent to a linear model or will be pass on to a spatially distributed parameter. In addition, the approximation of the electrical
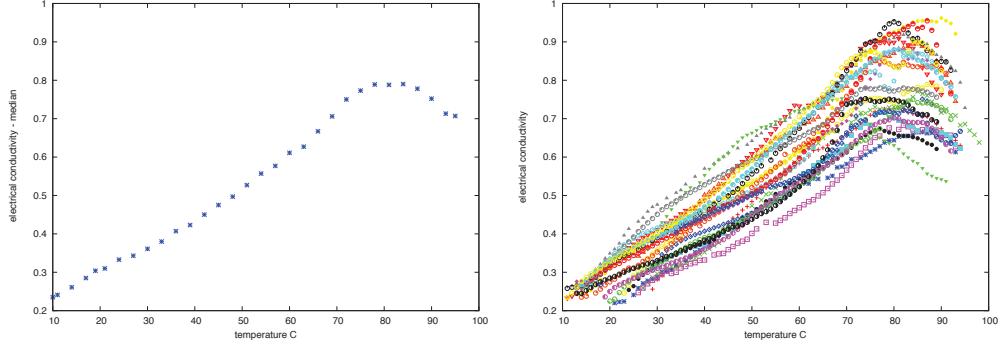
Figure 3.5: The median of the measured electrical conductivity in porcine livers, used for fitting the coefficients in the description of σ, c.f. (3.10) is depicted in the left figure. On the right, all measured values during the heating process are shown. Provided by *Charité - Universitätsmedizin Berlin*.

conductivity $\sigma(T)$ with a polynomial of fourth degree is adjusted to the ex-vivo experiments with porcine liver and will most likely not match for humans.

In the computational domain we have to deal with different tissue types as e.g. native liver tissue and tumorous tissue. As described above especially tumorous and native tissue have different conductivities. Therefore, in fact we should model varying conductivities for the different tissue types. For the modeling of the scaling factor $\frac{P_{\text{eff}}}{P_\Omega}$ we assumed an overall resistance R for the whole domain and therewith also an overall electrical conductivity $\sigma = \frac{1}{R}$. But now we will allow for differences in the conductivities of the different tissue types. To account for these differences in the modeling of the material parameters we assume that the material properties are constant for each tissue but differentiate between the diverse tissue types. We distinguish between tumorous tissue, native tissue and the vascular system such that we have three different tissue types with appropriate coefficients for the modeling of the material parameters.

3.4 Numerical solution with finite element method

In this section a short introduction to the discretization with finite element method (FEM) will be given as well as the application of the FEM to solve the potential equation (3.1) and the heat equation (3.8) numerically. This section is inspired by the first part of the lecture "Therapy planning with numerical mathematics" [52]. Further explanation on FEM is given e.g. by Braess [14] or Johnson [41].

The method of finite elements is based on the variational formulation of the PDEs and the so called weak theory. At first we will introduce functional spaces which are differentiable in a weak sense and state some lemmata which are needed in the following. Afterwards the variational formulation of a PDE will be explained.

Definition 3.1 (Weak derivative) *Let $y \in L^2(\Omega)$ be a function and $\alpha \in \mathbb{N}^n$ a multi-*

index. If there exists a function $y_\alpha \in L^2(\Omega)$ such that

$$\int_\Omega y(x)\partial^\alpha v(x)\, dx = (-1)^{|\alpha|} \int_\Omega y_\alpha(x)v(x)\, dx$$

holds for all $v \in C_0^\infty(\Omega)$, then y_α is called weak derivative of order α. *This function is denoted by $y_\alpha = \partial^\alpha y$.*

With this definition we can now introduce spaces which are differentiable in a weak sense.

Definition 3.2 (Sobolev space) *Let $1 \le p \le \infty$, $k \in \mathbb{N}$. The Sobolev Space $W^{k,p}(\Omega)$ is defined as the space of all functions $y \in L^p(\Omega)$, where the weak derivatives $\partial^\alpha y$ exist for all α with $|\alpha| \le k$ and belong to $L^p(\Omega)$.*
The corresponding norm for $1 \le p < \infty$ is

$$\|y\|_{W^{k,p}(\Omega)} = \left(\sum_{|\alpha| \le k} \int_\Omega |\partial^\alpha y|^p \, dx \right)^{1/p}.$$

The norm for $p = \infty$ is defined as

$$\|y\|_{W^{k,\infty}(\Omega)} = \max_{|\alpha| \le k} \|\partial^\alpha y\|_{L^\infty(\Omega)}.$$

For $p = 2$ we set $H^k(\Omega) := W^{k,2}(\Omega)$ and obtain the Sobolev space

$$H^k(\Omega) = \{y \in L^2(\Omega)|\, \partial^\alpha y \in L^2(\Omega) \text{ for all } |\alpha| \le k\}$$

with weak derivative $\partial^\alpha y$. The associated inner product and norm are as follows

$$(y,v)_{H^k} = \sum_{|\alpha| \le k} \int_\Omega \partial^\alpha y\, \partial^\alpha v\, dx, \qquad \|y\|_{H^k}^2 = \sum_{|\alpha| \le k} \int_\Omega (\partial^\alpha y)^2 \, dx.$$

The Lebesgue spaces $L^p(\Omega)$ are also a special case of Sobolev spaces with $k = 0$, i.e. $W^{0,p}(\Omega) = L^p(\Omega)$.

Lemma 3.1 (Trace lemma) *Let Ω be a bounded domain with Lipschitz boundary Γ. Then there exists a constant $c > 0$ such that*

$$\|v\|_{L^p(\Gamma)} \le c \, \|v\|_{W^{1,p}(\Omega)} \quad \text{for all } v \in C^1(\Omega).$$

This lemma guarantees the existence of linear continuous mapping

$$\gamma : W^{1,p}(\Omega) \to L^p(\Gamma)$$

which is called the *trace mapping* [28], p. 135.

Lemma 3.2 (Friedrichs' inequality) *Let $\Omega \subset \mathbb{R}^n$ be a bounded domain. Then there exists a constant $c > 0$ such that*

$$\|v\|_{L^2(\Omega)} \le c \, |v|_{W^{1,2}(\Omega)} \quad \text{for all } v \in H_0^1(\Omega). \tag{3.11}$$

The inequality (3.11) is known as *Friedrichs' inequality* or *Poincaré-Friedrichs' inequality* [28], p. 136.

The following theorem states that there is a unique solution of the PDE problem in a weak formulation under specified conditions, e.g. [24], p. 83.

Theorem 3.3 (Lax-Milgram) *Let H be a Hilbert space, $l(\cdot)$ be a continuous linear functional on H and $a(\cdot, \cdot)$ a continuous elliptic bilinear form on H. Then, for any $v \in H$, there exists a unique solution $y \in H$ such that $a(y, v) = l(v)$.*

For the variational formulation the PDEs are multiplied with a so called test function v and integrated over the whole domain Ω. We will illustrate this by a simplified PDE with homogeneous boundary values

$$-\nabla \cdot (p(x)\nabla y(x)) = f(x) \qquad \text{in } \Omega, \tag{3.12a}$$
$$y(x) = 0 \qquad \text{on } \Gamma_1, \tag{3.12b}$$
$$\nabla y(x) \cdot n(x) = 0 \qquad \text{on } \Gamma_2, \tag{3.12c}$$

with an open bounded computational domain $\Omega \in \mathbb{R}^n$, a piecewise smooth boundary domain $\Gamma = \Gamma_1 \cup \Gamma_2$, Γ_2 open in Γ, and a given function $f \in L^2(\Omega)$. The outer normal vector is denoted by $n(x)$ and $p(x) \in L^\infty(\Omega)$ represents the parameters.

To apply the existing theory to the present problem we define an appropriate space H

$$H(\Omega) := \{y \in H^1(\Omega) | \, y|_{\Gamma_1} = 0\},$$

The choice of H is reasonable since the existence of $y|_{\Gamma_1}$ can be proved by the Trace Lemma 3.1.

Multiplying (3.12a) with the test function $v(x) \in H(\Omega)$ and integrating over Ω leads to

$$-\int_\Omega \nabla \cdot (p(x)\nabla y(x)) \, v(x) \, dx - \int_\Omega f(x) \, v(x) \, dx = 0.$$

By utilizing partial integration and under the assumption that $y \in H(\Omega)$ solves the problem (3.12) and $v \in H(\Omega)$ satisfies at least the Dirichlet-condition on Γ_1 we obtain

$$\int_\Omega p(x)\nabla y(x) \cdot \nabla v(x) \, dx - \int_\Omega f(x) \, v(x) \, dx = 0. \tag{3.13}$$

By defining the linear form $l(\cdot)$ and the bilinear form $a(\cdot, \cdot)$ on $H(\Omega)$ as follows

$$l(v) = \int_\Omega f v \, dx, \qquad a(y, v) = \int_\Omega p \nabla y \cdot \nabla v \, dx, \tag{3.14}$$

we can rewrite (3.13) as

$$a(y, v) = l(v) \qquad \text{for all } v \in H(\Omega).$$

To apply the theorem of Lax-Milgram, Theorem 3.3, to the above PDE (3.12) we have to verify the preconditions of the theorem. The space $H(\Omega)$ is as closed subspace of $H^1(\Omega)$ a closed spaced, i.e. a Hilbert space. The remaining assumptions of the Lax-Milgram theorem are the continuity of the linear form $l(\cdot)$ and the continuity and ellipticity of the bilinear form $a(\cdot, \cdot)$. For the continuity of l we need at least $f \in L^2(\Omega)$

$$|l(v)| = \left| \int_\Omega v f \, dx \right| \leq \|v\|_{L^2(\Omega)} \|f\|_{L^2(\Omega)} \leq \|v\|_{H^1(\Omega)} \|f\|_{L^2(\Omega)}.$$

To show the continuity of the bilinear form $a(y, v)$ we need at least $p \in L^\infty(\Omega)$

$$
\begin{aligned}
|a(y, v)| &= \left| \int_\Omega p \nabla y \cdot \nabla v \, dx \right| \leq \|p\|_{L^\infty(\Omega)} \int_\Omega |\nabla y| |\nabla v| dx \\
&\leq \|p\|_{L^\infty(\Omega)} \|\nabla y\|_{L^2(\Omega)} \|\nabla v\|_{L^2(\Omega)} \\
&\leq \|p\|_{L^\infty(\Omega)} \|y\|_{H^1(\Omega)} \|v\|_{H^1(\Omega)}.
\end{aligned}
$$

If we can assure a positive parameter $p \geq p_0 > 0$ we have

$$a(v, v) = \int_\Omega p \, (\nabla v)^2 \, dx \geq p_0 \int_\Omega (\nabla v)^2 \, dx = p_0 |v|^2_{H^1(\Omega)},$$

with the semi-norm in $H^1(\Omega)$. With the so called Friedrichs' inequality, Lemma 3.2,

$$\|v\|_{L^2(\Omega)} \leq c |v|_{H^1(\Omega)}, \qquad \text{where } c \text{ depends only on } \Omega,$$

we obtain also the ellipticity if the part of the boundary with Dirichlet conditions has positive $(n-1)$ - dimensional Lebesgue-measure. In the case of the RFA this part of the boundary describes the surface of the electrodes which fulfills the conditions. Therefore we have

$$
\begin{aligned}
a(v, v) &\geq p_0 |v|^2_{H^1(\Omega)} \\
&= p_0 \frac{1}{2} |v|^2_{H^1(\Omega)} + p_0 \frac{1}{2} |v|^2_{H^1(\Omega)} \\
&\geq p_0 \frac{1}{2} |v|^2_{H^1(\Omega)} + \frac{p_0}{c^2} \frac{1}{2} \|v\|^2_{L^2(\Omega)} \\
&\geq \min\{p_0 \frac{1}{2}, \frac{p_0}{c^2} \frac{1}{2}\} \left(|v|^2_{H^1(\Omega)} + \|v\|^2_{L^2(\Omega)} \right) \\
&\geq \alpha \|v\|^2_{H^1(\Omega)}, \qquad \text{with } \alpha > 0.
\end{aligned}
$$

Altogether, the assumptions of the theorem are fulfilled and there is a unique $y \in H(\Omega)$ such that $a(y, v) = l(v)$ for all $v \in H(\Omega)$. This y is called *weak solution* of the boundary

value problem (3.12). If we have additionally $y \in C(\overline{\Omega}) \cap C^2(\Omega)$, $p \in C(\overline{\Omega}) \cap C^1(\Omega)$ and $f \in C(\overline{\Omega})$, y is also a strong solution.

In the model of the RFA we are also interested in modeling a discontinuous parameter $p(x)$. In the following we assume that the parameter p has jumps along a smooth interface M and that this interface divides the domain Ω into two open domains Ω_1 and Ω_2, i.e. $\Omega = \Omega_1 \cup \Omega_2$. Additionally we assume that the functions $p_1 := p|_{\Omega_1}$ and $p_2 := p|_{\Omega_2}$ and the corresponding solutions $y_1 := y|_{\Omega_1}$ and $y_2 := y|_{\Omega_2}$ can be continuously continued on the interface M. Let y be a weak solution of (3.12) which is globally continuous and C^2 in both domains Ω_1 and Ω_2. Let the solution also be C^1 continuable on M from both sides. The solution y is a strong solution at the interior of Ω_1 and Ω_2. Let $v \in C_0^\infty(\Omega)$ be a test function, then

$$
\begin{aligned}
0 &= \int_\Omega p\nabla y \cdot \nabla v \, dx - \int_\Omega fv \, dx \\
&= \int_{\Omega_1} (p_1 \nabla y_1 \cdot \nabla v - fv) \, dx + \int_{\Omega_2} (p_2 \nabla y_2 \cdot \nabla v - fv) \, dx \\
&= \int_{\Omega_1} (-\mathrm{div}(p_1 \nabla y_1)v - fv) \, dx + \int_{\partial\Omega_1} p_1 \nabla y_1 \cdot n_{\Omega_1} v \, ds \\
&\quad + \int_{\Omega_2} (-\mathrm{div}(p_2 \nabla y_2)v - fv) \, dx + \int_{\partial\Omega_2} p_2 \nabla y_2 \cdot n_{\Omega_2} v \, ds,
\end{aligned}
$$

with the outer normal vectors n_{Ω_1} and n_{Ω_2} for the domains Ω_1 and Ω_2 respectively. Since y_1 and y_2 are strong solutions in Ω_1 and Ω_2 respectively, the corresponding integrals are omitted. Hence the boundary integrals reduce to the integral over the manifold M since v disappears at the remaining boundary. The whole expression reduces with the outer normal $n_M = n_{\Omega_1} = -n_{\Omega_2}$ on M to

$$
0 = \int_M (p_1 \nabla y_1 - p_2 \nabla y_2) \cdot n_M v \, ds.
$$

With the arbitrary v we have the pointwise jump condition

$$
(p_1 \nabla y_1 - p_2 \nabla y_2) \cdot n_M = 0
$$

at the interface M. This gives us the same expression as we would obtain in the strong case with a discontinuous parameter. In both cases the jump condition constitutes an additional constraint to the system. Nevertheless, this illustrates that the weak formulation with the additional assumption of global continuity and C^2 in the two domains Ω_1 and Ω_2 is a better representation of the model than the strong one. The original formulation (3.12) is valid only for continuous parameter functions since otherwise $p(x)\nabla y(x)$ would not be differentiable. Whereas in the weak formulation (3.13) certain discontinuities of the parameters are permitted.

In a more general case we look at the PDE system with inhomogenous Dirichlet bound-

ary conditions on Γ_1, i.e. $y(x) = g(x)$ instead of the homogenous condition (3.12b). To solve this modified problem we determine any function $y_0 \in H^1(\Omega)$ which fulfills the new boundary conditions but not necessarily solves the PDE (3.12a). Further we look at the resulting boundary problem for the difference $\tilde{y} = y - y_0$:

$$
\begin{aligned}
-\nabla \cdot (p(x)\nabla\tilde{y}(x)) &= f(x) + \nabla \cdot (p(x)\nabla y_0(x)) & &\text{in } \Omega, \\
\tilde{y}(x) &= 0 & &\text{on } \Gamma_1, \\
\nabla\tilde{y}(x) \cdot n(x) &= 0 & &\text{on } \Gamma_2, \qquad (3.15)
\end{aligned}
$$

with the outer normal $n(x)$.

Altogether we obtain a problem in the form of (3.12), which can be solved as described before. Afterwards we calculate $y = \tilde{y} + y_0$ and obtain the solution of the original problem with inhomogenous boundary conditions. The same method can be applied to the potential equation (3.1).

For the solution of the instationary heat equation (3.8) we need additional strategies to handle the time dependency. A common practice to solve instationary PDE is to solve piecewise in time. We will discuss this on the basis of the following parabolic problem, a generalized form of the heat equation (3.8)

$$
\mu(x)\partial_t y(t,x) - \nabla \cdot (p(x)\nabla y(t,x)) = f(t,x) \text{ in } \mathbb{R}^+ \times \Omega, \qquad (3.16)
$$

with appropriate boundary conditions.

At first we choose a time step size $\tau > 0$ and calculate an approximation $y^n(x)$, $n \in \mathbb{N}$, for the solution $y(n\tau, x)$. To calculate the time derivative we use for example an implicit Euler method such that the derivative becomes

$$
\partial_t y(n\tau, x) \approx \frac{y^n(x) - y^{n-1}(x)}{\tau}, \quad n \in \mathbb{N}.
$$

Thus, if the solution $y^{n-1}(x)$ is known, the equation (3.16) can be approximated as follows

$$
\frac{1}{\tau}\mu(x)\left(y^n(x) - y^{n-1}(x)\right) - \nabla \cdot (p(x)\nabla y^n(x)) = f(n\tau, x), \quad n \in \mathbb{N}. \qquad (3.17)
$$

As weak formulation of (3.17) we obtain for a test function $v \in H^1(\Omega)$

$$
\int_\Omega p\nabla y^n \cdot \nabla v \, dx + \int_\Omega \frac{\mu}{\tau} y^n v \, dx = \int_\Omega \left(\frac{\mu}{\tau} y^{n-1} + f\right) v \, dx, \quad n \in \mathbb{N}.
$$

This can be brought into the abstract form $a(y,v) = l(v)$ by using the following bilinear form $a(\cdot, \cdot)$ and linear form $l(\cdot)$ and the approximated solution $y = y^n$ in the n-th time step

$$
a(y,v) = \int_\Omega p\nabla y \cdot \nabla v \, dx + \int_\Omega \frac{\mu}{\tau} yv \, dx, \quad l(v) = \int_\Omega \left(\frac{\mu}{\tau}(y^{n-1} + f\right) v \, dx, \quad n \in \mathbb{N}.
$$

As in the elliptic case, the theorem of Lax-Milgram can be applied and the system can be solved with FEM as described in the next section. Moreover, we can translate the system to a system with inhomogenous boundary conditions in the same manner as described for the elliptic problem.

3.4.1 Spatial discretization with finite elements

This section will provide a short insight in the method of finite elements. The FEM is a special case of the so called Ritz-Galerkin method. The basic idea is the approximation of the solution $y \in H$ by a function $y_h \in V_h$ in an appropriate finite dimensional subspace $V_h \subset H$. This means we have to determine a function $y_h \in V_h$ such that

$$a(y_h, v_h) = l(v_h) \qquad \text{for all } v_h \in V_h. \tag{3.18}$$

The existence and uniqueness of such a function y_h is given by the theorem of Lax-Milgram, since all assumptions are translated to the subspace V_h. The performance of the approximation of y by y_h is shown by the lemma of Céa

Lemma 3.4 (Céa) *For $y \in H$ and $y_h \in V_h$ we have*

$$\|y - y_h\|_H \leq \frac{C}{\alpha} \inf_{v_h \in V_h} \|y - v_h\|_H,$$

where C and α denote the constants from the continuity and the ellipticity of the bilinear form a.

This means that the approximated solution y_h reaches the best possible solution in the subspace V_h as close as possible. It is worse only by a factor of $\frac{C}{\alpha}$.
A generalization of Céa's lemma is given by the lemma of Strang. It is needed in those cases where the finite element space is not a subspace of the corresponding Sobolev space of an elliptic problem. Beside the approximation error the consistency error occurs. The consistency verifies if the given problem is solved effectively. The following first lemma of Strang is described e.g. in [14] (lemma 1.1, p. 100) or [28] (lemma 4.52, p. 244).

Lemma 3.5 (Strang) *Let $V_h \subset H$ be a finite dimensional subspace and $a_h(\cdot, \cdot)$ a uniform elliptic bilinear form, i.e.*

$$a_h(v_h, v_h) \geq \alpha \|v_h\|_H^2, \quad \alpha > 0, \, v_h \in V_h,$$

where α does not depend on h. Further $l_h(\cdot)$ denotes a linear form on V_h. Then there exists a constant $c > 0$ such that

$$\|y - y_h\| \leq c \left(\inf_{v_h \in V_h} \{\|y - y_h\| + \sup_{w_h \in V_h} \frac{|a(v_h, w_h) - a_h(v_h, w_h)|}{\|w_h\|} + \sup_{w_h \in V_h} \frac{l(w_h) - l_h(w_h)}{\|w_h\|} \right).$$

The constant c is independent of h.

That means that the approximation y_h matches the best possible solution in V_h as good as possible under the additional consideration of the error in the linear form and the bilinear form. The first term is called approximation error, whereas the last two terms constitute the consistency error.

To solve the discrete problem (3.18) we use a basis $(\varphi_1, \ldots, \varphi_N)$ of the $N-$dimensional subspace $V_h \subset H$. We replace the test function with the elements of the basis. Further we describe y_h as linear combination of the basis functions

$$y_h = \sum_{i=1}^{N} y_i \varphi_i. \tag{3.19}$$

Altogether the equation (3.18) becomes

$$a \left(\sum_{i=0}^{N} y_i \varphi_i, \varphi_j \right) = \sum_{i=0}^{N} y_i a(\varphi_i, \varphi_j) = l(\varphi_j) \qquad \text{for all } j \in \{1, \ldots, N\}.$$

Therewith the discrete problem is equivalent to a system of linear equations

$$L\vec{y} = \vec{b},$$

with

$$L = \begin{pmatrix} a(\varphi_1, \varphi_1) & \ldots & a(\varphi_1, \varphi_N) \\ \vdots & & \vdots \\ a(\varphi_N, \varphi_1) & \ldots & a(\varphi_N, \varphi_N) \end{pmatrix}, \quad \vec{y} := \begin{pmatrix} y_1 \\ \vdots \\ y_N \end{pmatrix} \text{ and } \vec{b} := \begin{pmatrix} l(\varphi_1) \\ \vdots \\ l(\varphi_N) \end{pmatrix}.$$

The matrix L is positive definite and symmetric, since the used bilinear form $a(y, v)$ is symmetric and elliptic. The actual structure of the matrix depends on the choice of the basis functions. Therefore it makes sense to choose a basis such that the matrix structure is sparse. In the following $\vec{y}$ will always denote the coefficient vector of the linear combination for y_h.

To solve the PDE in the model we cover the domain Ω with a three dimensional uniform cartesian grid G. That means the domain is divided into a finite number of subdomains $S_k \subset \Omega$, $k = 1, \ldots, N$, the finite elements, with

$$G = \bigcup_{k=1}^{N} S_k.$$

Further, V_h is defined as the subspace of all globally continuous functions v_h which are piecewise trilinear on the elements S_k, $k = 1, \ldots, N$. The functions $v_h \in V_h$ are uniquely determined by the values at the supporting points. If all supporting points, where v_h is not equal to zero according to the Dirichlet boundary conditions, are numbered serially

by $x_1, \cdots, x_n$, $n \in \mathbb{N}$, a basis of V_h is given by

$$\varphi_i(x_j) = \delta_{ij} = \begin{cases} 1, & i = j, \; i,j = 1, \ldots, n, \\ 0, & i \neq j, \; i,j = 1, \ldots, n. \end{cases}$$

These functions have a small support and therefore the matrix L has a sparse structure. To calculate the entries of L, e.g. for the generalized form (3.12), we assume that the parameter $p(x)$ is constant for each element S_k, $k = 1, \ldots, N$, of the grid G. That means we define $p(x) \equiv p_{S_k}$ for $x \in S_k$, $k = 1, \ldots, N$. Under this assumption we obtain

$$L_{ij}^p = a(\varphi_i, \varphi_j) = \int_\Omega p \nabla \varphi_i \cdot \nabla \varphi_j \, dx \approx \sum_{S_k} p_{S_k} \int_{S_k} \nabla \varphi_i \cdot \nabla \varphi_j \, dx, \quad i,j, = 1, \ldots, n,$$

for all elements S_k, $k = 1, \ldots, N$. Hence it will suffice to calculate the local integrals $\int_{S_k} \nabla \varphi_i \cdot \nabla \varphi_j$ for all functions φ_i, φ_j, $i,j = 1, \ldots, n$. The results will give us the so called *stiffness matrix*. Analogously we can calculate the *mass matrix* from the linear form, i.e. the local integrals $\int_{S_k} \varphi_i \cdot \varphi_j \, dx \, i,j = 1, \ldots, n$, $k = 1, \ldots, N$. Hence the PDEs reduce to systems of linear equations with stiffness matrix and mass matrix. For example, the PDE (3.12a) reduces to

$$L^p \vec{y} = M \vec{f},$$

where L^p denotes the stiffness matrix with weighting parameter p and M denotes the mass matrix without any special weighting function.

Applying the method of finite elements to the modeling of RFA we first solve the potential equation (3.1) and afterwards the bio-heat equation (3.8), since the potential is needed to calculate the right hand side Q_{rf} of the bio-heat equation. For the FEM the mass matrix M and the stiffness matrices L^σ and L^λ are used, where L^σ denotes the stiffness matrix weighted with the electrical conductivity σ and L^λ denotes the stiffness matrix weighted with the thermal conductivity λ. In the heat equation the mass matrix is also weighted with the weighting factor for the blood perfusion ν (cf. (3.7)) and the product ρc of the density ρ and the heat capacity c, divided by the time step size τ. The matrices can be calculated by integration rules as e.g. quadrature formulas.

The inhomogeneous Dirichlet conditions are incorporated as described in (3.15). That means for the potential ϕ we solve for $\tilde{\phi} := \phi - g$ instead, where g fulfills the Dirichlet conditions at the electrodes. For the temperature we solve for $\tilde{T} := T - b$ instead, where b satisfies the condition $b = T_{\mathrm{body}}$ at the probe Ω_{pr}. Afterwards the proper functions are obtained by subtracting the boundary conditions again. The Neumann conditions at the outer boundary are included in the stiffness and mass matrix.

The whole process with FEM discretization is summarized in the following algorithm
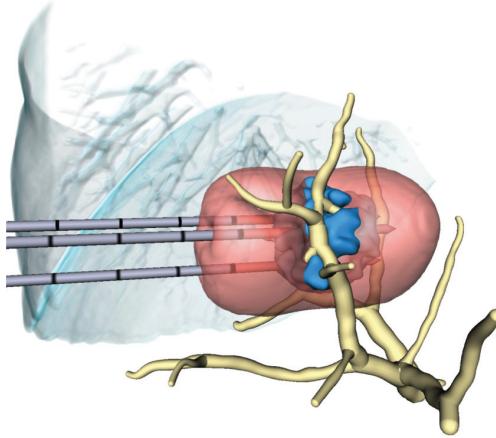
Figure 3.6: Simulation result for a cluster of three coupled probes (from the left) and a tumor (blue) in the vicinity of the vascular system (yellow). The simulated $60\,°C$ temperature iso-surface is depicted in red. Due to the cooling effect of the vessels the tumor is not completely destroyed. The picture is published in the paper of Preusser and Peitgen [67].

Algorithm 1

1. Solve the potential equation (3.1) with homogeneous Dirichlet conditions on the outer boundary by discretization with FEM and $\tilde{\phi} := \vec{\phi} - \vec{g}$

$$L^{\sigma}\tilde{\phi} = L^{\sigma}\vec{g}. \tag{3.20}$$

2. Calculate the heat source Q_{rf} for the right hand side of the heat equation (3.8) in a discrete form

$$\vec{Q}_{\mathrm{rf}} = \frac{P_{\mathrm{eff}}}{P_{\Omega}}\vec{\sigma}|\vec{\nabla\phi}|^2.$$

3. Solve the bio-heat transport equation (3.8) with implicit Euler method for the time derivative (cf. (3.17)) and FEM for discretization in space. Due to the inhomogeneous boundary conditions for a cooled probe it is solved for $\tilde{T} = \vec{T} - \vec{b}$

$$L^{\lambda}\tilde{T} + M^{\frac{\rho c}{\tau}+\nu}\tilde{T} = M\vec{Q}_{\mathrm{rf}} - M^{\nu}\vec{T}_{\mathrm{body}} + L^{\lambda}\vec{b} + M^{\frac{\rho c}{\tau}}\vec{T}^{n-1}. \tag{3.21}$$

Since the stiffness matrix and the mass matrix are symmetric and positive definite by construction we can apply a conjugate gradient method to solve (3.20) and (3.21). The electric field $\nabla\phi$ in step 2 is calculated with central differences.

The simulation result for a cluster of three coupled probes is shown in figure 3.6.

3.4.2 Non-matching Banach-spaces

To model the RFA we need the coupled system of PDEs (3.1) and (3.8). Even though the computational domain $\Omega \setminus \overline{\Gamma}$ of the present problem is not convex because of the electrodes we know from standard finite element methods that the potential equation (3.1) has a unique solution $\phi \in H^1(\Omega \setminus \overline{\Gamma})$, e.g. Großmann and Roos [28] or Braess [14]. To calculate the temperature distribution we need the expression $|\nabla \phi|^2$ in the source term Q_{rf} on the right hand side of the bio-heat transport equation (3.8). However, the problem is that for $\phi \in H^1(\Omega \setminus \overline{\Gamma})$ we know $|\nabla \phi|^2 \in L^1(\Omega \setminus \overline{\Gamma})$ but a right hand side in $L^1(\Omega \setminus \overline{\Gamma})$ does not assure a unique solution. Under some assumptions it can be shown that ϕ is also in $H^2(\Omega \setminus \overline{\Gamma})$ and hence $|\nabla \phi|^2 \in L^2(\Omega \setminus \overline{\Gamma})$, see [24]. However, in the present case the solution fails to be in $H^2(\Omega \setminus \overline{\Gamma})$ since this result requires a boundary in $C^2(\Omega \setminus \overline{\Gamma})$. But due to the electrodes the boundary is not as smooth as required. Therefore, we have to look more precisely at the regularity of the solution ϕ to assure a unique solution of the heat equation. The following results are based on [50] and a similar proof can be found in the paper of Antontsev et al. [6].

The following lemma is needed for the proof additionally to the lemmata and theorems stated above.

Lemma 3.6 *Let $u \in W^1(\Omega)$. Then u^+, u^-, $|u| \in W^1(\Omega)$, with*

$$u^+ := \max\{u, 0\}, \ u^- := \min\{u, 0\} \ and \ |u| := u^+ - u^-.$$

This lemma is stated and proved in Gilbarg and Trudinger [24], p. 152.

To assure a unique solution for an elliptic PDE the right hand side needs only to be in $H^{-1}(\Omega \setminus \overline{\Gamma})$, the dual space of $H_0^1(\Omega \setminus \overline{\Gamma})$. That means it is sufficient to show $|\nabla \phi|^2 \in H^{-1}(\Omega \setminus \overline{\Gamma})$. Let us consider (3.1) in a weak form and with generalized boundary conditions $h \in L^\infty(\partial \Omega), h \geq 0$,

$$\int_{\Omega \setminus \overline{\Gamma}} \sigma \nabla \phi \nabla v \, dx = - \int_{\partial \Omega} \sigma h v \, ds \tag{3.22}$$

for every $v \in H(\Omega \setminus \overline{\Gamma}) := \left\{ v \in H^1(\Omega \setminus \overline{\Gamma}) | \, v|_{\partial \Gamma} = 0 \right\}$.
We can split ϕ as follows $\phi = \tilde{\phi} + \phi_0$ with $\tilde{\phi} \in H(\Omega \setminus \overline{\Gamma})$, $\phi_0 \in C^\infty\left(\overline{\Omega} \setminus \Gamma\right)$ and $\nabla \phi_0$ has compact support in $\Omega \setminus \Gamma$. This splitting is not unique but for the following results a unique splitting is not necessary. For the following we assume $\sigma \in L^\infty(\Omega \setminus \Gamma)$ with $\sigma \geq \sigma_0 > 0$. The electrical power density $q := \sigma |\nabla \phi|^2$ can be written as

$$q = \sigma \left(\nabla \phi_0 \cdot \nabla \phi_0 + 2 \nabla \phi_0 \cdot \nabla \tilde{\phi} + \nabla \tilde{\phi} \cdot \nabla \tilde{\phi} \right).$$

The aim is to show that the right hand side is in $H^{-1}(\Omega \setminus \overline{\Gamma})$, i.e. we want to show $q \in H^{-1}(\Omega \setminus \overline{\Gamma})$. The first two terms are in $L^2(\Omega \setminus \overline{\Gamma})$, thus we can restrict our investigations to the last term $\nabla \tilde{\phi} \cdot \nabla \tilde{\phi}$. Since $C^\infty\left(\overline{\Omega \setminus \Gamma}\right)$ is dense in $H^1(\Omega \setminus \overline{\Gamma})$ we can approximate

functions in $H^1(\Omega \setminus \overline{\Gamma})$ with functions in $C^\infty(\Omega \setminus \overline{\Gamma})$. The dual space $H^{-1}(\Omega \setminus \overline{\Gamma})$ includes all linear and continuous functionals on $H^1(\Omega \setminus \overline{\Gamma})$, hence it is sufficient to show

$$\left| \int_{\Omega \setminus \overline{\Gamma}} \sigma |\nabla \tilde{\phi}|^2 w \, dx \right| \le C \|w\|_{H^1(\Omega \setminus \overline{\Gamma})}, \quad w \in C^\infty\left(\overline{\Omega \setminus \Gamma}\right). \tag{3.23}$$

The integral above is defined since w is bounded and $|\nabla \tilde{\phi}|^2 \in L^1(\Omega \setminus \overline{\Gamma})$. Therefore, we can start to estimate the integral

$$\left| \int_{\Omega \setminus \overline{\Gamma}} \sigma |\nabla \tilde{\phi}|^2 w \, dx \right| = \left| \int_{\Omega \setminus (\overline{\Gamma})} \sigma \nabla \tilde{\phi} \cdot \left(\nabla \tilde{\phi} w \right) \, dx \right|$$

$$= \left| \int_{\Omega \setminus \overline{\Gamma}} \sigma \nabla \tilde{\phi} \cdot \left(\nabla(\tilde{\phi} w) - \tilde{\phi} \nabla w \right) \, dx \right|$$

$$\le \left| \int_{\Omega \setminus \overline{\Gamma}} \sigma \nabla \tilde{\phi} \cdot \nabla(\tilde{\phi} w) \, dx \right| + \left| \int_{\Omega \setminus \overline{\Gamma}} \tilde{\phi} \sigma \nabla \tilde{\phi} \cdot \nabla w \, dx \right|. \tag{3.24}$$

For further estimation we look at the first summand to begin with. Since we know $\tilde{\phi} w \in H(\Omega \setminus \overline{\Gamma})$, the weak formulation of the potential equation (3.22) with test function $v = \tilde{\phi} w$ leads to

$$\left| \int_{\Omega \setminus \overline{\Gamma}} \sigma \nabla \tilde{\phi} \cdot \nabla(\tilde{\phi} w) \, dx \right| \le \left| \int_{\Omega \setminus \overline{\Gamma}} \sigma \nabla \phi_0 \cdot \nabla\left(\tilde{\phi} w\right) \, dx \right| + \left| \int_{\partial \Omega} \sigma h \tilde{\phi} w \, ds \right|$$

$$\le \|\sigma\|_{L^\infty(\Omega \setminus \overline{\Gamma})} \|\phi_0\|_{C^1(\Omega \setminus \overline{\Gamma})} \int_{\Omega \setminus \overline{\Gamma}} |\tilde{\phi} \nabla w + w \nabla \tilde{\phi}| \, dx$$

$$+ \|\sigma\|_{L^\infty(\Omega \setminus \overline{\Gamma})} \|h\|_{L^\infty(\Omega \setminus \overline{\Gamma})} \int_{\partial \Omega} |\tilde{\phi} w| \, ds$$

$$\le 2\|\sigma\|_{L^\infty(\Omega \setminus \overline{\Gamma})} \|\phi_0\|_{C^1(\Omega \setminus \overline{\Gamma})} \|\tilde{\phi}\|_{H^1(\Omega \setminus \overline{\Gamma})} \|w\|_{H^1(\Omega \setminus \overline{\Gamma})}$$

$$+ \|\sigma\|_{L^\infty(\Omega \setminus \overline{\Gamma})} \|h\|_{L^\infty(\Omega \setminus \overline{\Gamma})} \|\tilde{\phi}\|_{H^1(\Omega \setminus \overline{\Gamma})} \|w\|_{H^1(\Omega \setminus \overline{\Gamma})},$$

where the Trace Lemma 3.1 has been used to estimate the boundary integral. If we are able to show that $\tilde{\phi} \in L^\infty(\Omega \setminus \overline{\Gamma})$, the second summand of the integral inequality (3.24) can be estimated as follows

$$\left| \int_{\Omega \setminus \overline{\Gamma}} \tilde{\phi} \sigma \nabla \tilde{\phi} \cdot \nabla w \, dx \right| \le \|\tilde{\phi}\|_{L^\infty(\Omega \setminus \overline{\Gamma})} \|\sigma\|_{L^\infty(\Omega \setminus \overline{\Gamma})} \|\tilde{\phi}\|_{H^1(\Omega \setminus \overline{\Gamma})} \|w\|_{H^1(\Omega \setminus \overline{\Gamma})}.$$

Therefore, let

$$v = \max\{\phi - 1, 0\} \ge 0. \tag{3.25}$$

If we show that $v = 0$ almost everywhere this will imply $\phi \leq 1$ almost everywhere. If analogously $\phi \geq -1$ is shown we obtain finally $\phi \in L^\infty(\Omega \setminus \overline{\Gamma})$ and since $\phi = \tilde{\phi} + \phi_0$ also $\tilde{\phi} \in L^\infty(\Omega \setminus \overline{\Gamma})$.

From Lemma 3.6 we know $v \in H^1(\Omega \setminus \overline{\Gamma})$ for v defined as in (3.25) and $v = 0$ on $\partial \Gamma$ since there we have $\phi - 1 = 0$ or $\phi - 1 = -2$ due to the chosen values of $+1$ and -1 at the electrodes. Therefore, it follows that $v \in H(\Omega \setminus \overline{\Gamma})$ and we may apply the weak form of the potential equation to v. Hence, from the definition of v we know $\nabla v = 0$ for those regions where $v = 0$ and $\nabla v = \nabla \phi$ everywhere else. Therewith, we get from the weak form (3.22) the following inequality

$$\int_{\Omega \setminus \overline{\Gamma}} \sigma \nabla v \cdot \nabla v \, dx \leq 0.$$

With $\sigma \geq \sigma_0 > 0$ we obtain $|v|_{H^1(\Omega \setminus \overline{\Gamma})} = 0$ and it follows $\|v\|_{L^2(\Omega \setminus \overline{\Gamma})} = 0$ with the Friedrichs' inequality (3.11). This last result implies that $v = 0$ almost everywhere and hence $\phi \in L^\infty(\Omega \setminus \overline{\Gamma})$ and therewith also $\tilde{\phi} \in L^\infty(\Omega \setminus \overline{\Gamma})$.

Altogether by proving the estimate (3.23) we showed that $q \in H^{-1}(\Omega \setminus \overline{\Gamma})$ and this implies that the source term Q_{rf} of the heat equation is in $H^{-1}(\Omega \setminus \overline{\Gamma})$ and we will get a unique solution of the heat equation.

4 Mathematical theory for parameter identification problems

The identification of the material parameters from given temperature measurements is the aim of the present thesis. The problem will be defined as an optimal control problem where we want to fit the calculated temperature to measured data. In the present chapter the basic theory of optimization and optimal control problems is introduced as well as some basic algorithms to solve them. At the end of this chapter we will have also a brief look on the method of Tikhonov regularization.

Optimization, optimal control and closed-loop control have become an important part of our life. You will find it in many areas, from natural sciences over economics and finance to biology. Especially open-loop control and closed-loop control play an important role, for example for cars and radiators. But we may find also closed-loop control as biological functions in the human body, for example the control of the pupil's size in the human eyes or the cardiovascular system. One of the first known man-made closed-loop control takes part of the water clock of Ktesibios, who lived in the 3rd century BC.
But what does optimization or optimal control actually mean?
Optimization at all means to choose the best element of an available set of elements. Though the meaning of *best* depends on the underlying problem, it can be the minimum or the maximum or a balance between different things or conditions. In economy we are often interested in minimizing the cost and maximizing the production, whereas both are linked.
A control is a pre-defined input which influences a system and accordingly the output. If the control further optimizes the system somehow it is called optimal control. Further, control is dived into two parts, open-loop control and closed-loop control. Open-loop control intends to optimize a process or a system by using initial information. That means a priori unknown perturbations are not reduced during the optimization. Whereas closed-loop control uses additionally observations or measurements during the process to optimize the system. That means the actual values are continuously compared with the desired state and a priori unknown perturbations can be incorporated and reduced during the optimization.
In mathematics we differentiate further between optimization problems and optimal control problems. In optimization the control which minimizes (or maximizes) the objective function is a finite-dimensional vector. Whereas in optimal control problems the control is defined as a function. That means the control can additionally depend on the time or the space. Dynamical optimization problems are often associated with optimal control problems.

In practice, both optimization problems and optimal control problems are often constrained by ordinary differential equations or partial differential equations. The problems may arise in different contexts and in various formulations. For example identification problems represent one special part of optimization problems. Actually, identification problems belong to the field of inverse problems, which describe a problem where we are looking for adequate parameters which lead to a known outcome. In real applications such identification problems are formulated as optimization problems where we want to find a set of parameters such that the resulting outcome matches a desired state as good as possible. If the parameter is defined as a function we obtain an optimal control problem. Both descriptions lead to a minimization problem with appropriate constraints.

In the present work we will consider a parameter identification problem in the context of RFA, where the parameters are defined as spatially distributed or as temperature dependent functions. Accordingly, the problem is described as an optimal control problem. The intention is to find the material parameters which lead to a certain temperature distribution during the RFA. The basic idea is to improve the simulation of the RFA by calculating online the material parameters from given temperature measurements during the RFA.

4.1 Necessary and sufficient conditions

The so-called Lagrange-technique which is used to derive the optimality systems for the parameter identification problems in the present thesis is based on the mathematical theory for optimization problems we will outline in the following.

To solve an optimization problem for a local minimum we use the necessary conditions to derive the algorithms for the optimization problems. The sufficient conditions are used to decide if a solution which satisfies the necessary conditions, is a local minimum of the problem. The theory of optimization problems in general spaces can be found for example in [40]. The following definitions are described by Tröltzsch in [88], chapter 6. The theorems and associated proofs as well as further theorems, definitions and remarks can be found also in the paper of Maurer and Zowe [60]. In [88] as well as in the works of Kurcyusz [55] and Maurer and Zowe [60] the problem is described in a more general case. However we will restrict the investigations in the following to equality constraints, cf. (OP), and derive the necessary and sufficient conditions by the Lagrange multiplier theory.

Let V and Z be real Banach spaces, $C \subset V$ a non empty convex subset and $f : V \to \mathbb{R}$ and $h : V \to Z$ two-times Fréchet-differentiable. The optimization problem (OP) is stated as follows

$$\begin{aligned} \min f(v) & \\ \text{subject to } h(v) = 0 & \qquad\qquad \text{(OP)} \\ v \in C, & \end{aligned}$$

The set $C \subset V$ is called *feasible set* of (OP).

The Lagrangian to the problem (OP) is defined by the following function $\mathcal{L} : V \times Z^* \to \mathbb{R}$, with

$$\mathcal{L}(v, z^*) := f(v) + \langle z^*, h(v) \rangle_{Z^*, Z},$$

where Z^* denotes the dual space of Z and $\langle \cdot, \cdot \rangle_{Z^*, Z}$ denotes the dual pairing with respect to Z.

Definition 4.1 *An element $\bar{v}$ is called* local solution *of* (OP) *if for $\varepsilon > 0$*

$$f(\bar{v}) \leq f(v)$$

for all $v \in C$ with $h(v) = 0$ and $\|v - \bar{v}\|_V \leq \varepsilon$.

Definition 4.2 *If $\bar{v}$ is a local solution of* (OP) *and the following condition*

$$D_v \mathcal{L}(\bar{v}, z^*)(v - \bar{v}) \quad \geq \quad 0 \quad \forall v \in C \tag{4.1}$$

holds for $z^* \in K^+ := \{z^* \in Z^* | \langle z^*, z \rangle_{Z^*, Z} \geq 0 \quad \forall z \in K\}$ where $K \subset Z$ is a convex cone and D_v denotes the partial Fréchet derivative with respect to v. Then z^* is called corresponding Lagrange multiplier for $\bar{v}$.

If the problem is not reduced to a problem with equality constraints we need additionally the so-called complementary slack condition $\langle z^*, h(\bar{v}) \rangle_{Z^*, Z} = 0$.

To show the existence of a Lagrange multiplier we need so-called *constraint qualifications*. For convex problems, i.e. problems with convex functions f and h, we may use the *Slater condition*

> There exists an element $\tilde{v} \in C$ with $h(\tilde{v}) <_K 0$, i.e. $-h(\tilde{v}) \in int\, K$.

For problems with equality constraints this does not work and we will need other conditions. For non-convex functions there exist various possible conditions as e.g. the conditions by Mangasarian-Fromowitz or the Linear Independent Constraint Qualification (LICQ). Another condition is developed by Zowe and Kurcyusz [94], based on stability results of Robinson. The following definition can be found in a more general case in [88], page 249.

Definition 4.3 *Let $\bar{v} \in C$ with $h(\bar{v}) = 0$. The canonical hull of C in $\bar{v}$ is defined as*

$$C(\bar{v}) = \{\lambda(v - \bar{v}) | \lambda \geq 0, v \in C\}.$$

The condition

$$h'(\bar{v})C(\bar{v}) = Z \tag{4.2}$$

is called constraint qualification of Kurcyusz and Zowe, where $h'(v)$ denotes the Gâteaux derivative with respect to v.

The following theorem ensures the existence of a Lagrange multiplier, cf. Tröltzsch [88]

Theorem 4.1 *Let $\bar{v}$ be a local solution of* (OP) *and f and h are continuous Fréchet differentiable in a neighborhood of $\bar{v}$. If the constraint qualification* (4.2) *is satisfied then there exists a Lagrange multiplier $z^* \in Z^*$ corresponding to $\bar{v}$. The set of Lagrange multipliers for $\bar{v}$ is bounded.*

From this theorem and the definition of the Lagrange multipliers it follows that if the condition (4.2) is satisfied there exists a Lagrange multiplier $z^* \in Z^*$ such that (4.1) is fulfilled, i.e.

$$\langle f'(\bar{v}) + h'(\bar{v})^* z^*, v - \bar{v} \rangle_{Z^*, Z} \geq 0 \quad \forall v \in C, \tag{4.3}$$

where f' and h' denote the Gâteaux derivatives of f and h respectively. This gives us a first-order necessary condition. A similar formulation and the associated proofs can be found in the paper of Maurer and Zowe [60].
If we consider only equality constraints $h(v) = 0$ with additional $C = V$, the inequality (4.1) becomes an equality

$$f'(\bar{v}) + h'(\bar{v})^* z^* = 0.$$

Due to $C = V$ the constraint qualification (4.2) becomes $h'(\bar{v})U = Z$ and hence the operator $h'(\bar{v})$ has to be surjective, which leads to the above equation.
To derive a second-order sufficient condition we consider problem (OP) with f and h two times Fréchet-differentiable. The element $\bar{v}$ satisfies with $z^* \in Z^*$ the necessary conditions (4.3) and there exists a $\delta > 0$ such that

$$D_{vv}\mathcal{L}(\bar{v}, z^*)[v, v] := f''(\bar{v})[v, v] + \langle z^*, h''(\bar{v})[v, v] \rangle_{Z^*, Z} \geq \delta \|v\|_V^2 \tag{4.4}$$

for all $v \in C(\bar{v})$ with

$$h'(\bar{v})v = 0. \tag{4.5}$$

Therewith $D_{vv}\mathcal{L}(\bar{v}, z^*)[v, v]$ denotes the second partial derivative of the Lagrangian with the argument $[v, v]$ and $f''(\bar{v})[v, v]$ and $h''(\bar{v})[v, v]$ with the arguments $[v, v]$ denote the second derivatives of $f(\bar{v})$ and $h(\bar{v})$ respectively. The derivatives can be calculated as directional derivatives along v. Further, $\| \cdot \|_V$ denotes a norm in V.

Lemma 4.2 *If $\bar{v}$ satisfies the conditions of the problem* (OP) *and if the conditions* (4.3), (4.4) *and* (4.5) *are satisfied as well, then $\bar{v}$ is a local optimal solution of problem* (OP).

This second-order sufficient condition is depicted in [88] and follows from the general results in the paper of Maurer and Zowe [60].

4.2 Basic optimization algorithms

Based on the theory of the section above different basic optimization algorithms will be derived in the following. The above results will be used mainly to derive the necessary

conditions with the help of the Lagrangian function for a general optimal control problem.

At first we will introduce a gradient descent method and second a method of higher order, a so called Newton method. Originally, Newton methods are designed to calculate the root of a function. In the context of optimization they are used to calculate the root of the first-order necessary condition. The general theory and numerics for optimization problems is described in several textbooks as e.g. in the books of Gill et al. [25], Bonnans et al. [11], Geiger and Kanzow [22] and Großmann and Terno [29].

4.2.1 Gradient descent method

The main idea of a gradient descent methods is to find a local minimum of an objective function under consideration of the constraints by proceeding in the direction of the negative gradient. The negative gradient is the steepest descent towards the minimum. The appropriate descent is calculated as the direction which minimizes the derivative of the objective functional. If the calculated derivative is small, i.e. smaller than a certain value $\varepsilon > 0$, the algorithm stops. Otherwise we have to determine a step size which leads to a decreasing of the objective function if we proceed according to the calculated direction.

The main aspect for the algorithm is the determination of the descent direction and therefore the determination of the directional derivative of the objective function with respect to the optimization variable. The constraints has to be considered in the derivative, i.e. it has to be assured that they are adhered. In the following we will state a general optimal control problem to obtain a basis for the optimal control problems which are investigated in the following chapter. The corresponding optimality system will be derived from this general problem by using the Lagrange technique and a gradient descent algorithm will be formulated afterwards.

Let Y, U, Z be Hilbert spaces and we define Fréchet differentiable functions $F : Y \times U \to \mathbb{R}$ and $h : Y \times U \to Z$, where the space V from the general problem (OP) is replaced by $V := Y \times U$ and accordingly we have $v := (y, u)$. Later on we will obtain $Z = Y^*$ for specific problems.

The optimal control problem becomes

$$
\begin{aligned}
\min_v f(v) &:= F(y, u) \\
\text{subject to} \quad & h(y, u) = 0 \\
& u \in U_{\text{ad}}
\end{aligned}
\tag{OCP}
$$

where h represents the weak form of a PDE, e.g. the potential equation, and $U_{\text{ad}} \subset U$ denotes the feasible set for the control u. To set up the optimality system we deduce the necessary condition as defined in (4.3). Therefore, we have to formulate the corresponding Lagrange function at first. For the evaluation of the variational inequality we need the Lagrange multiplier which can be derived by the formal Lagrange technique as well. We know that there exists a Lagrange multiplier if the constraint qualification, see

definition 4.3, is satisfied.

The Lagrange function

$$\mathcal{L} : Y \times U \times Z^* \to \mathbb{R}$$

with Lagrange multiplier $z^* \in Z^*$ is defined as

$$\mathcal{L}(y, u, z^*) = F(y, u) + \langle z^*, h(y, u) \rangle_{Z^*, Z}.$$

The Lagrange multiplier z^* can be calculated via the adjoint equation which is derived by differentiating the Lagrange function with respect to the state y. The state y is the solution of the constraining PDE in (OCP). The adjoint equation is obtained by setting the derivative of the Lagrangian equal to zero

$$D_y \mathcal{L}(\bar{y}, \bar{u}, z^*)(y) = \langle D_y F(\bar{y}, \bar{u}) + D_y h(\bar{y}, \bar{u})^* z^*, y \rangle_{Y^*, Y} = 0 \quad \forall y \in Y, \qquad (4.6)$$

where $D_y \mathcal{L}$ denotes the Fréchet derivative of the Lagrangian with respect to the state y. If we set $\mu := -z^*$ the equation above (4.6) leads to

$$D_y h(y, u)^* \mu = D_y F(y, u), \quad \forall y \in Y, \qquad (4.7)$$

which is named adjoint equation with the adjoint state μ. Analogously, we derive the variational inequality from the derivative of the Lagrange function with respect to the control u

$$D_u \mathcal{L}(\bar{y}, \bar{u}, z^*)(u - \bar{u}) = \langle D_u F(\bar{y}, \bar{u}) + D_u h(\bar{y}, \bar{u})^* z^*, u - \bar{u} \rangle_{U^*, U} \geq 0 \quad \forall u \in U_{\text{ad}}.$$

Or accordingly with the adjoint state $\mu \in Y$

$$D_u \mathcal{L}(\bar{y}, \bar{u}, \mu)(u - \bar{u}) = \langle D_u F(\bar{y}, \bar{u}) - D_u h(\bar{y}, \bar{u})^* \mu, u - \bar{u} \rangle_{U^*, U} \geq 0 \quad \forall u \in U_{\text{ad}}. \qquad (4.8)$$

The inequalities (4.6) and (4.8) define the necessary conditions for the optimal control problem (OCP).

If we define for a Lipschitz-domain Ω the Hilbert spaces as $Y := H_0^1(\Omega)$ and $U := L^2(\Omega)$ and assume for the PDE constraints

$$h(y, u) = 0 \Leftrightarrow (\nabla y, \nabla w)_{L^2(\Omega)} = (u, w)_{L^2(\Omega)} \quad \forall w \in H_0^1(\Omega),$$

with the inner product $(\cdot, \cdot)_{L^2(\Omega)}$ in $L^2(\Omega)$ and where ∇y denotes the gradient of the state y with respect to the space, then we have $Z = Y^* = H_0^1(\Omega)$, since $H_0^1(\Omega)$ is a Hilbert space. By using Riesz representation theorem (e.g. [88], p. 34) the corresponding weak form of the adjoint equation, with adjoint state $\mu \in H_0^1(\Omega)$, is given by

$$(\nabla \mu, \nabla w)_{L^2(\Omega)} = (D_y F(y, u), w)_{L^2(\Omega)} \quad \forall w \in H_0^1(\Omega).$$

And the corresponding variational inequality is as follows

$$(D_u F(\bar{y}, \bar{u}) - \mu, u - \bar{u})_{L^2(\Omega)} \geq 0 \quad \forall u \in U_{\mathrm{ad}}.$$

With the adjoint state μ and the derivative with respect to the control u we are now able to describe a gradient descent method with projection for the general optimal control problem (OCP), as described e.g. in [88], p. 76. Further theoretical investigations can be found in [30]. As descent direction the derivative of the Lagrangian with respect to the control u is used. If the gradient is equal to zero, the algorithm stops. Numerically this means the gradient has to be smaller than a certain value $\varepsilon > 0$.

Algorithm 2

1. *Initialize.* Set $n := 0$ and choose initial $u_0 \in U_{\mathrm{ad}}$.

2. *State.* Calculate corresponding y_n to u_n from the state system $h(y_n, u_n) = 0$.

3. *Adjoint state.* Calculate corresponding μ_n from the adjoint system (4.7).

4. *Descent direction.* Calculate descent direction d_n from the negative gradient

$$\begin{aligned} d_n := & - D_u \mathcal{L}(y_n, u_n, \mu_n) \\ = & - D_u F(y_n, u_n) + D_u h(y_n, u_n)^* \mu_n. \end{aligned}$$

   If $D_u \mathcal{L}(y_n, u_n, \mu_n)(d_n) < \varepsilon$, STOP.

5. *Step size.* Determine the step size s_n by

$$F(y_n, P_{U_{\mathrm{ad}}}(u_n + s_n d_n)) = \min_{s>0} F(y_n, P_{U_{\mathrm{ad}}}(u_n + s d_n)), \tag{4.9}$$

   where $P_{U_{\mathrm{ad}}}$ denotes a projection onto the space of admissible controls U_{ad}.

6. *Update.* Set $u_{n+1} = P_{U_{\mathrm{ad}}}(u_n + s_n d_n)$ and $n = n + 1$ and go back to 2.

Since the case $d_n = 0$ is hard to reach numerically, the method stops if some termination criteria take effect or a maximal number of iterations is reached. For the termination criterion it is expedient to choose a condition which checks not only the absolute values like the gradient and the improvement in the target function or the difference of the succeeding iterates, but also the relation to the current objective value and the current iterate. In section 5.3 a possible termination criterion is described.

To assure an admissible new iterate, we have to determine an appropriate step size s_n such that the condition (4.9) in the fifth step of algorithm 2 is satisfied. For the determination of the step size in each iteration step there exists a variety of methods like e.g. the bisection method or the Armijo step size rule. For the bisection method we start with a step size s_0 and bisect this until a step size $s_k := s_0 2^{-k}, k \in \mathbb{N}$ is found which minimizes the current objective value $F(y_n, P_{U_{\mathrm{ad}}}(u_n + s d_n))$ with respect to s. This rule can be altered by using another factor instead of 2^{-1}. Further, it can be improved by

choosing the initial step size in dependence of the objective functional and the current derivative.

Another popular step size rule is the Armijo rule, where the current objective is compared with the last objective value and a term involving the gradient.

We assume, we have a descent direction d_n for the current value u_n. For given values $l \in (0, 1)$ and $\kappa \in (0, 1)$ and an initial value $s_0 \in \mathbb{R}$ we determine a step size

$$s_n := \max\{s_0 l^i \,|\, i = 0, 1, 2, \dots\}$$

such that

$$\varphi(s_n) \leq \varphi(0) + \kappa s_n \varphi'(0). \tag{4.10}$$

The function $\varphi : \mathbb{R} \to \mathbb{R}$ is defined as $\varphi(s) := f(u_n + sd_n)$. Accordingly, the gradient of φ at $s = 0$ is $\varphi'(0) = f'(u_n)^T \cdot d_n$. The final step size s_n is obtained by iteratively setting $s := sl$ until the condition (4.10) holds. In general the initial step size is chosen as $s_0 = 1$. But sometimes it is advisable to choose s_0 according to the size of the gradient values and the size of the optimization variable to avoid too large or too small values for s_0. Too large values may lead to a time consuming step size determination whereas too small values may slow down the iteration process due to too small steps in the right direction. Another possible modification is the so called expansion of the Armijo rule. Thereby we start with $s_0 = 1$ and if the condition (4.10) holds already, we choose the new step size $s := s_0 l^{-1}$ instead of accepting $s = 1$. This will be continued until (4.10) is no longer fulfilled.

Moreover, there exist other step size rules like e.g. the Wolfe-Powell rule, the strict Wolfe-Powell rule or the Goldstein rule. The Wolfe-Powell rule includes an additional condition on the gradient $\varphi'(s)$. All these rules tend to avoid too small step sizes. Further explanations can be found e.g. in [11, 23, 29].

4.2.2 Newton method and sequential quadratic programming

The idea of the Newton method for optimization and optimal control problems is the application of the classical Newton's method to the first order necessary condition. The classical Newton's method is an iterative method to find the roots of a function. The derivation of the Newton method will be illustrated at a real valued function $g : \mathbb{R} \to \mathbb{R}$ without any constraints.

To calculate the root of g we have the iteration instruction

$$u_{n+1} = u_n - \frac{g(u_n)}{g'(u_n)}.$$

We will apply this method to the necessary condition $f'(\bar{u}) = 0$ for a local solution $\bar{u}$ of an optimization problem without constraints. That means we approximate the necessary condition linearly to find the root of the derivative. We obtain

$$u_{n+1} = u_n - f'(u_n) \left(f''(u_n)\right)^{-1},$$

if the inverse $f''(u_n)^{-1}$ exists, which is equivalent to the linear approximation

$$f'(u_n) + f''(u_n)(u_{n+1} - u_n) = 0. \tag{4.11}$$

This equation is solvable if the matrix $f''(u_n)$ is regular.

Another motivation for the Newton method is the quadratic approximation of the objective function at w for w close to the iterate u_n, i.e.

$$\hat{f}(w) = f(u_n) + f'(u_n)^T(w - u_n) + \frac{1}{2}(w - u_n)^T f''(u_n)(w - u_n). \tag{4.12}$$

The necessary condition for $\hat{f}$ in a local optimum $\bar{w}$ leads to the condition

$$\hat{f}'(\bar{w}) = f'(u_n) + f''(u_n)(\bar{w} - u_n) = 0,$$

which corresponds to the above equation (4.11) with $\bar{w} = u_{n+1}$. Both equations can be reformulated to

$$f''(u_n)v_n = -f'(u_n),$$

with descent direction $v_n = (u_{n+1} - u_n)$ or $v_n = (\bar{w} - u_n)$ respectively.

A related point of view is to consider the equation (4.11) as necessary condition of the following quadratic optimization problem

$$\min_u f'(u_n)^T(u - u_n) + \frac{1}{2}(u - u_n)^T f''(u_n)(u - u_n). \tag{4.13}$$

Hence, applying the Newton method to the problem $f'(u) = 0$ can be accomplished alternatively by solving the sequence of quadratic minimization problems (4.13) and we obtain a so called sequential quadratic programming (SQP) method.

For problems with equality constraints the above results can be transferred to the Lagrange function and the SQP method is derived analogously. Also problems with inequality constraints can be solved with an SQP method, whereas the derivation is a little bit different. Detailed descriptions of the SQP method is presented in the textbook of Geiger and Kanzow [22] as well as in [11] or for PDE constrained problems in [27] and [88].

Turning now to the question of solving the optimal control problem as stated in (OCP). Let Ω denote a Lipschitz-domain and define the Hilbert spaces as $Y := H_0^1(\Omega$ and $U := L^2(\Omega)$ and $Z = Y^* = H_0^1(\Omega)$. Therewith we obtain as necessary conditions in (y_n, u_n) the condition

$$D_y\mathcal{L}(y_n, u_n, \mu_n)(y - y_n) = 0 \quad \forall y \in H^1(\Omega),$$

needed for the calculation of the adjoint state μ, and the variational inequality

$$D_u\mathcal{L}(y_n, u_n, \mu_n)(u - u_n) \geq 0 \quad \forall u \in U_{\text{ad}}. \tag{4.14}$$

Altogether we have $\nabla\mathcal{L}(y_n, u_n, \mu_n)(y - y_n, u - u_n) = 0$, where $\nabla\mathcal{L}$ denotes the gradient of the Lagrange function with respect to y and u. If we expand this equation in a quadratic approximation as in (4.12) or apply the Newton's method on this equation, we will obtain the following optimal control problem, similar to the previous problem without constraints but with the Lagrange function $\mathcal{L}$ instead of the basic function f.

$$\min_{(y,u)} \nabla F(y_n, u_n)^T d_n + \frac{1}{2} d_n^T \nabla^2 \mathcal{L}(y_n, u_n, \mu_n) d_n \tag{QP}$$
$$\text{subject to} \quad h(y_n, u_n) + \nabla h(y_n, u_n)^T d_n = 0,$$

where $d_n = (y - y_n, u - u_n)$ denotes the descent direction, ∇F the gradient of the objective with respect to the state y and the control u and $\nabla^2 \mathcal{L}$ the Hessian matrix of the Lagrange function with respect to the state y and the control u. Hence, the algorithm for the SQP method can be described as

Algorithm 3

1. *Initialize.* Set $n := 0$ and choose initial control u_0, initial state y_0 and initial Lagrange multiplier μ_0.

2. *Check optimality conditions.* If $\nabla\mathcal{L}(y_n, u_n, \mu_n) = 0$ and $h(y_n, u_n) = 0$, i.e. (y_n, u_n, μ_n) satisfies the necessary conditions of the primal optimal control problem (OCP), STOP.
   Thereby
   $$\nabla\mathcal{L}(y_n, u_n\mu_n) = 0 \Leftrightarrow \begin{pmatrix} D_y\mathcal{L}(y_n, u_n, \mu_n) \\ D_u\mathcal{L}(y_n, u_n, \mu_n) \end{pmatrix} = \begin{pmatrix} 0 \\ 0 \end{pmatrix}$$

3. *Solve QP.* Calculate a solution $(y - y_n, u - u_n, \mu_{n+1})$ of the quadratic problem (QP). That means the following equation system has to be solved with respect to $(y - y_n, u - u_n, \mu_{n+1})$, where $d_n = (y - y_n, u - u_n)$.
   $$\begin{pmatrix} \nabla^2\mathcal{L}(y_n, u_n, \mu_n) & \nabla h(y_n, u_n) \\ \nabla h(y_n, u_n)^T & 0 \end{pmatrix} \begin{pmatrix} d_n \\ \mu_{n+1} \end{pmatrix} = -\begin{pmatrix} \nabla F(y_n, u_n) \\ h(y_n, u_n) \end{pmatrix}.$$

4. *Update.* Set $y_{n+1} := y_n + (y - y_n)$, $u_{n+1} := u_n + (u - u_n)$ and $n := n + 1$ and go back to 2.

Since the SQP method converges only locally like the Newton method (cf. [23], p. 206, [87]), we need some globalization strategies. We may achieve global convergence by introducing a step size into the algorithm. Then the new iterate is given by a modified update

$$y_{n+1} := y_n + s_n(y - y_n) \quad u_{n+1} := u_n + s_n(u - u_n).$$

The step size s_n can be calculated by a line search as in the gradient method, e.g. bisection method or Armijo rule. The main question is, when does a new iterate improve the system? It is not sufficient to compare the objective values because the state might be

unfeasible, i.e. the constraints are violated. In the gradient method the new state y_n has been calculated from the state system for the iterate u_n. Whereas in the SQP method, the new state y_{n+1} and the new control u_{n+1} are both obtained iteratively. Hence, we have to assure that the constraints are adhered.

Therefore, we may use a so called penalty function to measure the quality of the solution. That means the penalty function is used instead of the objective functional for the calculation of the step size. Usually, this penalty function combines the objective and the feasibility conditions. An early approach concerning such globalization strategies is given by Han [34]. The new iterate is deemed as better than the last one if either the objective improves or the violation of the objective decreases. In a general form this penalty functions can be written as

$$P(y, u, \eta) := F(y, u) + \eta R(y, u) \tag{4.15}$$

with $\eta > 0$ and the continuous function $R : L^2(\Omega) \times L^2(\Omega) \to [0, \infty)$ where $R(y, u) = 0$ if and only if y and u are feasible, i.e. the constraints are adhered. There exist various penalty functions, e.g. penalty functions based on the q-norm

$$P(y, u; \eta) = F(y, u) + \eta \|h(y, u)\|_{L^q(\Omega)}$$

or the augmented Lagrangian

$$P(y, u, \mu; \eta) = \mathcal{L}(y, u, \mu) + \frac{\eta}{2} \|h(y, u)\|_{L^2(\Omega)}^2,$$

with $\eta > 0$. A detailed analysis for the l_1-penalty function is given by Geiger and Kanzow in [22], sec. 5.5.4., whereas Bonnans et al. [11] focus more on the determination and proper choice of the parameter η. A summary of different aspects can be found in [23].

4.3 Inverse problems

After considering the basic idea of constrained optimization in the last sections we will turn now to the field of inverse problems and the connection to the aim of this work, the parameter identification.

In the last century the topic of inverse problems has become more and more relevant in technical developments and in the second half of the 20th century the mathematical theory and analysis has evolved to a significant part of mathematics. An introduction to the theory of inverse problems is for example given by the book of Louis [57] or the book of Hofmann [37]. Contrary to a direct problem, an inverse problem is aimed at finding the causes or the terms which lead to a particular effect. Therewith, we need to concentrate on particular causes or terms, the remaining are assumed as known.

Hofmann distinguishes two typical cases of inverse problems. The first one is a problem where we have some measurements and want to know the original setting, i.e. the parameters or other conditioning terms. He calls it an *identification problem*. These

problems can be described as operator problems

$$F(x) = y, \quad x \in D \subset X, y \in Y,$$

where y is the known measurements and x the parameter we are looking for. In real applications the measurements will not satisfy these idealized situation. But it can be assumed that we have defective data y_δ which fulfill the estimate

$$\|y_\delta - y\| \le \delta$$

for the level of data error $\delta > 0$.

The second type of inverse problems is named *control problems*. There we want to find a parameter or term that leads to a desired effect and the problems are defined as minimization problems

$$\min \ \|F(x) - y\|_Y, \quad x \in D \subset X,$$

which can be solved with the methods from optimization or optimal control.

The identification of the thermal conductivity and the electrical conductivity from temperature measurements is formulated as control problem, i.e. we want to determine a parameter such that the measured temperature is reached in the best way.

Nevertheless, in the following identification and identification problems will always be meant in the sense of the control problem above, where we want to determine the appropriate parameters for given measurements. Beside that every control problem as defined above, can be described as identification problem as well [37].

The main difficulty for the solution is that most inverse problems are so called ill-posed problems, i.e. there does not exist a unique solution or small perturbations in the parameters will lead to high variations in the outcome. In the following U and Y denote Banach spaces if they are not further specified. The following definition of well-posed problems (the contrary to ill-posed problems) was given by Jacques Hadamard (1865-1963) ([37], p. 32).

Definition 4.4 *The equation*

$$F(u) = y, \quad u \in D \subset U, y \in Y \tag{4.16}$$

is called well-posed *if the following holds*

- *For every $y \in Y$ there exists a solution $u \in D$ for $F(u) = y$.*

- *The solution u for $F(u) = y$ is unique in D.*

- *The solution u depends continuously on the right hand side y.*

If at least one of the conditions is not fulfilled, the problem is called ill-posed*.*

The main idea to solve such problems is to find a solution that fits to the desired or given state. To be able to solve these problems even if they are ill-posed, we use so

called regularization methods. These regularization methods aim at turning the ill-posed problems into well-posed problems to guarantee the existence of a unique and stable solution. In the following we will briefly introduce the idea of regularization, especially the way of Tikhonov regularization.

Let y_δ be given defective data, which are connected with the exact data $y \in Y$ via the relation

$$\|y - y_\delta\|_Y \leq \delta, \quad \delta \in \mathbb{R}.$$

The given data y_δ are not necessarily in the range of the operator F that we want to fit to the data. That means the typical formulation as output least square problem, i.e.

$$\min_{u \in D \subset U} \|F(u) - y_\delta\|_Y^2$$

will fail in these cases. Even if the data are in the range of F, solving the minimization problem will lead to the inverse operator $F^{-1}(y)$ which is discontinuous if the third condition in the above definition is not satisfied. That means small perturbations in the data will lead to large errors. Therefore, the idea is to fit the operator F not as good as possible to the given data y_δ but as good as necessary. The regularization method of Tikhonov, developed in the 1960's, has become quite common to solve ill-posed problems in practical applications.
In the following we will introduce at first the regularization for a linear operator equation. Afterwards the regularization will be applied to a non-linear operator equation.
For a linear operator $A \in \mathcal{L}(U, Y)$ with adjoint operator $A^* \in \mathcal{L}(Y, U)$ and defective data y_δ we consider the problem

$$A^* A u = A^* y_\delta \quad u \in U, \, y_\delta \in Y.$$

The method of Tikhonov regularization is based on the fact that we may solve instead of the above ill-posed problem the following indexed family of functions

$$(A^* A + \alpha I)u = A^* y_\delta, \quad u \in U, \, y_\delta \in Y, \tag{4.17}$$

with the identity operator I in X. With the following lemma ([37], lemma 4.2, p. 135) we can show that for every $\alpha > 0$ the corresponding equation in (4.17) is well-posed by the definition of Hadamard.

Lemma 4.3 *A selfadjoint operator $B \in \mathcal{L}(U, Y)$, which is positive definite in the Hilbert space U, that means for a constant $\beta > 0$ the inequality $(Bu, u)_U \geq \beta \|u\|_U^2$ is satisfied for all $u \in U$, has a continuous inverse operator $B^{-1} \in \mathcal{L}(U, U)$ with $\|B^{-1}\|_{\mathcal{L}(U,U)} \leq \frac{1}{\beta}$. Further the minimization problem*

$$\min_{u \in U} (Bu, u)_U - 2(u, z)_U$$

is for every fixed $z \in U$ equivalent to the operator equation

$$Bu = z, \quad u \in U$$

and both have the same unique solution $u = B^{-1}z$.

If we define $B := A^*A + \alpha I$ and $z := A^*y_\delta$ the well-posedness of (4.17) is given by the above lemma with $\beta = \alpha$. Furthermore (4.17) is equivalent to the minimization of

$$\left((A^*A + \alpha I)u, u\right)_U - 2(u, A^*y_\delta)_U = \|Au - y_\delta\|_Y^2 + \alpha\|u\|_U^2 - \|y_\delta\|_Y^2,$$

for all $u \in U$. Since the constant term $\|y_\delta\|_Y$ does not influence the minimization problem, the Tikhonov functional is defined as follows

$$T_\alpha(u) := \|Au - y_\delta\|_Y^2 + \alpha\|u\|_U^2 \tag{4.18}$$

and the regularized solution u_α^δ is the unique solution to every $y_\delta \in Y$ which minimizes the corresponding Tikhonov functional T_α.

For a non-linear operator equation

$$F(u) = y, \quad u \in D \subset U, \, y \in Y \tag{4.19}$$

a regularized solution u_α^δ is calculated as the solution of the minimization problem

$$\min_{u \in D} T_\alpha(u) = \|F(u) - y_\delta\|_Y^2 + \alpha\|u - u^*\|_U^2, \quad \alpha > 0, \tag{4.20}$$

with a positive regularization parameter $\alpha \in \mathbb{R}$ and defective data $y_\delta \in Y$ with

$$\|y_\delta - y\|_Y \le \delta,$$

where $\delta > 0$ denotes the level of data error. Thereby $u^* \in U$ denotes a given reference element.

For practical applications, the main problem is the balance between regularity and approximation. One criteria which became more and more popular in the last years is the so called L-curve-criteria from P. C. Hansen [35]. The L-curve-criteria leads to admissible regularization parameters for a lot of practical applications. This heuristic criteria uses a logarithmic 2D plot of the norm $\|F(u_\alpha^\delta) - y_\delta\|$ versus the norm $\|u_\alpha^\delta - u^*\|$. Both norms are parameterized by the regularization parameter α. If we start with $\alpha = 0$ the norm $\|F(u_\alpha^\delta) - y_\delta\|$ stays nearly the same whereas the regularization term $\|u_\alpha^\delta - u^*\|$ typically decreases considerably. From a certain point the relation reverses, i.e. the error in the approximation to the data increases whereas the regularization term remains nearly the same. The resulting curve is in many cases L-shaped and the parameter which leads to the values in the angle of this curve could be a suitable regularization parameter for the inverse problem. However, as every other method, this criterion can fail and we will need further investigations then to find the best parameter. A typical shape of such an
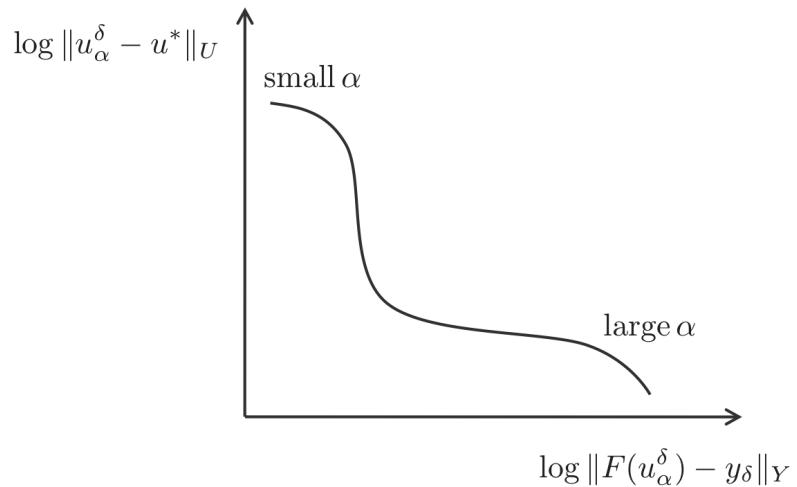
Figure 4.1: A typical shape of an L-curve for the determination of a regularization parameter α.

L-curve is presented in figure 4.1.

5 Identification of the material parameters

The main part of this work is the identification of the material parameters for given temperature data from radio frequency ablation, especially the identification of the unknown thermal conductivity and unknown electrical conductivity. The purpose of the identification is the improvement of the model for the RFA, since an exact modeling of the material parameters is important for a realistic RFA simulation. The material parameters influence the simulation via the PDEs in the modeling. However, these parameters are not known exactly and the approximations are based on the results from animal experiments. Beside the fact that most of this results are from ex vivo experiments we neither know if these results are transferable to humans at all.

Hence, the material parameters will be identified from temperature measurements by solving an inverse problem. The temperature depends on the parameters and the prediction for the treatment with RFA is based on the temperature distribution. Furthermore, the temperature can be measured during the treatment by MRI thermometry. Therewith, the inverse problem including the temperature distribution gives us a good opportunity to improve the whole simulation patient individually during the treatment. The possibility of a patient individual identification is a significant improvement for the simulation since the material parameters vary a lot for different patients but also for one patient. The parameters depend on the patient's constitution and also on the diverse tissue types, especially the difference between tumorous and native tissue. Moreover the parameters vary during the treatment due to the temperature dependence but also because of vaporization of water or the denaturation of the cells.

In figure 5.1 the median electrical conductivity, measured in various porcine livers (ex vivo), is depicted together with the smallest and largest values as well as the standard deviation at the certain temperature points. The measurements are executed at the *Charité - Universitätsmedizin Berlin* (Germany) and are published in the paper of Zurbuchen et al. [95]. The data shows a great variety between the different livers during the heating. During the cooling down of the tissue after the ablation, the variety is much less, see the diagrams at the bottom of figure 5.1.

The basic inverse problem (BIP) for the identification of the spatially distributed material parameters from a given temperature distribution T_g at a certain time point t_{fin} can be described by the following optimal control problem

$$\min_{T,\lambda,\sigma} F(T,\lambda,\sigma) = \frac{1}{2}\big\|T(t_{\text{fin}},x) - T_g(x)\big\|^2_{H^1(\Omega)} + \text{Reg}_\lambda(\lambda) + \text{Reg}_\sigma(\sigma) \qquad \text{(BIP)}$$

subject to

$$\rho c \partial_t T - \text{div}\left(\lambda(x)\nabla T\right) + \nu(T - T_{\text{body}}) = \frac{P_{\text{eff}}}{P_\Omega}\sigma(x)|\nabla\phi|^2 \qquad \text{in } \Omega \qquad (5.1)$$

$$-\text{div}\left(\sigma(x)\nabla\phi\right) = 0 \qquad \text{in } \Omega \setminus \overline{\Gamma}, \qquad (5.2)$$

with the thermal conductivity $\lambda \in H^m(\Omega)$, $m > 0$ and the electrical conductivity $\sigma \in H^s(\Omega)$, $s > \frac{3}{2}$. The terms $\text{Reg}_\lambda(\lambda)$ and $\text{Reg}_\sigma(\sigma)$ denotes the regularization terms for λ and σ respectively. The appropriate boundary conditions for (5.1) and (5.2) can be found in (3.8) and (3.1) respectively.

Here the material parameters are assumed to be spatially distributed. But as described in section 3.3.3 in fact the parameters are also temperature dependent. However, using spatially distributed parameters will incorporate the temperature dependence since the temperature is also spatially distributed. Nevertheless, the modeling of temperature dependent parameters as described in (3.9) and (3.10) has different advantages.
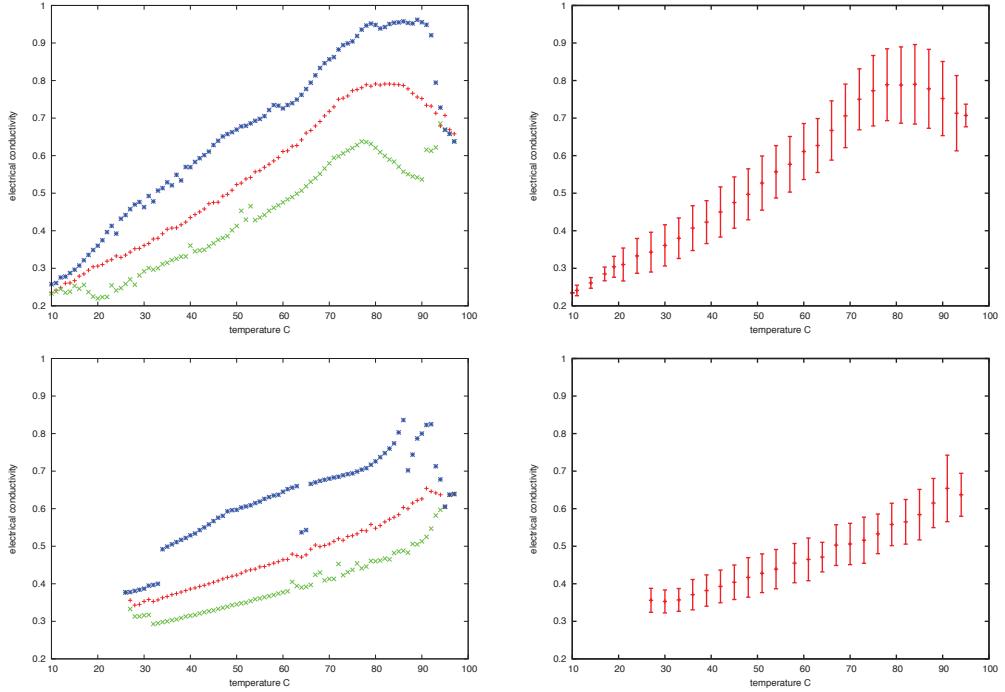
Figure 5.1: The electrical conductivity, measured in several porcine livers. On the left we have the median (red plus), the smallest measured values (green crosses) and the largest measured values (blue asterisks). On the right the median with standard deviation is depicted for a selection of measuring points. The figures at top show the results obtained during the heating, whereas the figures at the bottom represent the measurements during the cooling. The data are provided by *Charité - Universitätsmedizin Berlin*.

Mainly, the local impact of the temperature distribution is used sensibly, since for the identification of spatially distributed parameters the local impact of the temperature is a particular challenge. Due to the minor effect of the temperature distribution and the electrical potential on the peripheral region an identification of spatially distributed parameters is very difficult. The minor effect on the outer regions is reflected in a locally steep gradient for the parameters whereas in the most parts the gradient is flat. This highly complicates the optimization. Especially for the electrical conductivity this effect is intensified by the scaling term $\frac{P_{\text{eff}}}{P_\Omega}$. By using temperature dependent parameters the only local impact of the temperature does not matter.

To incorporate the advantages of the different models for the material parameters we will investigate different identification problems, that are distinguished by the different models for the parameters. We distinguish three main problems, which are all based on the problem with spatially distributed parameters. In figure 5.2 a schematic is presented to illustrate the different identification problems. Problem A is the basic problem with spatially distributed parameters. Problem B denotes the case where we use tissue dependent parameters and Problem C is given by a temperature dependent modeling of the parameters. However, Problem A is splitted further into several problems. Because of the coupling of the two PDEs via the right hand side and the unequal influence of the parameters on the temperature distribution it is difficult to solve the problem for both
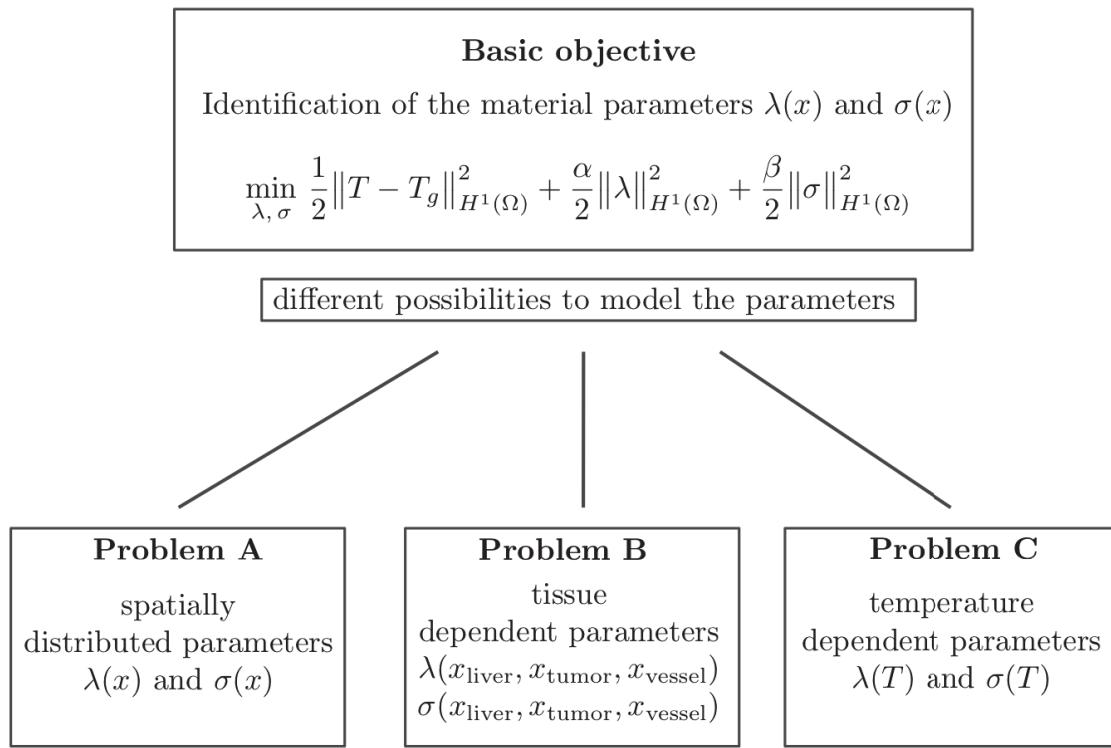
Figure 5.2: A schematic to illustrate the different types of identification problems.
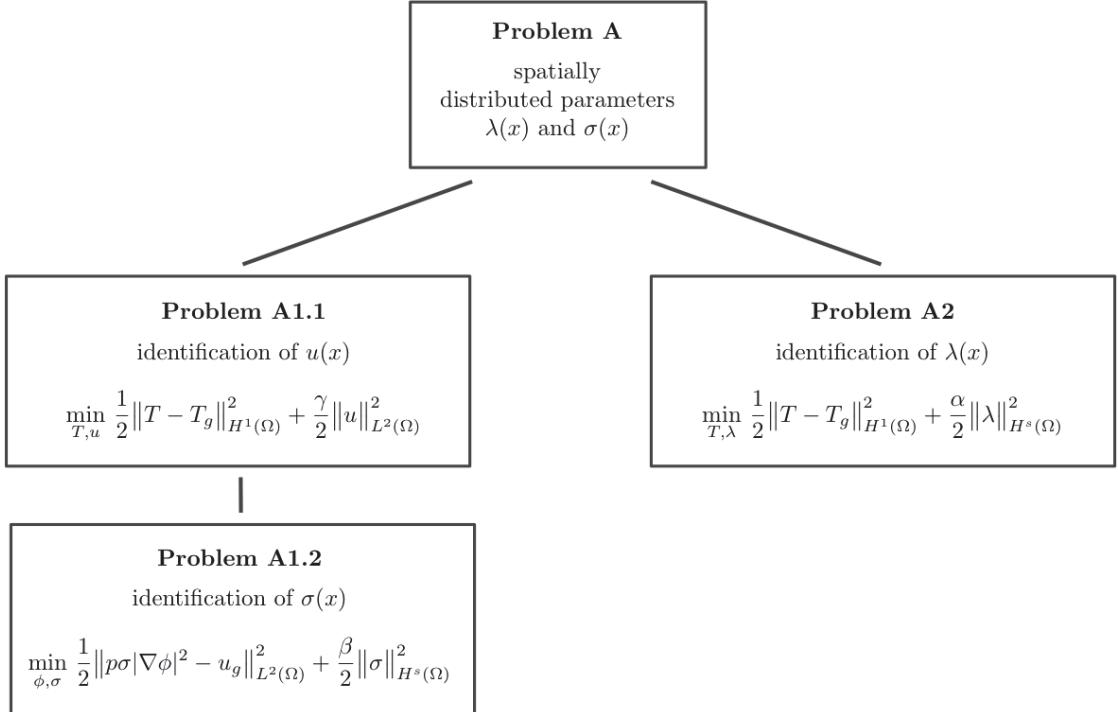
Figure 5.3: A schematic to illustrate the splitting of Problem A into two subproblems, one for the identification of the electrical conductivity (Problem A1) and one for the thermal conductivity (Problem A2). Thereby Problem A1 is further separated into two problems, one for the identification of the heat source u (Problem A1.1) and one for the identification of the electrical conductivity σ (Problem A1.2).

parameters in a satisfactory manner. Further, an identification of a spatially distributed electrical conductivity directly from the temperature distribution is difficult.

To get these problems under control yet without reducing the problem to constant parameters, we consider two subproblems where the optimization of the thermal conductivity and the electrical conductivity are separated. That means we split the above main optimal control problem (BIP) into two optimal control subproblems, one for the identification of the electrical conductivity (Problem A1) and one subproblem for the thermal conductivity (Problem A2). This splitting is schematically illustrated in figure 5.3. For the identification of the electrical conductivity Problem A1 is separated further into two problems, the identification of the heat source from temperature measurements (Problem A1.1) and the identification of the electrical conductivity (Problem A1.2), by fitting the power density to the previously identified heat source.

In the following section the existence of optimal controls for the different identification problems is investigated.

Therewith the basic problem, the identification of both parameters the electrical con-

ductivity and the thermal conductivity in one problem will not be considered. The numerical results have shown that the separated identification of spatially distributed parameters performs better than the combined identification. However, for constant or piecewise constant parameters the performance of the coupled optimization is well. For that reason there are also numerical results presented in the next chapter for the coupled optimization of constant parameters. A related optimal control problem with a coupled system of PDEs and temperature dependent electrical conductivity is described by Hömberg et al. [38]. Though in the paper of Hömberg et al. the direct current induced on a part of the boundary is optimized.

5.1 Existence of solutions for the different optimal control problems

In this section we will look into the existence of optimal controls for the identification problems. All problems have in common that the domain $\Omega \subset \mathbb{R}^N$ is a bounded Lipschitz domain with outer boundary $\partial\Omega$. As before, Γ, Γ_- and Γ_+ are parts of the domain Ω. Before we begin with the investigations some spaces and terms are defined and different theorems are cited which are needed to prove the existence of optimal controls for the diverse problems.

At first the *Bochner spaces* are defined ([88], p. 114)

Definition 5.1 (Bochner space) *For $1 \leq p < \infty$ and a Banach-space X, the space of all (equivalent classes of) measurable functions $y : [a, b] \to X$ with $[a, b] \subset \mathbb{R}$ and*

$$\int_a^b \|y(t)\|_X^p \, dt < \infty$$

is denoted by $L^p(a, b; X)$. The corresponding norm is defined as

$$\|y\|_{L^p(a,b;X)} := \left(\int_a^b \|y(t)\|_X^p \, dt \right)^{1/p}.$$

For $p = \infty$ the space $L^\infty(a, b; X)$ is defined as the space of all measurable functions $y : [a, b] \to X$ with $[a, b] \subset \mathbb{R}$ and

$$\|y\|_{L^\infty(a,b;X)} := \operatorname*{ess\,sup}_{[a,b]} \|y(t)\|_X < \infty.$$

For $p = 2$ and $X = H^1(\Omega)$ the above space $L^2(0, t_{\text{fin}}; H^1(\Omega))$ coincides for $Q := [0, t_{\text{fin}}] \times \Omega$ with the space

$$W_2^{1,0}(Q) := \{y \in L^2(Q) \mid \partial^\alpha y \in L^2(Q), \ \forall i = 1, \ldots, N\}.$$

Further we define $W(0, t_{\text{fin}})$ as the space of all functions $y \in L^2(0, t_{\text{fin}}; H^1(\Omega))$ with derivative $y' = \partial_t y \in L^2(0, t_{\text{fin}}; H^{-1}(\Omega))$ and associated with the norm

$$\|y\|_{W(0,t_{\text{fin}})} = \left(\int_0^{t_{\text{fin}}} \left(\|y(t)\|_{H^1(\Omega)}^2 + \|y'(t)\|_{H^{-1}(\Omega)}^2 \right) dt \right)^{1/2},$$

see also [88], p. 117. The following theorem is given by Showalter [76], section III.4., p. 120, theorem 4.1. For the theorem the needed definitions are introduced at first (Showalter [76], sec. II.2, p. 37 ff.). For the following let V be a reflexive Banach space with dual V^*.

Definition 5.2 *The function $\mathcal{A} : V \to V^*$ is said to be* monotone *if*

$$\langle \mathcal{A}(y) - \mathcal{A}(v), y - v \rangle_{V^*, V} \geq 0 \quad \forall y, v \in V.$$

Definition 5.3 *The function $\mathcal{A} : V \to V^*$ is said to be* hemicontinuous *if for each $y, v \in V$ the real valued function $t \mapsto \mathcal{A}(y + tv)(v)$ is continuous.*

Definition 5.4 *The function $\mathcal{A} : V \to V^*$ is* type M *if $y_n \rightharpoonup y$, $\mathcal{A}y_n \rightharpoonup f$ and $\limsup \mathcal{A}y_n(y_n) \leq f(y)$ imply that $\mathcal{A}y = f$.*

The following lemma is taken from [76], p. 38, Lemma 2.1.

Lemma 5.1 *If $\mathcal{A}$ is hemicontinuous and monotone then it is type M.*

Theorem 5.2 *Let V be a reflexive Banach space with dual space V^* and H a Hilbert space. Further V is assumed to be separable and dense in H. Assume that the operator $\mathcal{A} : V \to V^*$ is given such that its realization in $L^p(0, \tau; V)$ is type M, bounded and coercive with*

$$\mathcal{A}v(v) \geq \alpha \|v\|_{L^p(0,\tau;V)}, \quad v \in L^p(0, \tau; V).$$

Then for each $u \in L^{p'}(0, \tau; V^*)$ (the dual space of $L^p(0, \tau; V)$) and $y_0 \in H$ there is a solution of the Cauchy Problem

$$\begin{aligned} \text{find} \quad & y \in L^p(0, \tau; V) \\ \text{such that} \quad & \partial_t y(t) + \mathcal{A}(y(t)) = u(t) \quad \text{in } L^{p'}(0, \tau; V^*), \\ & y(0) = y_0 \text{ in } H. \end{aligned} \quad (5.3)$$

The solution is unique if the operator $\mathcal{A}$ is monotone, hemicontinuous, bounded and coercive. This is given by the next proposition ([76], sec. III.4., p. 122, Proposition 4.1)

Proposition 5.3 *Let the spaces V, H, $L^2(0, \tau; V)$ be given as in 5.2 with V separable. Assume a family of operators $\mathcal{A}(t, \cdot) : V \to V^*$, $0 \leq t \leq \tau$, is given such that*

(i) for each $v \in V$ the function $\mathcal{A}(\cdot, v) : [0, \tau] \to V^*$ is measurable,

(ii) *for a.e.* $t \in [0, \tau]$ *the operator* $\mathcal{A}(t, \cdot) : V \to V^*$ *is monotone, hemicontinuous and bounded by*

$$\|\mathcal{A}(t, v)\|_{V^*} \leq C(\|v\|_V + k(t)), \quad v \in V,$$

where $k \in L^2([0, \tau])$,

(iii) *there is a seminorm* $|\cdot|_V$ *on* V *and numbers* $\gamma > 0$, $\alpha > 0$ *such that*

$$|v|_V + \gamma |v|_H \geq \alpha \|v\|_V, \quad and$$
$$\mathcal{A}(t, v)(v) \geq \alpha |v|_V^2, \quad a.e. \ t \in [0, \tau], v \in V,$$

with $|v|_H^2 = (v, v)_H$.

Then for each $u \in L^2(0, \tau; V^*)$ *and* $y_0 \in H$ *problem* (5.3) *has a unique solution.*

A general theorem for the existence of optimal controls is given in [88], Theorem 2.14, p. 39.

Theorem 5.4 *Let* $(U, \|\cdot\|_U)$ *and* $(H, \|\cdot\|_H)$ *be real Hilbert spaces and* $U_{ad} \subset U$ *a nonempty, bounded, closed and convex subset of* U. *Suppose* $\alpha \geq 0$ *to be a constant value and* $y_g \in H$. *Further let* $S : U \to H$ *be a linear and continuous operator. Then the quadratic optimization problem*

$$\min_{u \in U_{ad}} f(u) = \frac{1}{2} \|Su - y_g\|_H^2 + \frac{\alpha}{2} \|u\|_U^2$$

has an optimal solution $\bar{u}$, *which is unique for* $\alpha > 0$.

For the identification of the electrical conductivity we refer to the paper of Assmann [9] and consider for a Lipschitz domain Ω with boundary $\partial\Omega$ the following parameter identification problem

$$\min_{y,p} \ F(y, p) := \frac{1}{2} \|y - y_g\|_{L^2(\Omega)}^2 + \frac{\alpha}{2} \|p\|_{H^s(\Omega)}^2$$

$$\text{subject to} \quad -\operatorname{div}(p\nabla y) = g \quad \text{in } \Omega$$
$$y = 0 \quad \text{on } \partial\Omega$$

(5.4)

with $0 < p_{\min} \leq p(x) \leq p_{\max}$ a.e. in Ω, $y \in H_0^1(\Omega)$, $p \in H^s(\Omega)$, $s > 0$ and where y_g, $g \in L^2(\Omega)$ and $\alpha > 0$ are given and $p_{\min} < p_{\max}$ are constant values.
The admissible set U_{ad}^p is defined as

$$U_{ad}^p := \{p \in H^s(\Omega) | \, 0 < p_{\min} \leq p(x) \leq p_{\max} \text{ a.e. in } \Omega\}.$$

A parameter-to-state operator is given by $S : L^\infty(\Omega) \to H^1(\Omega)$.

Theorem 5.5 *The parameter identification problem* (5.4) *has at least one solution* $\bar{p} \in U_{ad}^p$ *with the optimal state* $\bar{y} = S(\bar{p})$, *which means*

$$F(\bar{y}, \bar{p}) \leq F(y, p) \quad \forall p \in U_{ad}^p, y = S(p).$$

Turning now to the identification problems, we will investigate the identification problems which are based on the main problem (BIP) first. Thereby we separate the identification of the thermal conductivity and the electrical conductivity (Problem A), i.e. we look into the existence of solutions for the subproblems Problem A1.1, Problem A1.2 and Problem A2. Finally, we will investigate the existence of solutions for temperature dependent parameters, as described in Problem C. The identification of tissue dependent parameters (Problem B) can be considered as a special case of Problem A with piecewise constant parameters. Hence we will not separately consider Problem B in the following.

5.1.1 Problem A1.1: Identification of the heat source

As described above we split the identification of the electrical conductivity, Problem A1, into two subproblems, one for the heat source $u(x)$ and one for the electrical conductivity $\sigma(x)$ itself. At first we investigate the identification of the heat source from a given temperature distribution $T_g(x)$ at a certain time point t_{fin}. The aim is to fit the measured temperature $T(t_{\text{fin}}, x)$, calculated by the bio-heat transport equation, to the measured data $T_g(x)$. This leads to the following optimal control problem

$$\min_{T,\,u} F(T, u) := \frac{1}{2}\|T(t_{\text{fin}}, x) - T_g(x)\|_{H^1(\Omega)}^2 + \frac{\gamma}{2}\|u(t_{\text{fin}}, x)\|_{L^2(\Omega)} \tag{A1.1}$$

subject to

$$\begin{aligned}
\rho c \partial_t T - \operatorname{div}(\lambda \nabla T) + \nu(T - T_{\text{body}}) &= u && \text{in } Q := [0, t_{\text{fin}}] \times \Omega, \\
\nabla T \cdot n &= 0 && \text{on } \Sigma := [0, t_{\text{fin}}] \times \partial\Omega, \quad \text{(C A1.1)} \\
T &= T_{\text{body}} && \text{in } \Omega
\end{aligned}$$

with outer normal n and with

$$u_a(t, x) \le u(t, x) \le u_b(t, x) \quad \text{a.e. in } Q.$$

With $T_g \in L^2(Q)$, $u_a, u_b \in L^2(Q)$, $T_{\text{body}} \in L^2(\Omega)$ and $\nu \in L^\infty(Q)$, there exists for every $u \in L^2(Q)$ a unique weak solution $T \in W(0, t_{\text{fin}})$, see section 3.4 in [88]. And it follows from theorem 3.16 in [88] that there exists an optimal control $\overline{u}$ for this problem. With the additional condition $\gamma > 0$ for the regularization parameter we will have also uniqueness for the optimal control.

These results can also be transferred to the case that we have $u \in L^2(0, t_{\text{fin}}; H^{-1}(\Omega))$, where $H^{-1}(\Omega)$ denotes the dual space of $H^1(\Omega)$. Theorem 5.2 gives us the existence of a solution for the PDE (C A1.1) if the preconditions are satisfied. Let $V = H^1(\Omega)$ and $H = L^2(\Omega)$. The heat source is given by $u \in L^2(0, t_{\text{fin}}; H^{-1}(\Omega))$ and the coercive and

linear operator $\mathcal{A}$, where the term νT_{body} is moved to the right hand side, is given by

$$\mathcal{A}T(v) = \int\limits_0^{t_{\mathrm{fin}}}\!\!\int\limits_\Omega \lambda\nabla T\nabla v + \nu T v \, dx \, dt, \quad v \in L^2(0, t_{\mathrm{fin}}; H^1(\Omega))$$

which is measurable as function of time and monotone since

$$\int\limits_0^{t_{\mathrm{fin}}}\!\!\int\limits_\Omega (\lambda\nabla T - \lambda\nabla v)\nabla(T - v) + \nu(T - v)(T - v) \, dx \, dt$$

$$= \int\limits_0^{t_{\mathrm{fin}}}\!\!\int\limits_\Omega \lambda \left(\nabla(T - v)\right)^2 + \nu(T - v)^2 \, dx \, dt$$

$$\geq \lambda_a\|\nabla(T - v)\|^2_{L^2(0,t_{\mathrm{fin}};L^2(\Omega))} + \|\nu\|_{L^\infty(Q)}\|T - v\|^2_{L^2(0,t_{\mathrm{fin}};L^2(\Omega))}$$

$$\geq c_0 \, \|T - v\|^2_{L^2(0,t_{\mathrm{fin}};H^1(\Omega))}$$

$$\geq 0, \quad \forall v \in L^2(0, t_{\mathrm{fin}}; H^1(\Omega)),$$

with $0 < \lambda_a \leq \lambda(x) \leq \lambda_b$, where $\lambda_a, \lambda_b \in \mathbb{R}$ and a bounded coefficient $0 < \nu_0 \leq \nu(x)$. The hemicontinuity is given by the following inequality, for a value $c > 0$ and a bounded coefficient $0 < \nu(x) < \infty$

$$\int\limits_0^{t_{\mathrm{fin}}}\!\!\int\limits_\Omega \lambda\nabla(T + sv)\nabla v + \nu(T + sv)v \, dx \, dt = \int\limits_0^{t_{\mathrm{fin}}}\!\!\int\limits_\Omega \lambda\nabla T\nabla v + \lambda s\nabla v\nabla v \, dx \, dt$$

$$+ \int\limits_0^{t_{\mathrm{fin}}}\!\!\int\limits_\Omega \nu(Tv + svv) \, dx \, dt$$

$$\leq \lambda_b \left(\|\nabla T\|_{L^2(Q)}\|\nabla v\|_{L^2(Q)} + |s| \, \|\nabla v\|^2_{L^2(Q)}\right)$$

$$+ \|\nu\|_{L^\infty(Q)} \left(\|T\|_{L^2(Q)}\|v\|_{L^2(Q)} + |s| \, \|v\|^2_{L^2(Q)}\right)$$

$$\leq c \, \|v\|_{L^2(0,t_{\mathrm{fin}};H^1(\Omega))}$$

which gives the boundedness of the real valued linear function $\mathcal{A}(y + sv)(v)$, $s \in \mathbb{R}$ and therewith the continuity. Similar the boundedness of $\mathcal{A}v(v)$ can be shown

$$\int\limits_0^{t_{\mathrm{fin}}}\!\!\int\limits_\Omega \lambda\nabla v\nabla v + \nu vv \, dx \leq \lambda_b\|\nabla v\|^2_{L^2(0,t_{\mathrm{fin}};L^2(\Omega))} + \|v\|^2_{L^2(0,t_{\mathrm{fin}};L^2(\Omega))} \leq C \, \|v\|^2_{L^2(0,t_{\mathrm{fin}};H^1(\Omega))}.$$

For the coercivity in theorem 5.2 we have to show

$$\mathcal{A}v(v) \geq \alpha\|v\|_{L^2(0,t_{\mathrm{fin}};H^1(\Omega))}, \quad v \in L^2(0, t_{\mathrm{fin}}; H^1(\Omega)).$$

For a bounded coefficient $0 < \nu_0 \le \nu(x)$ and $v \in L^2(0, t_{\text{fin}}; H^1(\Omega))$ we have

$$\int\limits_0^{t_{\text{fin}}} \int\limits_\Omega \lambda \nabla v \nabla v + \nu \, vv \, dx \, dt \ge \int\limits_0^{t_{\text{fin}}} \left(\lambda_a \|\nabla v\|_{L^2(\Omega)}^2 + \nu_0 \|v\|_{L^2(\Omega)}^2 \right) dt$$

$$\ge \alpha \, \|v\|_{L^2(0,t_{\text{fin}};H^1(\Omega))}^2,$$

with an appropriate $\alpha > 0$.

The solution is unique if the operator $\mathcal{A}$ is monotone, hemicontinuous, bounded and coercive. This is given by Proposition 5.3 Conditions (i) and (ii) are fulfilled as shown above. The first condition in (iii) in the above proposition is satisfied with $v \in H^1(\Omega)$

$$\int_\Omega \nabla v \nabla v \, dx + \gamma \int_\Omega vv \, dx \ge \alpha \int_\Omega \nabla v \nabla v + vv \, dx,$$

with $\alpha := \min\{1, \gamma\}$. Additionally the second condition in (iii) holds, since

$$\int_\Omega \lambda \nabla v \nabla v \, dx \ge \alpha \int_\Omega \nabla v \nabla v \, dx$$

and $0 < \lambda_a \le \lambda \le \lambda_b$.

Therewith the problem (C A1.1) has a unique solution $T \in L^2(0, t_{\text{fin}}; H^1(\Omega))$ also for $u \in L^2(0, t_{\text{fin}}; H^{-1}(\Omega))$.

To prove the existence of an optimal control for a heat source $u \in L^2(0, t_{\text{fin}}; H^{-1}(\Omega))$ we can proceed as described by Tröltzsch [88]. That means we need to verify that the control-to-state operator S with $u \mapsto T = S(u)$ is continuous. Then we can apply theorem 5.4 and obtain the existence of an optimal control. In the proof of proposition 5.3, see [76], sec. III.4., p. 123, a bound for the solution by the initial condition and the right hand side is given similar to that needed for the proofs in [88], i.e. there exists a constant c such that

$$\|T\|_{L^2(0,t_{\text{fin}};H^1(\Omega))} \le c \left(\|T_{\text{body}}\|_{L^2(\Omega)} + \|u\|_{L^2(0,t_{\text{fin}};H^{-1}(\Omega))} \right). \tag{5.5}$$

A general description for parabolic problems and the derivation of such an estimate is given also in section 7.2 in [88]. Therewith we can show that the weak solution $T \in L^2(0, t_{\text{fin}}; H^1(\Omega))$ also belongs to $W(0, t_{\text{fin}})$ as described in [88], sec. 3.4.4, p. 119 ff.. Finally, the existence of a solution for the optimal control problem with an adjusted norm in the regularization term or with $\gamma = 0$ can be proved in the same way as described in section 3.5 in [88], p. 123 ff.. The proof is based on Theorem 5.4 and uses the above estimate (5.5) to show the existence of a continuous control-to-state operator $S : L^2(0, t_{\text{fin}}; H^{-1}(\Omega)) \to H^1(\Omega)$ with $u(t, x) \mapsto T(t_{\text{fin}}, x)$.

5.1.2 Problem A1.2: Identification of the electrical conductivity

For the second part of Problem A1, the identification of the electrical conductivity σ from the previously identified heat source u, a steady state optimal control problem is formulated. The idea is to fit the heat source, scaled with a constant factor $p \in \mathbb{R}$ instead of the factor $\frac{P_{\text{eff}}}{P_\Omega}$ to a given heat source u_g. In the following we will model a monopolar probe but the results are transferable as well to a bipolar probe. Moreover, we will assume a higher regularity of the potential ϕ as is given by the original problem of RFA.

The problem we will consider is as follows

$$\min_{\phi,\sigma} F(\phi,\sigma) = \frac{1}{2}\big\|p\sigma|\nabla\phi|^2 - u_g\big\|_{L^2(\Omega)}^2 + \frac{\beta}{2}\|\sigma\|_{H^s(\Omega)}^2 \tag{A1.2}$$

subject to

$$\begin{aligned}
-\mathrm{div}(\sigma\nabla\phi) &= g && \text{in } \Omega \setminus \overline{\Gamma} \\
\phi &= 0 && \text{on } \partial\Omega \\
\phi &= 1 && \text{on } \Gamma
\end{aligned} \tag{C A1.2}$$

where $\Gamma \subset \Omega$ is the electrode of the probe, $\beta \geq 0$ the regularization parameter and $s > \frac{3}{2}$. The factor s needs to be large enough to assure that $\sigma \in H^s(\Omega)$ is also in $L^\infty(\Omega)$ which is given by Sobolev's imbedding theorem if $s > \frac{N}{2}$, where N is the dimension of the space Ω, see e.g. [3], Theorem 4.12, p. 84 ff.. Further, to obtain a heat source $u \in L^2(\Omega)$ we need a potential $\phi \in H^2(\Omega)$. From the imbedding theorem we know that $H^2(\Omega) = W^{2,2}(\Omega) \subset W^{1,4}(\Omega)$ and for $\phi \in H^2(\Omega)$ it follows that $|\nabla\phi| \in L^2(\Omega)$. In Gilbarg and Trudinger [24], theorem 8.8, p. 183, it is shown that the H^2 regularity holds only locally in the inner of the computational domain. For a smooth boundary, i.e. the boundary $\partial\Omega \cup \partial\Gamma$ has to be of class C^2, the results with the higher regularity can be extended to the whole domain ([24], theorem 8.12, p. 186). Due to the shape of electrodes for the RFA the boundary of the computational domain is not as smooth as needed. However, for the following results we will assume a smooth boundary, i.e. a smooth shape of the electrodes. Then, we can assume $|\nabla\phi|^2 \in L^2(\Omega)$.

Due to the fact that a monopolar probe is modeled we can not use Neumann conditions at the outer boundaries. We use Dirichlet conditions or Robin conditions instead. In the bipolar case the boundary conditions will be adjusted to

$$\begin{aligned}
\nabla\phi \cdot n &= 0 && \text{on } \partial\Omega \\
\phi &= \pm 1 && \text{on } \Gamma := \Gamma_- \cup \Gamma_+.
\end{aligned}$$

The parameter $\sigma \in H^s(\Omega), s > \frac{3}{2}$, is bounded by $0 < \sigma_a \leq \sigma(x) \leq \sigma_b$ for all $x \in \Omega$ and $\sigma_a, \sigma_b \in \mathbb{R}$. Further we have $u_g \in L^2(\Omega)$ for the given heat source as well as $g \in L^2(\Omega)$, whereas in the identification problem we set $g = 0$. With the given assumptions the existence of an optimal control can be proved in the same way as described by Aßmann et al. [9] for Theorem 5.5. The only condition we need to verify is that the *control-to-state operator* $S : L^\infty(\Omega) \to L^2(\Omega)$ with $S(\sigma) = \sigma|\nabla\phi|^2$ exists and that it is continuous.

From Sobolev's imbedding theorem we know that $H^s(\Omega)$ is imbedded continuously in $L^\infty(\Omega)$ for $s > \frac{3}{2}$, that means $\sigma \in L^\infty(\Omega)$. Further, from Hölder's inequality ([4], Lemma 1.16, p. 51) we obtain that $S(\sigma) = \sigma|\nabla\phi|^2 \in L^2(\Omega)$ and hence the operator is continuous. Therefore, the results from [9] can be used and the existence of an optimal control for Problem A1.2 is ensured.

5.1.3 Problem A2: Identification of the thermal conductivity

In this section we will consider Problem A2, that means the identification of a spatial distributed thermal conductivity $\lambda(x)$ from temperature measurements $T_g(x)$ at a certain time t_{fin}. As in Problem A1.1 the intention is to fit the calculated temperature to the measured data and use the bio-heat transport equation as constraints. The problem is defined as

$$\min_{T,\lambda} F(T,\lambda) = \frac{1}{2}\|T(t_{\text{fin}}, x) - T_g(x)\|^2_{H^1(\Omega)} + \frac{\alpha}{2}\|\lambda\|_{H^s(\Omega)} \tag{A2}$$

subject to

$$
\begin{aligned}
\rho c \partial_t T - \operatorname{div}(\lambda \nabla T) + \nu(T - T_{\text{body}}) &= u &&\text{in } Q := [0, t_{\text{fin}}] \times \Omega, \\
T(0, x) &= T_{\text{body}} &&\text{in } \Omega \\
\nabla T \cdot n &= 0 &&\text{on } [0, t_{\text{fin}}] \times \partial\Omega,
\end{aligned}
\tag{C A2}
$$

and with

$$\lambda_a \le \lambda(x) \le \lambda_b \quad \text{a.e. in } \Omega.$$

We know that for $T_g \in L^2(Q)$, $\nu \in L^\infty(Q)$, $u \in L^2(Q)$ and $\lambda \in H^s(Q)$ with $s > 0$ we have a unique weak solution $T \in W(0, t_{\text{fin}})$, see Problem A1.1 above. However, for the following results we will consider a modified problem which is discretized in time such that we can apply again the results from [9]. Therefore, we will use a Helmholtz-term for linearizing in time and obtain a time-discrete heat equation

$$-\operatorname{div}(\lambda \nabla T) + \left(\tfrac{\rho c}{\tau} + \nu\right)T = u + \tfrac{\rho c}{\tau}T_0 + \nu T_{\text{body}},$$

where T_0 defines the initial temperature and τ the time step size. To apply the results from Aßmann et al. [9] we have to prove that the additional linear term $\left(\tfrac{\rho c}{\tau} + \nu\right)T$ does not influence the proof. As shown in section 3.4 the lemma of Lax-Milgram can be applied as well, since the coefficient $\left(\tfrac{\rho c}{\tau} + \nu\right)$ is bounded. Hence, we have the same preconditions as in [9] with a control-to-state mapping $S : L^\infty(\Omega) \to H^1(\Omega)$ such that the results can be applied and the existence of an optimal control for (A2) is ensured.

5.1.4 Problem C: Identification of temperature dependent parameters

At last we will look at an identification problem where the parameter we want to identify, depends on the temperature. For the identification of the thermal conductivity $\lambda(T)$ from temperature measurements T_g this leads to an optimal control problem constrained by

a quasi-linear PDE

$$\min_{T,\lambda} F(T,\lambda) = \frac{1}{2}\big\|T(t_{\text{fin}},x) - T_g(x)\big\|^2_{H^1(\Omega)} + \frac{\alpha}{2}\|\lambda\|_{H^s(\Omega)} \tag{C}$$

subject to

$$\begin{aligned}
\rho c\partial_t T - \operatorname{div}(\lambda(T)\nabla T) + \nu(T - T_{\text{body}}) &= u &&\text{in } Q := [0, t_{\text{fin}}] \times \Omega \\
T(0,x) &= T_{\text{body}} &&\text{in } \Omega \\
\nabla T \cdot n &= 0 &&\text{on } \partial Q,
\end{aligned} \tag{C C}$$

and with

$$\lambda_a \leq \lambda(T) \leq \lambda_b \quad \text{a.e. in } Q.$$

All functions are assumed to be as in Problem A2 above with $s > 0$.

To solve this PDE we would need either a non-linear solver or a linearization in the temperature. We will use a horizontal method of lines with respect to the time, also called method of Rothe. Method of lines are numerical techniques to solve partial differential equations, especially parabolic equations. The basic idea is to discretize the PDE in all but one dimension. The resulting equations can be solved afterwards with standard techniques [69, 70]. The method of Rothe is a semi-discrete time stepping scheme, where a nonlinear parabolic PDE is linearized with respect to the state [43]. For the present problem (C C) this means that we approximate the time derivative $\partial_t T$ with a backward Euler method and replace the temperature in the function of the thermal conductivity $\lambda(T)$ with the temperature from the previous time step, i.e. we obtain accordingly $\lambda(T^{n-1})$, $n \in \mathbb{N}$, where T^{n-1} denotes the temperature at the $(n-1)$th time step. The resulting PDE from this semi-implicit method, which is now linear in the temperature, is as follows

$$-\operatorname{div}\big(\lambda(T^{n-1})\nabla T^n\big) + \big(\tfrac{\rho c}{\tau} + \nu\big) T^n = u + \tfrac{\rho c}{\tau}T^{n-1} + \nu T_{\text{body}},$$

where $\tau > 0$ denotes the time step size for the Euler method.

The lemma of Lax-Milgram provides a unique solution $T \in H^1(\Omega)$ for every $\lambda \in L^2(\Omega)$, if λ is bounded as described above. If we set $T := T^n$ and use a linear modeling for the thermal conductivity, as described in (3.9), we have $\lambda(T^{n-1}) \in L^p(\Omega)$ for $T^{n-1} \in L^p(\Omega), 1 \leq p \leq \infty$. Thus, there exists a continuous control-to-state operator $S : L^2(\Omega) \to H^1(\Omega)$, with $\lambda \mapsto T$, such that we can apply Theorem 5.4 which gives us the existence of an optimal control for Problem (C).

5.2 The optimality systems for the identification problems

After the theoretical investigations concerning the existence of optimal controls for the different identification problems in the last section, we will go into detail for the application for the method of RFA. That means the identification problems will be described as they are used for the numerical investigations in the next chapter. Particularly the

optimality system will be derived, which means we will calculate the adjoint equations and the variational equations for the different problems. At first we will investigate the identification of the heat source and resultant the identification of the electrical conductivity. Afterwards we will turn to the identification of the thermal conductivity and an approach to optimize both parameters in one problem.

5.2.1 Problem A1.1: Identification of the heat source

As described above the identification of the electrical conductivity is divided into two steps, the identification of the heat source u, problem A1.1, and the identification of the electrical conductivity σ from the heat source, problem A1.2. Therefore, we will start with the identification of the heat source. That means we are interested in identifying the right hand side of the bio-heat transport equation and formulate this as an optimal control problem with a tracking type objective functional, as described in (A1.1). This kind of optimal control problem is well known from literature, see [88] and the references therein. Even though it is well known it is an ill-posed problem. Even small perturbations in the measured heat distribution will produce large variations in the heat source. Therefore, we will not obtain an exact numerical solution of this problem considering the absolute values of the right hand side.

Looking at the optimal control problem depicted in (A1.1) we calculate the corresponding adjoint system and variational inequality by using the Lagrange technique. For theoretical reasons we have to assume $u \in L^2(0, t_{\text{fin}}; H^{-1}(\Omega))$, whereas for practical application we assume additionally $\int_{\Omega} (\nabla u(t_{\text{fin}}, x)^2 \, dx < \infty$. The assumed higher regularity of the control u permits the use of a modified regularization term to reduce the variations in the heat source u. That means we will use $\frac{\gamma}{2} \int_{\Omega} (\nabla u(t_{\text{fin}}, x))^2 \, dx$ instead of the H^{-1}-norm at the final time t_{fin} as regularization

The Lagrange function $\mathcal{L} : W(0, t_{\text{fin}}) \times L^2(0, t_{\text{fin}}; H^{-1}(\Omega)) \times W(0, t_{\text{fin}}) \to \mathbb{R}$ with the Lagrange multiplier $\mu \in W(0, t_{\text{fin}})$ is given by the following equation

$$
\begin{aligned}
\mathcal{L}(T, u, \mu) &= F(T, u) - (h(T, u), \mu)_{L^2(Q)} \\
&= \frac{1}{2} \int_{\Omega} (T(t_{\text{fin}}, x) - T_g(x))^2 \, dx + \frac{1}{2} \int_{\Omega} (\nabla (T(t_{\text{fin}}, x) - T_g(x)))^2 \, dx \\
&\quad + \frac{\gamma}{2} \int_{\Omega} (\nabla u(t_{\text{fin}}, x))^2 \, dx - \int_0^{t_{\text{fin}}} \int_{\Omega} \rho c \partial_t T \mu \, dx \, dt \\
&\quad - \int_0^{t_{\text{fin}}} \int_{\Omega} \lambda \nabla T \nabla \mu \, dx \, dt - \int_0^{t_{\text{fin}}} \int_{\Omega} \nu \left(T - T_{\text{body}}\right) \mu \, dx \, dt \\
&\quad + \int_0^{t_{\text{fin}}} \int_{\Omega} u \mu \, dx \, dt - \int_0^{t_{\text{fin}}} \int_{\Omega_{\text{pr}}} \left(T - T_{\text{body}}\right) \mu \, dx \, dt,
\end{aligned}
$$

where $h(T, u)$ denotes the constraints described in (C A1.1) and $\gamma \in \mathbb{R}$ denotes the regularization parameter. To derive the adjoint equation we have to differentiate the Lagrange function with respect to the state T. Using integration by parts we obtain the following adjoint equation

$$\begin{aligned}
\rho c \partial_t \mu - \operatorname{div}(\lambda \nabla \mu) + \nu \mu &= 0 && \text{in } Q \\
\mu(t_{\text{fin}}, x) &= T(t_{\text{fin}}, x) - T_g - \operatorname{div}\left(\nabla(T(t_{\text{fin}}, x) - T_g)\right) && \text{in } \Omega, \\
\mu(t, x) &= 0 && \text{on } [0, t_{\text{fin}}] \times \Omega_{\text{pr}}, \\
\nabla \mu(t, x) \cdot n &= 0 && \text{on } [0, t_{\text{fin}}] \times \partial \Omega,
\end{aligned}$$

with $Q := [0, t_{\text{fin}}] \times \Omega$. And for the corresponding variational inequality we have

$$D_u \mathcal{L}(T, u, \mu)(v - u) = \gamma \int_{\Omega} \nabla u \nabla (v(t_{\text{fin}}) - u) \, dx + \int_0^{t_{\text{fin}}} \int_{\Omega} \mu(v - u) \, dx \, dt \geq 0 \quad \forall v \in U_{\text{ad}}^u, \tag{5.6}$$

with $U_{\text{ad}}^u = \{u \in L^2(0, t_{\text{fin}}; H^{-1}(\Omega)) \mid u_a \leq u \leq u_b \text{ a.e. in } \Omega \text{ and } \int_{\Omega} (\nabla u(t_{\text{fin}}, x))^2 \, dx < \infty\}$.

Due to the restriction of the objective functional on the final time t_{fin} the derivative of the objective can be found now in the boundary condition of the adjoint system. Altogether we obtain a time dependent system with a boundary condition at the final time t_{fin} and on the spatial boundaries. This end-time condition makes the whole system hard to solve. We would need a simple shooting method or for a more stable result a multiple shooting method. Another possibility is to simplify the whole problem by using either only one time step, which can be described by a Helmholtz-term, or to reduce the whole problem to a steady state system

$$\min_{T, u} F(T, u) := \frac{1}{2} \|T - T_g\|_{H^1(\Omega)}^2 + \frac{\gamma}{2} \int_{\Omega} (\nabla u)^2 \, dx \tag{A1.1'}$$

such that

$$\begin{aligned}
-\operatorname{div}(\lambda \nabla T) &= u - \nu(T - T_{\text{body}}) && \text{in } \Omega, \\
T &= T_{\text{body}} && \text{on } \Omega_{\text{pr}}, \tag{C A1.1'} \\
\nabla T \cdot n &= 0 && \text{on } \partial \Omega,
\end{aligned}$$

and with

$$u_a(x) \leq u(x) \leq u_b(x) \quad \text{a.e. in } \Omega.$$

The resulting simplified Lagrange functional $\mathcal{L}$ with the Lagrange multiplier $\mu \in H^1(\Omega)$ and the corresponding adjoint system are as follows

$$
\begin{aligned}
\mathcal{L}(T, u, \mu) \quad = \quad & \frac{1}{2} \int_\Omega (T - T_g)^2 \, dx + \frac{1}{2} \int_\Omega (\nabla(T - T_g))^2 \, dx + \frac{\gamma}{2} \int_\Omega (\nabla u)^2 \, dx \\
& - \int_\Omega \lambda \nabla T \nabla \mu \, dx - \int_\Omega \nu (T - T_{\text{body}}) \mu \, dx \\
& - \int_{\Omega_{\text{pr}}} (T - T_{\text{body}}) \mu \, dx
\end{aligned}
$$

and hence the adjoint system

$$
\begin{aligned}
-\text{div}(\lambda \nabla \mu) + \nu \mu &= (T - T_g) - \text{div}\,(\nabla(T - T_g)) & & \text{in } \Omega, \\
\mu &= 0 & & \text{on } \Omega_{\text{pr}}, \\
\nabla \mu \cdot n &= 0 & & \text{on } \partial \Omega.
\end{aligned}
\tag{5.7}
$$

The variational inequality is apart from the integrals mainly the same as in (5.6)

$$
D_u \mathcal{L}(T, u, \mu)(v - u) = \int_\Omega \mu(v - u) \, dx + \gamma \int_\Omega \nabla u \nabla(v - u) \, dx \geq 0
\tag{5.8}
$$

for all $v \in U^u_{\text{ad}}$ with $U^u_{\text{ad}} := \{u \in H^{-1}(\Omega) | \, u_a(x) \leq u(x) \leq u_b(x) \text{ and } \int_\Omega (\nabla u)^2 \, dx < \infty\}$.

5.2.2 Problem A1.2: Identification of the electrical conductivity

For the second step in the splitted identification problem A1 for the electrical conductivity we consider two different settings. The first one is the original problem with the scaling term $\frac{P_{\text{eff}}}{P_\Omega}$. The second one is a simplified model, where we replace the scaling term $\frac{P_{\text{eff}}}{P_\Omega}$ by a constant factor $p \in \mathbb{R}$, as described in (A1.2) and (C A1.2). In both cases we assume a higher regularity for the heat source u than provided by the RFA model to ensure the existence of an optimal control as described in section 5.1.2. For the numerical implementation, presented in the next chapter, the optimization works despite the fact that the boundary of the computational domain is not as smooth as necessary due to the shape of the electrodes. This is based on the spatial discretization. Probably, for a discretization where the grid size tends to zero the optimization will fail.

5.2.2.1 The model including the scaling term

In this first approach to identify a spatially distributed electrical conductivity σ we consider the optimal control problem (A1.2) with the actual scaling term $\frac{P_{\text{eff}}}{P_\Omega}$ instead of the approximation p.. The aim is to determine the electrical conductivity σ from a given heat source u_g calculated before. At first we need to derive the optimality system. This is done by using the Lagrange method to calculate the adjoint system and the variational inequality. Again the regularization is slightly modified. Instead of using the

full H^s-norm, with $s > \frac{3}{2}$, we will regularize the gradient only, i.e. we use $\frac{\beta}{2}\|\nabla\sigma\|^2_{L^2(\Omega)}$ as regularization term. The Lagrange function $\mathcal{L}(\phi, \sigma, \mu) : H^1(\Omega) \times H^s(\Omega) \times H^1(\Omega) \to \mathbb{R}$, $s > \frac{3}{2}$, with the Lagrange multiplier $\mu \in H^1(\Omega)$ for the considered problem is as follows

$$\mathcal{L}(\phi, \sigma, \mu) = \frac{1}{2} \int_\Omega \left(\frac{P_{\text{eff}}}{P_\Omega} \sigma |\nabla\phi|^2 - u_g \right)^2 dx + \frac{\beta}{2} \int_\Omega (\nabla\sigma)^2 dx$$
$$- \int_\Omega \sigma \nabla\phi \nabla\mu \, dx - \int_{\Gamma_+} (\phi - 1) \, \mu \, dx$$
$$- \int_{\Gamma_-} (\phi + 1) \, \mu \, dx.$$

To derive the corresponding adjoint equation of the problem, we need to consider the derivative of the Lagrangian function with respect to the potential ϕ. In the following we will concentrate on the model for a bipolar probe. The only term in the bio-heat transfer equation which is influenced by the polarity of the applicator is the term P_{eff}. This term can be considered separately in case of a monopolar probe.

The derivative of the Lagrangian is as follows

$$D_\phi \mathcal{L}(\phi, \sigma, \mu)(h) = 2 \int_\Omega q(\phi, \sigma) \left(\frac{P_{\text{eff}}}{P_\Omega} \sigma \nabla\phi \nabla h \right) dx$$
$$- \int_\Omega q(\phi, \sigma) \frac{64 R_I^2 P_{\text{set}}}{(4 + R_I P_\Omega)^3} \sigma |\nabla\phi|^2 \, dx \int_\Omega \sigma \nabla\phi \nabla h \, dx$$
$$- \int_\Omega \sigma \nabla h \nabla\mu \, dx - \int_{\Gamma_+} h\mu \, dx - \int_{\Gamma_-} h\mu \, dx,$$

with

$$q(\phi, \sigma) := \tfrac{P_{\text{eff}}}{P_\Omega} \sigma |\nabla\phi|^2 - u_g \tag{5.9}$$

and

$$P_\Omega(\phi, \sigma) = \int_\Omega \sigma |\nabla\phi|^2 \, dx,$$
$$\frac{P_{\text{eff}}}{P_\Omega} = \frac{16 R_I P_{\text{set}}}{(4 + R_I P_\Omega)^2},$$
$$D_\phi P_\Omega(\phi, \sigma)(h) = \int_\Omega 2\sigma(x) \nabla\phi(x) \nabla h(x) \, dx,$$
$$D_\phi \left(\frac{P_{\text{eff}}}{P_\Omega} \right)(h) = -2 \frac{16 R_I^2 P_{\text{set}}}{(4 + R_I P_\Omega)^3} \int_\Omega \sigma \nabla\phi \nabla h \, dx.$$

In case of a monopolar probe only the term $\frac{P_{\text{eff}}}{P_\Omega}$ and its derivative change. For $\phi = 1$ at the electrode we obtain

$$
\frac{P_{\text{eff}}}{P_\Omega} = \frac{4R_I P_{\text{set}}}{(1 + R_I P_\Omega)^2},
$$

$$
D_\phi\left(\frac{P_{\text{eff}}}{P_\Omega}\right)(h) = -2\frac{4R_I^2 P_{\text{set}}}{(1 + R_I P_\Omega)^3}\int_\Omega \sigma\nabla\phi\nabla h\, dx.
$$

These terms can be set appropriately in the Lagrangian. For the derivation of $\frac{P_{\text{eff}}}{P_\Omega}$ see chapter 3.

By solving $D_\phi\mathcal{L}(\phi, \sigma, \mu)(h) = 0$ for all functions $h \in H^1(\Omega)$ and defining the Lagrange multiplier appropriately, we obtain the corresponding adjoint equation

$$
\begin{aligned}
-\operatorname{div}(\sigma\nabla\mu) =\ & \operatorname{div}(\sigma\nabla\phi)\int_\Omega q(\phi,\sigma)2\frac{16R_I^2 P_{\text{set}}}{(4+R_I P_\Omega)^3}\,\sigma|\nabla\phi|^2\, dx \\
& -2\operatorname{div}\left(q(\phi,\sigma)\frac{P_{\text{eff}}}{P_\Omega}\sigma\nabla\phi\right) && \text{in } \Omega\setminus\overline{\Gamma}, \\
\nabla\phi\cdot n =\ & 0 && \text{on } \partial\Omega, \\
\phi =\ & 0 && \text{on } \Gamma_+\cup\Gamma_-.
\end{aligned}
$$

For the variational inequality we need $D_\sigma\mathcal{L}(\overline{\phi},\overline{\sigma},\mu)(\sigma-\overline{\sigma}) \geq 0$. The derivative with respect to the electrical conductivity σ is given as

$$
\begin{aligned}
D_\sigma\mathcal{L}(\phi,\sigma,\mu)(v-\sigma) = & \int_\Omega \left(g(\sigma)\sigma|\nabla\phi|^2 - u_g\right)g(\sigma)(v-\sigma)|\nabla\phi|^2 \\
& + \int_\Omega \left(g(\sigma)\sigma|\nabla\phi|^2 - u_g\right)g'(\sigma)P_\Omega(v-\sigma)\sigma|\nabla\phi|^2\, dx \\
& + \beta\int_\Omega \nabla\sigma\nabla(v-\sigma)\, dx - \int_\Omega \nabla\phi\nabla\mu(v-\sigma)\, dx \\
\geq & 0 \qquad \forall v \in U_{\text{ad}}^\sigma,
\end{aligned}
$$

with the admissible set for the control σ for a certain $s > \frac{3}{2}$

$$
U_{\text{ad}}^\sigma := \{\sigma \in H^s(\Omega)\,|\, 0 < \sigma_a(x) \leq \sigma(x) \leq \sigma_b(x)\}.
$$

And with the auxiliary function

$$
g(\sigma) := \frac{P_{\text{eff}}}{P_\Omega(\sigma)},
$$

$$
\partial_\sigma g(\sigma)(v) = \begin{cases} -2\frac{16R_I^2 P_{\text{set}}}{(4+R_I P_\Omega(\sigma))^3}P_\Omega(v) & \text{(bipolar applicator)}, \\[2mm] -2\frac{4R_I^2 P_{\text{set}}}{(1+R_I P_\Omega(\sigma))^3}P_\Omega(v) & \text{(monopolar applicator)}. \end{cases} \tag{5.10}
$$

Finally, if we consider $f(\sigma) := F(\phi(\sigma), \sigma)$ as a function of σ, the total derivative $f'(\sigma)$ of the objective functional with respect to the electrical conductivity σ for the setting

with a bipolar probe is

$$f'(\sigma) = |\nabla\phi|^2 \int_\Omega q(\phi,\sigma) \frac{32 R_I^2 P_{\text{set}}}{(4 + R_I P_\Omega)^3} \sigma |\nabla\phi|^2 \, dx$$
$$- q(\phi,\sigma) \frac{P_{\text{eff}}}{P_\Omega} |\nabla\phi|^2 - \alpha \text{div}(\nabla\sigma) + \nabla\phi\nabla\mu,$$

with the adjoint state μ and $q(\phi,\sigma)$ as defined in (5.9). As mentioned before, the scaling term produces difficulties for the optimization if we assume a spatially distributed electrical conductivity σ. Due to the locally varying effect of the power density we obtain a local highly steep gradient which precludes an optimization for the current setting. The steepness of the gradient is increased by the scaling term which depends on the electrical conductivity again.

To deal with these limitations we will reformulate the problem in the next section with a constant scaling term.

5.2.2.2 Simplifying the model to evade the scaling term

The whole identification problem is simplified by replacing the actual scaling factor by a real value $p \in \mathbb{R}$, cf. (A1.2). Let us assume that the setup power P_{set} and the inner resistance of the generator R_I are constant values, then we can consider the scaling factor as a real valued function in σ

$$g(\sigma) := \frac{P_{\text{eff}}}{P_\Omega}(\sigma) : H^s(\Omega) \to \mathbb{R}.$$

The assumption of constant values P_{set} and R_I is reasonable since these values may change only in time but the considered problem (A1.2) is not time-dependent. The function $g(\sigma)$ can be approximated by a constant value $p \in \mathbb{R}$. In the end the product $p\sigma$ is identified instead of σ. With this approximation the target functional reduces to

$$\min_{\phi,\sigma} F(\phi,\sigma) := \frac{1}{2} \left\| p\,\sigma |\nabla\phi|^2 - u_g \right\|_{L^2(\Omega)}^2 + \frac{\beta}{2} \left\| \nabla\sigma \right\|_{L^2(\Omega)}^2$$

The adjoint system and the variational inequality simplifies accordingly to

$$\begin{aligned}
-\text{div}(\sigma\nabla\mu) &= 2\text{div}\big(\big(p\,\sigma|\nabla\phi|^2 - u_g\big)\,p\,\sigma\nabla\phi \big) &&\text{in } \Omega \setminus \overline{\Gamma}, \\
\nabla\phi \cdot n &= 0 &&\text{on } \partial\Omega, \\
\phi &= 0 &&\text{on } \Gamma = \Gamma_+ \cup \Gamma_-.
\end{aligned}$$

and

$$D_\sigma \mathcal{L}(\phi, \sigma, \mu)(v - \sigma) = p \int_\Omega \left(p\,\sigma |\nabla\phi|^2 - u_g \right) (v - \sigma) |\nabla\phi|^2 \, dx$$

$$+ \beta \int_\Omega \nabla\sigma \nabla(v - \sigma) \, dx + \int_\Omega \nabla\phi \nabla\mu \, (v - \sigma) \, dx$$

$$\geq 0 \quad \forall v \in U^\sigma_{\text{ad}},$$

where U^σ_{ad} denotes the admissible set for the control σ as before.

The problem differs slightly from the original one since the value of σ depends now on the chosen approximation p for the scaling term.

5.2.2.3 Simplified model with an additional scaling term

Beside the problem with the scaling term the spatial high variety of the gradient persists, i.e. the gradient of the potential varies a lot on the spatial domain. Near the electrodes we have a really steep descent and at the outer boundary the gradient flattenes. Therefore, we introduce a scaling term in the objective to smooth the derivative and improve the optimization or rather make it possible. This can be achieved by scaling the fitting term in the target function with the piecewise reciprocal of the squared gradient, denoted by

$$\mathcal{S} := \begin{cases} \frac{1}{|\nabla\phi|^2}, & \text{if } \nabla\phi \neq 0, \\ 1, & \text{if } \nabla\phi = 0. \end{cases}$$

If the gradient is equal to zero, e.g. at the electrodes, the scaling $\mathcal{S}$ is set to 1. The target functional then becomes

$$\min_{\phi, \sigma} F(\phi, \sigma) := \frac{1}{2} \| \mathcal{S} \left(p\,\sigma |\nabla\phi|^2 - u_g \right) \|^2_{L^2(\Omega)} + \frac{\beta}{2} \|\nabla\sigma\|^2_{L^2(\Omega)}. \tag{A1.2'}$$

With this additional scaling the adjoint equation and the variational inequality change accordingly. The adjoint state can be calculated by the following adjoint system

$$\begin{aligned} -\text{div}(\sigma \nabla \mu) &= -\text{div}\left(2 \left(\mathcal{S} \right)^2 \left(p\,\sigma |\nabla\phi|^2 - u_g \right) \mathcal{S} u_g \nabla\phi \right) & \text{in } \Omega \setminus \overline{\Gamma} \\ \nabla\phi \cdot n &= 0 & \text{on } \partial\Omega, \\ \phi &= 0 & \text{on } \Gamma_+ \cup \Gamma_-. \end{aligned} \tag{5.11}$$

Further as variational inequality we obtain

$$D_\sigma \mathcal{L}(\phi, \sigma, \mu)(v - \sigma) = \int_\Omega \mathcal{S} \left(p\,\sigma |\nabla\phi|^2 - u_g \right) p(v - \sigma) \, dx$$

$$+ \beta \int_\Omega \sigma(v - \sigma) \, dx - \int_\Omega \nabla\phi \nabla\mu \, (v - \sigma) \, dx \tag{5.12}$$

$$\geq 0 \quad \forall v \in U^\sigma_{\text{ad}},$$
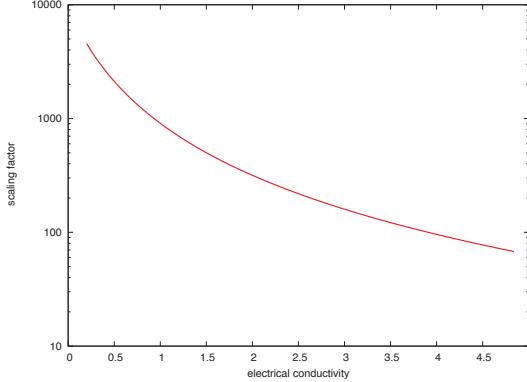
Figure 5.4: The scaling factor $\frac{P_{\text{eff}}}{P_\Omega}$ as function of the electrical conductivity $\sigma\,(\text{S m}^{-1})$, displayed in a logarithmic scale.

with the admissible set U_{ad}^σ for the control σ as before.

In the above modeling with the approximation p of the actual scaling term $\frac{P_{\text{eff}}}{P_\Omega}$ we must have in mind that the size of the scaling term depends on different values as the generator power P_{set}, the generator impedance R_I and last but not least on the parameter σ. Small changes in these values may cause large changes in the scaling term. Therefore, we need a really good approximation p to be able to calculate the correct electrical conductivity. The dependence of the scaling term $\frac{P_{\text{eff}}}{P_\Omega}$ on the electrical conductivity σ is shown in figure 5.4. Especially for the values of the electrical conductivity σ in human tissue, which are typically in the range of $[0,2]\,\text{Sm}^{-1}$, considerable differences for the scaling factor are observable.

In the above optimization problem we consider all the time the product $p\sigma$ of the approximated scaling factor and the electrical conductivity, which correlates to the desired product except that we do not know the exact factorization. That means for an over estimating of the approximated scaling term p in the beginning the resulting electrical conductivity σ is smaller than the optimal one and vice versa. Because of the complexity of the scaling term we are not able to solve this problem finally. However, for the aim of the above optimization problem the identification of the product is a good step towards the improvement for the modeling depending on temperature changes. The finally calculated heat source and the temperature distribution are not affected by the scaling. Otherwise, if we change e.g. the power during the ablation, it becomes important to know the electrical conductivity itself and not only the product of the scaling term and the conductivity. Therefore, it is still important to develop an identification problem for the electrical conductivity itself.

5.2.3 Problem A2: Identification of the thermal conductivity

For the identification of a spatially distributed thermal conductivity we consider problem A2. That means we want to identify the thermal conductivity λ from given temperature

measurements T_g at a certain time t_{fin}. The objective functional is described in (A2) and the constraints $h(T, \lambda)$ are described in (C A2). In the following we will assume $\lambda \in L^2(0, t_{\text{fin}}; H^1(\Omega))$ and use accordingly the H^1-norm for the regularization.
The Lagrange function $\mathcal{L} : W(0, t_{\text{fin}}) \times L^2(0, t_{\text{fin}}; H^1(\Omega)) \times W(0, t_{\text{fin}}) \to \mathbb{R}$ with the Lagrange multiplier $\mu \in W(0, t_{\text{fin}})$ is given by the following equation

$$
\begin{aligned}
\mathcal{L}(T, \lambda, \mu) \;=\;& F(T, \lambda) - (h(T, \lambda), \mu)_{L^2(\Omega)} \\
=\;& \frac{1}{2} \int_\Omega (T(t_{\text{fin}}, x) - T_g(x))^2 \, dx + \frac{1}{2} \int_\Omega \left(\nabla(T(t_{\text{fin}}, x) - T_g(x))\right)^2 dx \\
& + \frac{\alpha}{2} \int_\Omega \lambda^2 \, dx + \frac{\alpha}{2} \int_\Omega (\nabla\lambda)^2 \, dx - \int_0^{t_{\text{fin}}}\!\!\int_\Omega \rho c \partial_t T \mu \, dx \, dt \\
& - \int_0^{t_{\text{fin}}}\!\!\int_\Omega \lambda \nabla T \nabla \mu \, dx \, dt - \int_0^{t_{\text{fin}}}\!\!\int_\Omega \nu \left(T - T_{\text{body}}\right) \mu \, dx \, dt \\
& + \int_0^{t_{\text{fin}}}\!\!\int_\Omega \frac{P_{\text{eff}}}{P_\Omega} \sigma |\nabla\phi|^2 \mu \, dx \, dt - \int_{\Omega_{\text{pr}}} (T - T_{\text{body}}) \mu \, dx \, dt \\
& - \int_0^{t_{\text{fin}}}\!\!\int_{\Omega_{\text{pr}}} (T - T_{\text{body}}) \mu \, dx \, dt - \int_0^{t_{\text{fin}}}\!\!\int_{\partial\Omega} \nabla T \cdot n \mu \, dx \, dt.
\end{aligned}
$$

The corresponding adjoint equation to the problem can be obtained technically by differentiating the above Lagrange function with respect to the temperature T. By using integration by parts and reformulating the system we obtain the following adjoint system which is a backwards heat equation

$$
\begin{aligned}
\rho c \partial_t \mu - \text{div}(\lambda \nabla \mu) + \nu \mu &= 0 && \text{in } Q := [0, t_{\text{fin}}] \times \Omega, \\
\mu(t_{\text{fin}}, x) &= T(t_{\text{fin}}, x) - T_g(x) && \\
&\quad - \text{div}\big(\nabla(T(t_{\text{fin}}, x) - T_g(x))\big) && \text{in } \Omega, \quad\quad (5.13) \\
\mu(t, x) &= 0 && \text{on } [0, t_{\text{fin}}] \times \Omega_{\text{pr}}, \\
\nabla\mu(t, x) \cdot n &= 0 && \text{on } [0, t_{\text{fin}}] \times \partial\Omega,
\end{aligned}
$$

with the adjoint state μ. Such a PDE backward in time can be solved by a multiple shooting method (further explanations for multiple shooting are given e.g. in [79], section 7.3).
The variational inequality can be calculated by differentiating the Lagrangian with re-

spect to the control λ

$$D_\lambda \mathcal{L}(T, \lambda, \mu)(v - \lambda) = \alpha \int_\Omega \lambda(v - \lambda)\, dx + \alpha \int_\Omega \nabla\lambda\nabla(v - \lambda)\, dx - \int_0^{t_{\text{fin}}} \int_\Omega \nabla T \nabla\mu(v - \lambda)\, dx\, dt,$$

for all $v \in U_{\text{ad}}^\lambda := \{\lambda \in L^2(0, t_{\text{fin}}; H^1(\Omega)) \,|\, 0 < \lambda_a \leq \lambda \leq \lambda_b\}$. The derived adjoint equation and the variational inequality can be used to solve the optimal control problem for example with a gradient method, where the variational inequality provides the descent direction.

For practical application the identification of a spatially distributed thermal conductivity λ as described above is nearly impossible, like the identification of the electrical conductivity. Due to the only local influence of the temperature on the domain, the gradient is almost flat except for the vicinity of the probe, where the gradient with respect to the thermal conductivity is steep. Therefore, we would need an appropriate scaling as for the electrical conductivity. However, this will not be subject to the present investigations.

In the next section we will describe another idea for the identification of the thermal conductivity. This approach is later on used for the identification of temperature dependent conductivities as well as for tissue dependent parameters, which is then formulated as a nonlinear optimization problem.

5.2.4 Problem B and C: Identification of temperature and tissue dependent conductivities

In this section we will investigate an approach for the identification which neglects the temperature as optimization variable and reduces the whole problem to an identification problem without any constraints, beside the box constraints for the control. Correspondingly we would need another possibility to calculate the derivative of the objective functional with respect to the optimization variable, since we do not have an adjoint system any longer. This method is later on used for the identification of the temperature dependent parameters as well as for tissue dependent parameters. Theoretically, problem B with tissue dependent parameters is a special case of problem A with spatially distributed parameters, if we consider the parameter function as piecewise constant. But practically the following approach proved to be a good method for the identification of tissue dependent parameters as well.

At first we formulate a general optimal control problem where the control is used as optimization variable only and apply it afterwards to the identification of the material parameters in RFA. Later on the problem will be changed into a nonlinear optimization problem.

The general optimal control problem is given by

$$\min_u f(u) := F(y(u), u),$$

where the objective $F(y, u)$ is reduced to an objective $f(u)$ which depends on the control u only. The former constraints enter this problem via the state $y(u)$, which is calculated by solving $h(y, u) = 0$, compare with (OCP). To differentiate the objective properly we have to use the chain rule, i.e.

$$\frac{\partial}{\partial u} f[w] = \frac{\partial}{\partial y} F \frac{\partial}{\partial u} y[w], \tag{5.14}$$

where $\frac{\partial}{\partial u} f[w]$ denotes the directional derivative of the objective f along w with respect to the control u.

Usually the first factor, the derivative of the objective with respect to the state $\frac{\partial F}{\partial y}$, can be calculated without any difficulties. Whereas the second factor needs some further investigations. Assume we have given a general parabolic PDE

$$\partial_t y(t, x) - \text{div}(u(x) \nabla y(t, x)) = g(t, x)$$

with appropriate boundary conditions. For the derivative of the state y with respect to the control u we apply the differential operator to the above equation and obtain

$$\frac{\partial}{\partial u} \left(\partial_t y - \text{div}(u \nabla y) \right) [w] = \frac{\partial}{\partial u} g[w]$$

$$\partial_t \left(\frac{\partial}{\partial u} y[w] \right) - \text{div} \left(w \nabla y + u \nabla \left(\frac{\partial}{\partial u} y[w] \right) \right) = 0$$

$$\partial_t \left(\frac{\partial}{\partial u} y[w] \right) - \text{div} \left(u \nabla \frac{\partial}{\partial u} y[w] \right) = \text{div}(w \nabla y).$$

By defining $\psi := \frac{\partial}{\partial u} y[w]$ we may rewrite the above equation as a PDE in ψ

$$\partial_t \psi - \text{div}(u \nabla \psi) = \text{div}(w \nabla y). \tag{5.15}$$

That means we have to solve (5.15) for ψ to obtain the derivative $\frac{\partial}{\partial u} y[w]$.

To apply the above results to the identification of the thermal conductivity we will consider the following objective functional

$$f(\lambda) = F(T(\lambda), \lambda) := \frac{1}{2} \left\| T(t_{\text{fin}}, x) - T_g(x) \right\|_{L^2(\Omega)}^2 + \frac{\alpha}{2} \| \lambda \|_{L^2(\Omega)}^2. \tag{5.16}$$

Instead of the H^1-norm as used in (A2), the L^2-norm is used. This is justified because the thermal conductivity and the electrical conductivity are modeled as spatially constant or as piecewise constant at the different tissue types (liver, tumor, vascular system). Hence the temperature distribution will be smoother than for spatially varying conductivities

and accordingly the term $\int_{\Omega} \left(\nabla (T - T_g) \right)^2 dx$ influences the objective functional not that much. On the contrary, for the model with spatially distributed conductivities this term is the main part of the objective functional and has to be taken into account necessarily. According to the explanations above the derivative of the functional (5.16) with respect to the thermal conductivity λ can be calculated by using the chain rule (5.14) and we obtain

$$D_\lambda f(v) = D_T F(\partial_\lambda T)(v) = \int_{\Omega} (T - T_g) \partial_\lambda T v \, dx + \alpha \int_{\Omega} \lambda v \, dx,$$

where $\partial_\lambda T$ denotes the derivative of the temperature with respect to the thermal conductivity λ. The derivative $\partial_\lambda T$ can be calculated either by using the difference quotient or by solving an appropriate PDE in $\partial_\lambda T$, compare (5.15),

$$\rho c \partial_t (\partial_\lambda T) - \mathrm{div}(\lambda \nabla (\partial_\lambda T)) + \nu (\partial_\lambda T) = \mathrm{div}(v \nabla T).$$

With this formulation we are able to solve the problem without the need to solve a PDE backward in time as we will have to do if we use the adjoint equation (5.13) above.

If we model the thermal conductivity as a linear temperature dependent function as described in section 3.3.3, we obtain an additional factor in the chain rule and the derivative of the target functional becomes

$$D_{\lambda_{\mathrm{ref}}} f(v) = D_T F(\partial_\lambda T)(\partial_{\lambda_{\mathrm{ref}}} \lambda)(v)$$
$$= \int_{\Omega} (T - T_g) \partial_\lambda T (1 + \alpha_\lambda (T - T_{\mathrm{ref}})) v \, dx + \alpha \int_{\Omega} \lambda (1 + \alpha_\lambda (T - T_{\mathrm{ref}})) v \, dx$$

for the coefficient function $\lambda_{\mathrm{ref}}(x)$. For the coefficient function $\alpha_\lambda(x)$ we obtain analogously

$$D_{\alpha_\lambda} f(v) = D_T F(\partial_\lambda T)(\partial_{\alpha_\lambda} \lambda)(v)$$
$$= \int_{\Omega} (T - T_g) \partial_\lambda T \lambda_{\mathrm{ref}} (T - T_{\mathrm{ref}}) v \, dx + \alpha \int_{\Omega} \lambda \lambda_{\mathrm{ref}} (T - T_{\mathrm{ref}}) v \, dx.$$

Suppose that we define σ as a constant function in Ω or as a piecewise constant function on the three different tissue types (tumor, native liver and blood vessels), the approach can also be applied to the optimization of the electrical conductivity σ. Also a linear temperature dependent modeling for the electrical conductivity is possible. Let us consider the following objective functional, similar to (5.16)

$$f(\sigma) = F(T(\sigma), \sigma) := \frac{1}{2} \left\| T(t_{\mathrm{fin}}, x) - T_g(x) \right\|^2_{L^2(\Omega)} + \frac{\beta}{2} \|\sigma\|^2_{L^2(\Omega)}. \tag{5.17}$$

The derivative becomes little more complex as we have to differentiate the heat source on the right hand side of the heat equation too. The resulting PDE is nearly the same as for

the thermal conductivity except the right hand side. The derivative of the temperature with respect to the electrical conductivity $\partial_\sigma T$ can be calculated with the following PDE

$$\rho c \partial_t (\partial_\sigma T) - \text{div}(\lambda \nabla(\partial_\sigma T)) + \nu(\partial_\sigma T) = \partial_\sigma Q_{\text{rf}},$$

with

$$\begin{aligned}
\partial_\sigma Q_{\text{rf}}[w] &= \partial_\sigma \left(\frac{P_{\text{eff}}}{P_\Omega} \sigma |\nabla \phi|^2 \right) [w] \\
&= \partial_\sigma \left(\frac{P_{\text{eff}}}{P_\Omega} \right) \sigma |\nabla \phi|^2 + \frac{P_{\text{eff}}}{P_\Omega} w |\nabla \phi|^2 + 2 \frac{P_{\text{eff}}}{P_\Omega} \sigma \nabla \phi \nabla \psi[w].
\end{aligned}$$

The derivative of the potential with respect to σ is denoted by $\psi := \partial_\sigma \phi$ and can be calculated as solution of the PDE

$$-\text{div}(\sigma \nabla \psi) = \text{div}(w \nabla \phi).$$

The derivative of the scaling factor is given by

$$\partial_\sigma \left(\frac{P_{\text{eff}}}{P_\Omega} \right) [w] = \begin{cases} -2 \frac{16 R_I^2 P_{\text{set}}}{(4 + R_I P_\Omega(\sigma))^3} P_\Omega(w) & \text{(bipolar applicator)}, \\ -2 \frac{4 R_I^2 P_{\text{set}}}{(1 + R_I P_\Omega(\sigma))^3} P_\Omega(w) & \text{(monopolar applicator)}. \end{cases}$$

compare with (5.10) in section 5.2.2.1.

The advantage of the temperature or tissue dependent modeling is that the only local impact of the temperature does not matter. For the linear temperature dependent conductivities the influence of the temperature on the parameters is valid on the whole domain and not only locally. Therewith the locally steep descent as in problem A is avoided and an optimization is possible which is valid on the whole domain. Otherwise is the complexity of the modeling limited. That means it is impossible to use a polynomial of higher degree for the modeling of the electrical conductivity because that will lead to a loss of regularity for the optimization parameter. But a linear model for the electrical conductivity does not cope with the complex behavior of the parameter during the RFA, as can be seen in the measured data from porcine liver depicted in figure 5.1.

If the linear temperature dependent parameters are modeled with constant coefficients we obtain a nonlinear optimization problem instead of the original optimal control problem. That means the control reduces to a finite dimensional vector. For linear temperature dependent and additional tissue dependent parameters

$$\begin{aligned}
\lambda(T) &= \lambda_{\text{ref}}(1 + \alpha_\lambda(T - T_{\text{ref}})) \\
\sigma(T) &= \sigma_0 + \sigma_1(T - T_{\text{ref}})
\end{aligned}$$

we obtain at most a six-dimensional vector for each parameter. Two coefficients $(\lambda_{\text{ref}}, \alpha_\lambda)$ or (σ_0, σ_1) for each tissue type (liver, tumor and vascular system). Therewith the dimension for the controls is considerably reduced.

This optimization problem has to be solved in a different way as described above. Due to the small number of variables it is advisable to use an approximation of the derivative as for example central differences instead of the method described above. For the numerical results presented in the next chapter the nonlinear optimization solver WORHP [62] is used. The solver provides different approximation strategies for the gradient or the Hessian.

The reformulation of the problem as a nonlinear optimization problem has advantages as well as drawbacks. The reduced dimensionality is a great advantage and the consideration of the temperature dependence improves the optimization since the locally steep gradient is avoided. But for real applications we are not able to account for spatial variations in the measured data. If we have another kind of dependence on the temperature distribution than a linear dependency, we will get some troubles. That means we have to know the kind of temperature dependence in advance. Especially for the electrical conductivity this states a major problem, since the kind of temperature dependence is not known exactly.

5.3 Numerical implementation

In this section some aspects of the numerical implementation used in the next chapter are described. For the numerical implementation a spatial discretization is needed. Therefore, all functions are discretized in space with the method of finite elements described already in section 3.4.

Let us consider the following problem where the control u is the only optimization variable and the state y is calculated corresponding to u

$$\min_u F\left(y(u), u\right).$$

A discretization of the control u leads to the following modified problem, where the state y is now calculated with the discrete control u_h

$$\min_{u_h} F\left(y(u_h), u_h\right).$$

Further discretization of the state y will give us the final discrete version of the original problem

$$\min_{u_h} F\left(y_h(u_h), u_h\right), \tag{5.18}$$

which can be minimized with respect to the control u_h. In this case the state is calculated corresponding to the control and the constraints $h(y_h, u_h) = 0$ are satisfied accordingly. If the problem is formulated with both the state and the control as optimization variables

$$\min_{y_h, u_h} F\left(y_h, u_h\right)$$
$$\text{subject to } h(y_h, u_h) = 0$$

the constraints have to be considered explicitly in the optimization process to assure that they are satisfied.

In the following a brief example for the discretization of Problem (A1.1') is presented. For the solution with the gradient descent method we need the discretized objective functional as well as the discretized versions of the PDEs for the temperature T and the adjoint state μ and the descent direction d. In the following $\vec{u}$ will denote the vector of the coefficients in the linear combination of u_h, similar to the description in section 3.4.1, cf. (3.19). The same for all other functions.
The objective

$$
\begin{aligned}
F(T, u) &:= \frac{1}{2} \|T - T_g\|_{H^1(\Omega)}^2 + \frac{\gamma}{2} \int_\Omega (\nabla u)^2 \, dx \\
&= \frac{1}{2} \int_\Omega (T - T_g)^2 + (\nabla(T - T_g))^2 \, dx + \frac{\gamma}{2} \int_\Omega (\nabla u)^2 \, dx
\end{aligned}
$$

becomes with the coefficient vectors $\vec{T}$ and $\vec{u}$ of the already discretized temperature T_h and the discretized heat source u_h, respectively, which correspond to the state y_h and the control u_h from above,

$$
F(\vec{T}, \vec{u}) = \frac{1}{2} (\vec{T} - \vec{T}_g)^t M (\vec{T} - \vec{T}_g) + \frac{1}{2} (\vec{T} - \vec{T}_g)^t L (\vec{T} - \vec{T}_g) + \frac{1}{2} \vec{u}^t L \vec{u}.
$$

Here M denotes the mass matrix and L the stiffness matrix.
The PDEs for the constraints and the adjoint equation are discretized similar to the description in section 3.4, i.e. for the constraints (C A1.1') we obtain

$$
L^\lambda \vec{T} + M^\nu \vec{T} = M \vec{u} + M^\nu \vec{T}_{\text{body}} \tag{5.19}
$$

with the stiffness matrix L^λ weighted with λ and the mass matrices M and M^ν, where the latter one is weighted with the perfusion coefficient ν. If a cooled probe is modeled, i.e. $T = T_{\text{body}}$ holds on the probe, we have to modify the equation accordingly, cf. (3.21).
The discretized version of the adjoint (5.7) is

$$
L^\lambda \vec{\mu} + M^\nu \vec{\mu} = M(\vec{T} - \vec{T}_g) + L(\vec{T} - \vec{T}_g),
$$

with L^λ, M and M^ν as above.
The discretized descent direction $\vec{d}$, calculated from the variational inequality (5.8) is given as

$$
\vec{d} = -M \vec{\mu} - \gamma L \vec{u}.
$$

That means that we discretize the control u as well as the state T. The discrete state $\vec{T}$ is calculated from the discretized PDE (5.19) in dependence of the discrete control $\vec{u}$. For the gradient descent method only the control $\vec{u}$ is used as optimization variable. The temperature $\vec{T}$ is calculated according to the control in each iteration step. That means we have a situation similar to (5.18).

The discretization for the other problems is achieved in the same way. For those cases where the coupled system of potential equation and heat equation is used we apply algorithm 1 described on page 35 for the discretization.

Altogether this means that the optimal control problems from the beginning reduce to nonlinear optimization problems which can be solved e.g. with the SQP solver WORHP. However the optimization problems with spatially distributed controls will be solved with the gradient descent method described in algorithm 2. Whereas the optimization problems with constant, tissue dependent and temperature dependent parameters will be solved with WORHP.

Another important aspect for the implementation of the optimization algorithms is the termination criteria. Theoretically, we want to obtain a descent direction equal to zero but numerically this is hard to reach. Therefore, it is advisable to use further termination criteria. Possible termination criteria for unconstrained problems can be found for example in [25], section 8.2.3.

For the gradient descent method the constraints are always satisfied, since the temperature T_n is calculated from the constraining PDE according to the current iterate u_n. The same for the other problems, where the conductivities are used as controls. Therefore one of the termination criteria described in [25] is used for the numerical results presented in the next chapter. The algorithm stops if the variation in the objective value compared with the previous value is small in relation to the absolute value of the current objective, i.e. if

$$F(T_{n-1}, u_{n-1}) - F(T_n, u_n) \leq \varepsilon(1 + |F(T_n, u_n)|) \tag{5.20}$$

holds. This gives us the opportunity to compare not only the objective values from sequent iteration steps but also to relate to the absolute value of the objective. Thus, we do not need to adapt the tolerance factor ε to the size of the objective value.

6 Numerical results

In this section some applications of the optimization and optimal control problems to artificial data and to temperature data from an experiment with Agar-gel are described. That means the thermal conductivity and the electrical conductivity will be identified for the method of RFA from a given temperature distribution. The intention is to find parameters which match the original values as good as possible by fitting the calculated temperature to the given data. Due to the difficulties originating from the method of RFA and the resulting modeling, as e.g. the steep descent of the electric potential from the electrodes to the outer regions or the coupling of the PDEs via the heat source, we will consider different aspects and methods for the parameter identification as described in chapter 5. A particular challenge is posed by the scaling term P_{eff}/P_Ω.

For the identification we will use the algorithms presented in section 4. The described methods will need some modifications according to the current setting. We will start with an artificial setting and end up with temperature measurements from an ablation in Agar-gel. As described in the previous chapter we will split the optimization into two main parts, at first the identification of the electrical conductivity and second the identification of the thermal conductivity. The parameters are modeled in different ways, i.e. we will investigate the different types of problems from the previous chapter, Problem A, Problem B and Problem C or a combination of Problem B and Problem C.

6.1 Artificial temperature data

First we will consider an identification problem where we know the exact data. This will provide a basis for further investigations. The aim is to identify the material parameters from a given temperature distribution. In this first step we will use temperature distributions we have calculated in advance for a certain set of parameters, i.e. we know the parameters we want to identify. As described in the previous section we split the optimization into several parts, for the thermal conductivity and for the electrical conductivity as well as a further partitioning for the heat source and the electrical conductivity. To solve the optimization problems we use the SQP-solver `WORHP` [62] on the one hand and a gradient descent method on the other hand. The SQP-solver is integrated in `MeVisLab`, an application framework for medical image processing and visualization [1], based on `C++`. The gradient method is implemented with help of `QuocMesh`, a FEM toolbox [2]. All problems are spatially discretized with FEM, as exemplarily performed for Problem (A1.1') in section 5.3. Therewith all problems change to optimization problems finally.

6.1.1 Nonlinear optimization solver `WORHP`

The nonlinear optimization solver `WORHP` is an SQP solver combined with an interior point method, designed for sparse large-scale nonlinear problems [62]. `WORHP` is an iterative solver with some special characteristics. One apparent characteristic is the use of reverse communication architecture which makes the internal loops needless and offers a high flexibility over the optimal control process. In the computational part different methods for the calculation of the derivatives are possible. The user can provide the derivatives or they are calculated by a finite difference (FD) method that uses in addition the so called group strategy which accelerates the process extremely for sparse problems. The second derivatives, i.e. the Hessian matrix, can be provided by the user as well or it is approximated by a Broyden-Fletcher-Goldfarb-Shanno (BFGS) update formula, which assures positive definiteness. The quadratic subproblem is solved by a primal-dual interior point method. To ensure global convergency the step size for the main problem is determined by a line search with a merit function and the Armijo rule. Furthermore, several other characteristics as a regularization of the Hessian to ensure positive definiteness and recovery strategies in the line search, are implemented to stabilize and speed up the whole optimization process. All these specifics of `WORHP` lead to more than $90\,\%$ solved problems of the CUTEr (Constrained and Unconstrained Testing Environment, revisited) test set.

`WORHP` is used in the following to solve the optimization problems, where the parameters are assumed to be constant, piecewise constant on the different tissue types or linear temperature dependent. For the problems with spatially distributed parameters a gradient descent algorithm is used.

6.1.2 Identification of the electrical conductivity (Problem A1)

At first we will consider the identification of the electrical conductivity for artificial temperature data, i.e. we calculate the temperature in advance for a given set of parameters. The temperature is calculated by a steady state heat transfer equation as depicted in (C A1.1') with a source term u on the right hand side and a body temperature $T_{\text{body}} = 37\,°\text{C}\,(= 310.15\,\text{K})$. In the present setting we assume a non-cooled probe and ignore accordingly the conditions $T = T_{\text{body}}$ on Ω_{pr}, where Ω_{pr} denotes the probe. The source term $u = \frac{P_{\text{eff}}}{P_\Omega}\sigma|\nabla\phi|^2$ is calculated as described in section 3.2, i.e. ϕ is the solution of the potential equation (3.1) with Dirichlet conditions at the outer boundaries. The computational domain is given by a real data set from computer tomography (CT) measurements in the liver with a segmented tumor and a segmented vascular system. We use a grid with $65 \times 65 \times 65$ grid points, i.e. we have 2^6 elements in each direction for the FEM. The blood perfusion and the cooling effects of the vascular system is described by the term Q_{perf} as given in (3.7) with coefficients $\nu_{\text{v}} = 0.05\,\text{s}^{-1}$ and $\nu_{\text{c}} = 0.006067\,\text{s}^{-1}$, for the vascular cooling and the capillary perfusion respectively. The other values are set to $\rho_{\text{blood}} = 1059\,\text{kg m}^{-3}$ for the density and to $c_{\text{blood}} = 3850\,\text{J kg}^{-1}\text{K}^{-1}$ for the heat capacity. The values for the perfusion coefficients ν_{v} and ν_{c} are set arbitrarily since the real values are not known whereas the blood density ρ_{blood} and the heat capacity c_{blood}
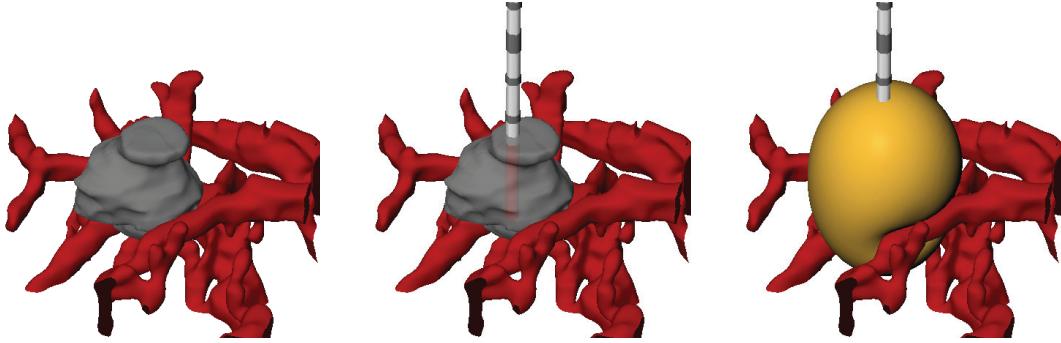
Figure 6.1: The setting for the identification of the heat source and the identification of the electrical conductivity afterwards. On the left the vascular system (red) and the tumor (grey) are displayed. In the middle the probe is placed in the tumor and on the right the 60 °C iso-surface of the temperature distribution (yellow) is shown.

are taken from table 10-4 in [78].

The piecewise constant material parameters are set to the following values, for the thermal conductivity we use $\bar{\lambda} = \{0.54,\, 0.62,\, 0.54\}\,\mathrm{W\,K^{-1}m^{-1}}$ and the electrical conductivity is set to $\bar{\sigma} = \{0.53,\, 0.64,\, 0.53\}\,\mathrm{S\,m^{-1}}$ for the three different tissue types native liver tissue, tumorous liver tissue and the vascular system. The heat capacity $c = 3455\,\mathrm{J\,kg^{-1}\,K^{-1}}$ is assumed to be constant for all tissue types and not temperature dependent as well as the density $\rho = 1080\,\mathrm{kg\,m^{-3}}$. We assume a monopolar probe, for this reason we use Dirichlet conditions at the outer boundary. The inner impedance of the generator is set to $R_I = 80\,\Omega$ and the generator power is defined as $P_{\mathrm{set}} = 60\,\mathrm{kg\,m^2\,s^{-3}}$. The probe is placed at the following position in the grid $(32, 24, 25)$ with an orientation of $(0, 0, -1)$. The setting is visualized in figure 6.1.

Turning now to the optimizational aspects of the problem. The intention is to identify a spatially distributed electrical conductivity from the given temperature, calculated as described above. As explained in the previous chapter for Problem A we will split the optimization into two separated parts, the identification of the heat source u and by using the calculated optimum u_g, the identification of the electrical conductivity. A direct identification of a spatially varying electrical conductivity from given temperature measurements is nearly impossible due to the only local impact of the heat source on the temperature distribution.

6.1.2.1 Optimize for the heat source from exact data set (Problem A1.1)

For the optimization of the heat source as described before we consider the optimal control problem (cf. (A1.1'))

$$F(T, u) = \frac{1}{2}\big\|T - T_g\big\|_{H^1(\Omega)}^2$$

with an appropriate boundary condition (C A1.1') and with Dirichlet conditions at the outer boundary $\partial\Omega$, because of the used monopolar probe. The regularization parameter α_u is set to zero, since we use the exact data T_g, obtained by forward simulation with the setting described above. Hence the optimality system is given by the state equation (C A1.1') and the adjoint equation (5.7), both with Dirichlet conditions on $\partial\Omega$ and the reduced variational inequality

$$D_u\mathcal{L}(T, u, \mu)(v - u) = \int_\Omega \mu(v - u)\, dx \geq 0 \quad \forall u \in U_{\text{ad}},$$

with a spatially distributed control u and $U_{\text{ad}} = \{u(x)\,|\, 0 \leq u(x)\}$. For the solution we apply the gradient descent method as described in algorithm 2 on page 45. The whole problem is discretized with FEM as described in 5.3 and hence the problem change to an optimization problem. The algorithm is implemented in `QuocMesh`. The descent direction v_n in the fourth step is given by the anti-gradient $v_n = -\mu$, i.e. the descent direction is determined by the negative adjoint state in the case we do not have any regularization. The step size is calculated by the Armijo rule with initial step size $s_0 = 10^5/\mathcal{M}(f')$ and $s_{\min} = 10^{-11}/\mathcal{M}(f')$ as smallest admissible step size. Thereby

$$\mathcal{M}(f') := \frac{1}{n}\sum_{i=0}^{n}|f_i'(u)|$$

denotes the mean value of all spatial values of the derivative $f'(u)$ of the objective $f(u) := F(y(u), u)$, considered as function of u, with respect to the control u. For the current setting the gradient is given as $f'(u) = D_u\mathcal{L}(T, u, \mu) = \mu$. The value of the derivative $f'(u)$ at the i-th element is denoted by $f_i'(u)$. That means the step size and the termination condition for the step size depend on the mean value of the derivatives to avoid too small or too large step sizes. As termination criterion for the optimization we use a comparison between the current objective value and the previous value in relation to the absolute value of the current objective as described in (5.20), with a tolerance of $\varepsilon = 10^{-6}$. Furthermore we use a projection in the Armijo rule to ensure only positive values for the heat source u. If a new iterate u_{n+1} is negative we define

$$u_{n+1} := \begin{cases} \frac{1}{2}(u_{n+1} + u_n), & \text{for } |u_{n+1}| < u_n, \\ u_n, & \text{else.} \end{cases}$$

The initial value is set to a constant value $u_0 = 100$.

In figure 6.3 a comparison of the calculated values and the given ones is shown. The heat source as well as the temperature distribution is displayed along a line in the three dimensional computational domain. The shown results and the progression of the objective values as well as the progression of the maximal absolute difference in the temperature (optimal vs given one), depicted in figure 6.2, illustrate that the identification of the heat source works very well for this artificial setting. The calculated temperature nearly matches the given one exactly. The heat source is also very similar to the given one
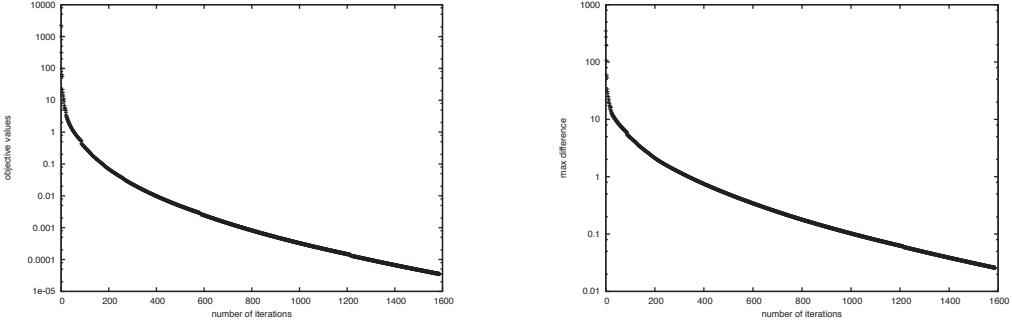
Figure 6.2: The progression of the objective functional for the identification of the heat source is displayed on the left. On the right the progression of the maximal absolute differences between the calculated and the given temperature is shown. Both are displayed with a logarithmic scale for the progression values.

but due to the really high values and the ill-posedness of the problem the values do not match exactly. The largest differences between optimal and calculated heat source can be found at the vascular structures and in the area of the tumorous tissue. These differences will be reflected in the results of the identification of the electrical conductivity in the next sections.

The ill-posedness is reflected in the large number of needed iterations as well. A smaller termination condition will probably lead to even better results but also to much more iterations. Since great modifications in the heat source lead only to small variations in the temperature distribution and if the modifications in the heat source become smaller, the differences in the temperature and therewith in the objective functional becomes even more smaller, which slows down the convergency much more. However the slow convergency rate might be improved by an optimization algorithm of higher degree (e.g. an SQP method) or further improvements in the algorithm for the determination of the step size.

6.1.2.2 Optimize for the electrical conductivity from the previously identified heat source (Problem A1.2)

Let us now turn to the main objective, the identification of the spatially distributed electrical conductivity σ, as described in Problem A1.2. We know that it will not be possible to identify the electrical conductivity directly from the temperature data, instead we will use the optimal control problem (A1.2), based on the calculated heat source from above. As already mentioned in section 5.2.2 the identification of the electrical conductivity will need some special investigations. Due to the effects of the scaling term P_{eff}/P_Ω on the system and the steep descent of the gradient of the potential $\nabla\phi$ we will apply the optimal control problem with the modified objective functional (cf. (A1.2'))

$$F(\phi, \sigma) = \frac{1}{2}\|\mathcal{S}\left(p\,\sigma|\nabla\phi|^2 - u_g\right)\|_{L^2(\Omega)}^2 + \frac{\beta}{2}\|\nabla\sigma\|_{L^2(\Omega)}^2$$

89
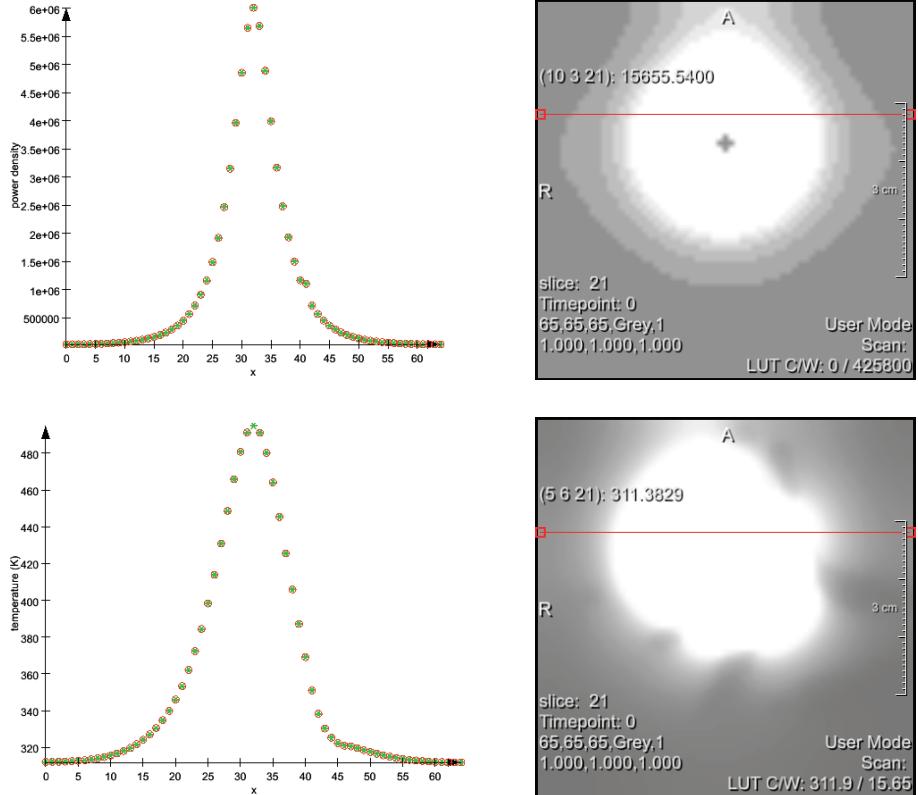
Figure 6.3: Results for the identification of the heat source for known parameters. At the top left the finally calculated heat source u (green asterisks) in comparison with the given heat source u_g (red circles) is depicted and at the bottom left the resulting temperature distribution T (green asterisks) is shown, together with the given temperature T_g (red circles). The shown values are plotted along the red line in the right figures, which represents the spatial position in the object. In the picture on the top right the applicator is denoted by the cross almost in the middle. The dark gray shadows in the picture at the bottom originate from the vascular system and the corresponding cooling effect.

to the data and the calculated u_g from above. That means we use the same setting as above for the domain, the RF probe and the generator. The new optimality system consists of the state equation (3.1) with Dirichlet boundary conditions on the outer boundary and the adjoint system as described in (5.11) as well as the variational inequality (5.12). Since the given data u_g for the heat source are the result from the above optimal control problem we need a regularization for the spatially distributed control σ. As described in (A1.2') we use the L^2-norm of the gradient as regularization term, i.e. the H^1-semi-norm, with regularization parameter $\beta = 10^{-8}$. In real applications the heat source and the electrical conductivity may not have the necessary regularity to apply to the theoretical result from the previous chapter. For the RFA the boundary of the domain is not as smooth as necessary to obtain $|\nabla\phi|^2 \in L^2(\Omega)$, because of the shape of the electrodes. However, due to the discretization the optimization works for the present setting. Probably, for a discretization where the grid size tends to zero the optimization will fail.

Again we use the gradient descent method as described in algorithm 2 with an Armijo rule for the step size and a termination condition as above. The derivative is given as (cf. (5.12))

$$f'(\sigma) = D_\sigma \mathcal{L}(T, \sigma, \mu) = \mathcal{S}(p\sigma|\nabla\phi|^2 - u_g)p + \beta\sigma - \nabla\phi\nabla\mu.$$

Due to the discretization with FEM the problem becomes an optimization problem. The initial step size in the Armijo rule is set to $s_0 = 1/\mathcal{M}(f')$, this is based on the fact that the values for the electrical conductivity are significantly smaller than for the heat source, usually they are in the range of $[0; 1]$. The smallest step size is set to $s_{\min} = 10^{-12}/\mathcal{M}(f')$. The admissible set for the given problem is $U_{\mathrm{ad}} = \{\sigma(x)| 10^{-4} < \sigma(x) < 100\}$. It is considerably larger than it has to be if we look at the typical values for σ however a smaller set may lead to limitations during the optimization.

Beside the modifications in the objective functional a good initial guess for the parameter σ is essential for a successful optimization. Due to the influence of the electrical conductivity on the scaling term $P_{\mathrm{eff}}/P_\Omega$, see figure 5.4, and the fact that we approximate the scaling term as $p = 1700$ we need an initial guess larger than 1.5. In the calculations for the following results we use $\sigma_0 = 3.0$ as initial guess.

The progression of the objective values in figure 6.4 shows that the convergency is much faster than for the heat source however the results do not match the given values as good as in the case of the identification of the heat source. In figure 6.5 the heat source and the temperature, calculated for the identified electrical conductivity is compared with the given values, i.e. the results from the previous identification of the heat source, and the originally given values. Again the values are displayed along a line in the three dimensional object, also shown in figure 6.5.

The displayed results illustrate that the identified parameters do not match the given ones. This is based on the fact that the used heat source is incorrect as well and do not comprehend the differences in the parameters for the different tissue types. As described above the main differences in the identified heat source are at the vascular structures and the tumorous tissue. Although the identification of the heat source is good enough
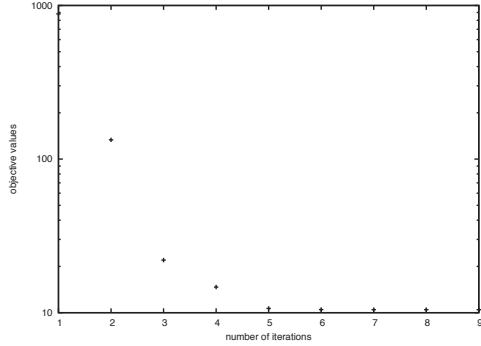
Figure 6.4: The progression of the objective for the identification of the electrical conductivity with a pre-optimized heat source. For the values of the objective a logarithmic scale is used.

to get a good approximation of the temperature it is not adequate for the identification of the parameters. Due to the ill-posedness of the identification problem for the heat source some information concerning the detailed distribution of the parameters get lost. In the last row of figure 6.5 the identified electrical conductivity is compared with the given values, where the calculated values are multiplied with the quotient of the used scaling factor $p = 1700$ and the scaling term for the original heat source $\frac{P_{\text{eff}}}{P_\Omega} = 1645.8$. However, the values do not match. The mismatch in the middle of the line is based on the fact described above, that some information concerning the tissue types get lost by using the identified heat source. However, the optimization realizes some differences in this area, indicated by the variation in the otherwise almost constant results.

The fact that all values are smaller than the given ones although the temperature nearly fits the originally temperature, is founded by a wrong final scaling. We chose the scaling factor $p = 1700$ in the beginning and identify an electrical conductivity σ except for the exact scaling. For the comparison we multiply the optimized values with the quotient of the used scaling factor p and the scaling term for the originally given heat source but in fact we use a heat source for the identification which differs from the given one. The scaling term depends on small variations in the parameters even if they are only in one tissue type. In table 6.1 three different settings for the electrical conductivity and the resulting scaling term are depicted. The results illustrate that only locally modified values for the electrical conductivity give rise to large changes in the scaling term. Therefore, the scaling in the present problem has to be different but we do not know the exact value we have to use instead of $p \cdot (\frac{P_{\text{eff}}}{P_\Omega})^{-1} = 1700 \cdot 1645.8 \cdot 10^{-1}$. In the diagram at the bottom right of the figure, the values are multiplied with an arbitrarily value such that the values nearly fit. In the end the identified values represents the given ones in a good way except the differences in the tissue types. For the matching of the temperature and the power density we need the given approximation value p only.

To find the most suitable regularization parameter the L-curve criterium has been applied but the results were not really applicable, which means that the shape of the
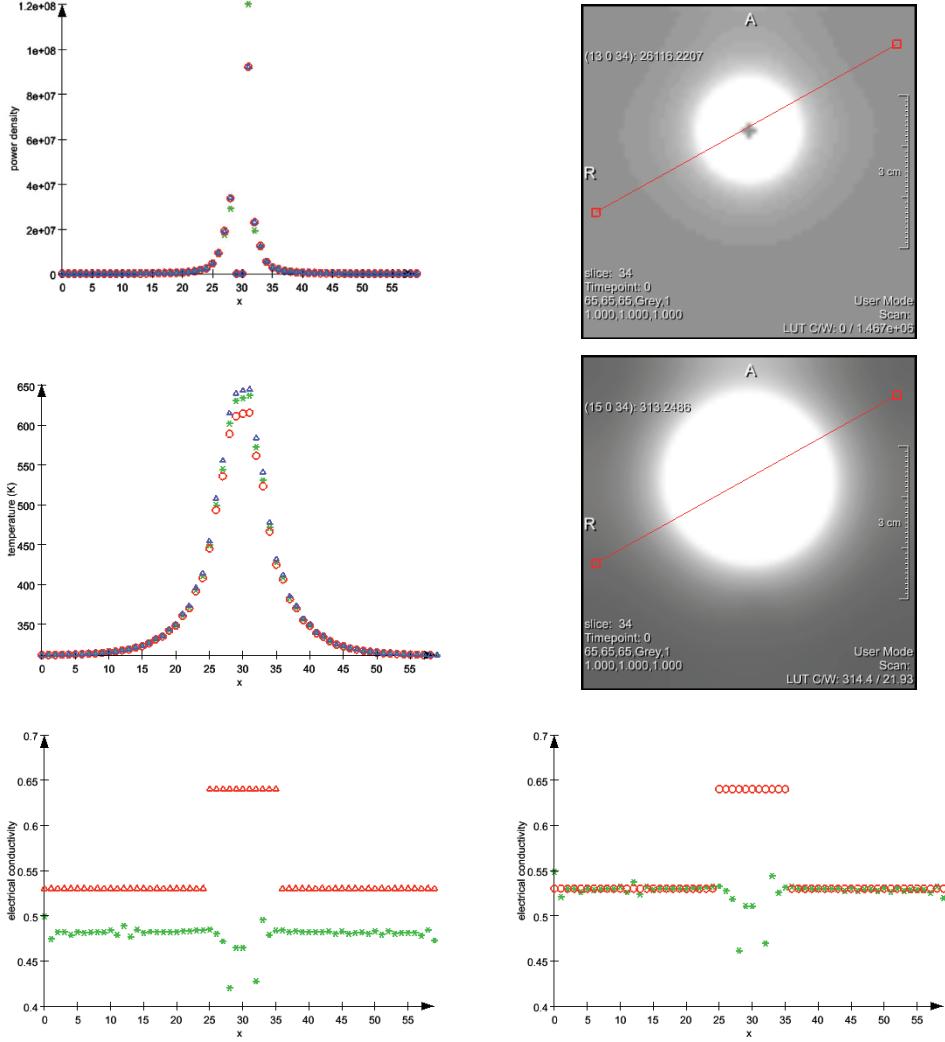
Figure 6.5: Results for the identification of the electrical conductivity from a previously identified heat source. In the figure at the top left the calculated power density (green asterisks) vs the given power density (red circles) as result from the prior optimization problem and the original heat source (blue triangles) is depicted. At the top right the spatial position of the shown values is marked as a red line. In the middle the originally given temperature distribution (blue triangles), the temperature as result of the identified heat source (red circles) and the temperature corresponding to the calculated electrical conductivity (green asterisks) are compared. At the bottom left the given values (red triangles) for the electrical conductivity and the calculated values (green asterisks), multiplied with $1.03293 = 1700 \cdot \left(\frac{P_\Omega}{P_{\text{eff}}} \right)$, are shown. At the bottom right the calculated values are multiplied with 1.135.

	liver tissue	tumorous tissue	vascular system	$\frac{P_{\text{eff}}}{P_\Omega}$
$\sigma\,(\mathrm{S\,m^{-1}})$	0.54	0.6	0.54	1276.62
$\sigma\,(\mathrm{S\,m^{-1}})$	0.54	0.85	0.54	808.215
$\sigma\,(\mathrm{S\,m^{-1}})$	0.54	1.23	0.54	439.98

Table 6.1: The scaling term $\frac{P_{\text{eff}}}{P_\Omega}$ for the heat source for varying electrical conductivity in the tumorous tissue. The inner resistance is set to $R_I = 80\,\Omega$, the generator power is set to $P_{\text{set}} = 60\,\mathrm{kg\,m^2\,s^{-3}}$ and as body temperature $T_{\text{body}} = 37\,°\mathrm{C}$ is used.
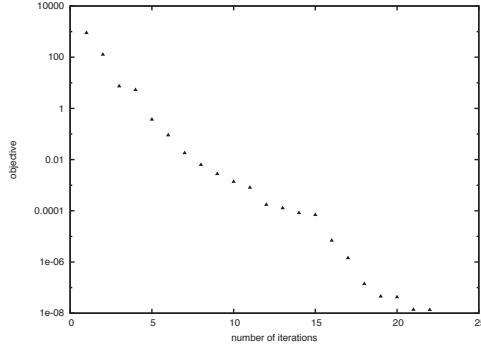

Figure 6.6: The progression of the objective function for the identification of the electrical conductivity for an exactly known heat source, displayed with a logarithmic scale.

resulting graph was not like an L-curve. Not even a tendency to an L-shaped curve was observable. Therefore, the regularization parameter has been chosen as $\beta = 10^{-8}$ by comparing the calculated power densities and the calculated conductivities. A stronger regularization leads in most cases not only to a smoother conductivity but also to larger values.

6.1.2.3 Optimize for the electrical conductivity with an exactly known heat source (Problem A1.2)

As above we are interested in the identification of a spatially distributed electrical conductivity $\sigma(x)$, as described for Problem A1.2. However, in the following we assume that we know the exact heat source $\bar{u}$. The setting for the calculations is the same as above but we use now the given heat source $\bar{u}$, calculated for the setting with the optimal electrical conductivity $\bar{\sigma}$. We do not use the identified u_g, obtained as result of the identification problem for the heat source. The optimality system is the same as above with u_g replaced by $\bar{u}$ and without any regularization term since we use the exact data and will not need any regularization for σ. The objective functional is accordingly as
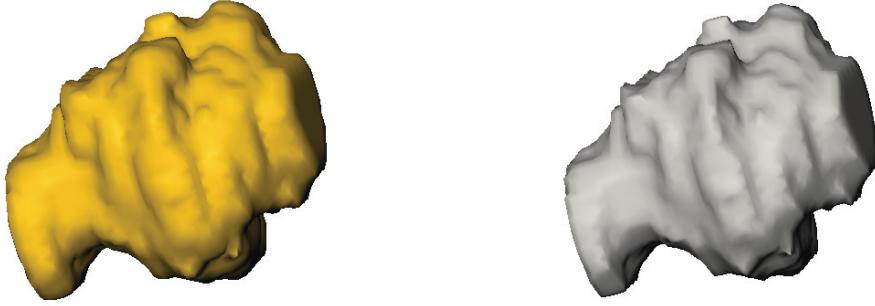
Figure 6.7: On the left we see the $0.4\,\mathrm{S\,m}^{-1}$ iso-surface for the calculated electrical conductivity, without the outer boundary. On the right we have the shape of the tumor.

follows

$$F(\phi, \sigma) = \frac{1}{2}\|\mathcal{S}\left(p\,\sigma|\nabla\phi|^2 - \bar{u}\right)\|^2_{L^2(\Omega)}.$$

For the optimization of the discretized problem the gradient descent algorithm 2 on page 45, implemented in `QuocMesh` is used. The optimal parameter values are set to $\sigma = (0.53, 0.62, 0.53)\,\mathrm{S\,m}^{-1}$ for native liver tissue, tumorous tissue and the vascular system respectively. As illustrated by the progression of the objective functional, displayed in figure 6.6, only few iterations are needed for convergence. Moreover the identified electrical conductivity is nearly the same as the given one. In figure 6.8 the calculated values for the electrical conductivity and the corresponding values for the heat source and the temperature distribution are compared with the given optimal values. In all cases the computed values fit the original ones. Only at the outer boundary they do not match, which is founded by the optimization problem and the usage of the finite elements which vanish at the boundaries. The good results are reflected in the final objective value $F(u, \sigma) = 1.34125 \cdot 10^{-8}$ for $\varepsilon = 10^{-9}$ in the termination condition (5.20).

Comparing the results with the results from above, we observe that not only the objective is considerably smaller also the calculated parameters are much more precise. Even the values on the different tissue types are noticeable distinct. In figure 6.7 the tumor and the identified parameters with a value above $0.4\,\mathrm{S\,m}^{-1}$ are displayed. Due to the scaling factor $p = 1800$ and the original $\frac{P_{\mathrm{eff}}}{P_\Omega} = 1311.8$ the calculated values for σ are smaller than the optimal ones and accordingly the threshold in the figure is set. The figure illustrates that the identification comprises the shape of the tissue structure almost exactly. Altogether the results corroborate that the identification of the electrical conductivity is well posed if the input data are correct, well known and smooth.
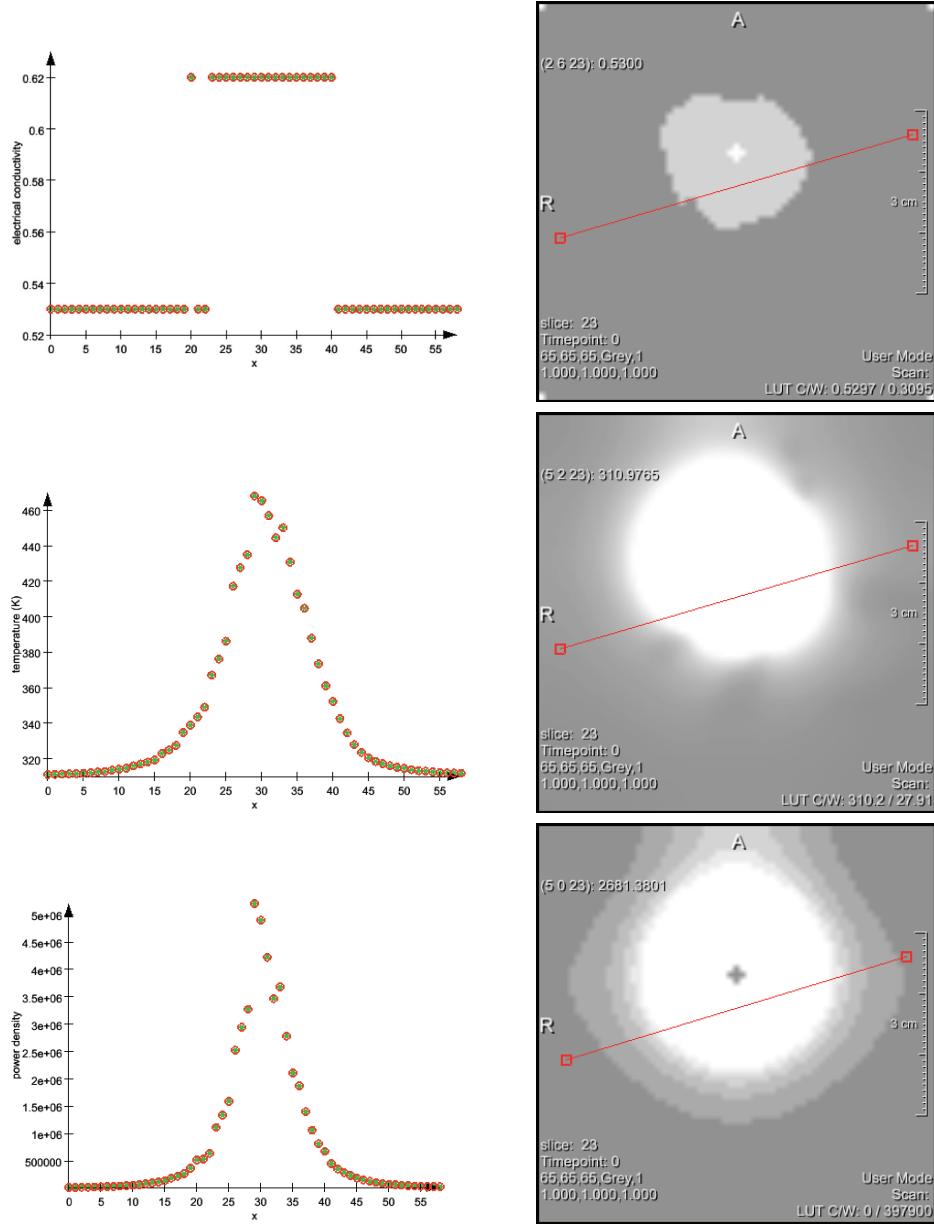
Figure 6.8: We depict the results for the identification of the electrical conductivity for an artificial setting with an exactly known heat source in comparison with the given (optimal) values. On the left the values at a line across the three dimensional object, depicted as red line in the pictures at the right, are shown. From top to bottom the calculated values (green asterisks) for the electrical conductivity, the corresponding temperature and the corresponding heat source are compared with the given values (red circles). The electrical conductivity is multiplied with $1.37216 = \frac{1800}{P_{\text{eff}}/P_{\Omega}}$, according to the used scaling factor.
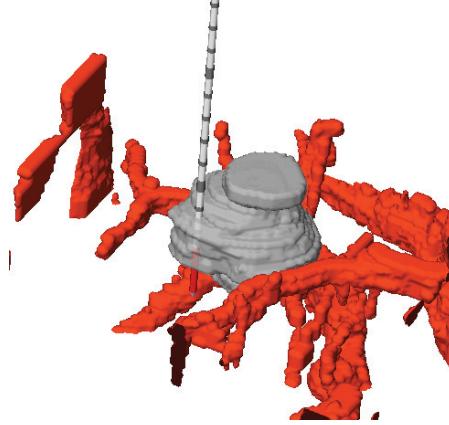
Figure 6.9: The CT data set with the placed RFA probe. The vascular structures are displayed in red and the tumor in grey. The probe is placed in the vicinity of the tumor.

6.1.3 Identification of the thermal conductivity (Problem B and C)

6.1.3.1 The tissue and temperature dependent thermal conductivity (Problem B and Problem C)

In this section we will investigate the identification of the thermal conductivity as described in section 5.2.4, where the conductivity depends linear on the temperature and additionally on the tissue types. The reduced optimization problem is used, i.e. the control is a finite dimensional vector, and we do not have any constraints beside the box constraints. For a certain setting of parameters we calculate the temperature distribution in advance and apply it as measurement data T_g to our problem. That is we know the parameter values and can test the algorithm and compare the results with the given values. We investigate a combination of Problem B and Problem C. That means we model a thermal conductivity which depends on the temperature and differs for the different tissue and structure types: native liver tissue, tumorous liver tissue and vascular structures, i.e.

$$\lambda(T(x)) = \begin{cases} \lambda_{\mathrm{ref}}^l(1 + \alpha_\lambda^l(T(x) - T_{\mathrm{body}})/\mathrm{K}), & \text{if } x \in \Omega_l, \\ \lambda_{\mathrm{ref}}^t(1 + \alpha_\lambda^t(T(x) - T_{\mathrm{body}})/\mathrm{K}), & \text{if } x \in \Omega_t, \\ \lambda_{\mathrm{ref}}^v(1 + \alpha_\lambda^v(T(x) - T_{\mathrm{body}})/\mathrm{K}), & \text{if } x \in \Omega_v, \end{cases}$$

where Ω_l and Ω_t denote the domains with native and tumorous liver tissue respectively and K the SI-unit Kelvin. The vascular structures are denoted by Ω_v. For the first results shown in table 6.2 we set the optimal values to $\lambda_{\mathrm{ref}}^l = 0.43\,\mathrm{W\,K^{-1}m^{-1}}$, $\lambda_{\mathrm{ref}}^t = 0.38\,\mathrm{W\,K^{-1}m^{-1}}$, $\lambda_{\mathrm{ref}}^v = 0.35\,\mathrm{W\,K^{-1}m^{-1}}$ and $\alpha_\lambda^l = 0.016$, $\alpha_\lambda^t = 0.014$, $\alpha_\lambda^v = 0.014$.

The computational domain is given by a real CT data set, including a tumor and vascular structures in the liver, displayed in figure 6.9, together with the RFA probe. We use a grid with $39 \times 26 \times 26$ grid points for the FEM, i.e. we have $26,364$ elements. The temperature

distribution is calculated with the time dependent bio-heat transport equation, described in equation (3.8). The body temperature T_{body} is set to $29\,°C\,(=\,302.15\,K)$ and the density ρ and the heat capacity c are both calculated in dependence of the dehydration state ϑ of the tissue and the portion of water w_W. The used formulas and values are described in more detail in [78]. The density is approximated by

$$\rho(T,\vartheta) = (\rho_G(1 - w_W) + \rho_W(1 - \vartheta)w_W)(1 + \alpha_\rho(T - T_{\text{body}})) \qquad (6.1)$$

and the specific heat capacity is described as

$$c(\vartheta) = c_G(1 - w_W) + (c_D\vartheta + c_W(1 - \vartheta))w_W, \qquad (6.2)$$

where ϑ denotes the current state of dehydration and $\rho_G = 1300\,\text{kg m}^{-3}$ the density of the tissue, $\rho_W = 993\,\text{kg m}^{-3}$ the density of water, $\rho_D = 2.89\,\text{kg m}^{-3}$ the density of dehydrated tissue, $w_W = 0.715$ the portion of water in the tissue, $c_W = 4215\,\text{J kg}^{-1}\,\text{K}^{-1}$ the heat capacity of water, $c_G = 1550\,\text{J kg}^{-1}\,\text{K}^{-1}$ the heat capacity of native tissue and $c_D = 1334\,\text{J kg}^{-1}\,\text{K}^{-1}$ the heat capacity of dehydrated tissue. All parameter values are set to the appropriate values for body temperature. The coefficient $\alpha_\rho = -0.00056$ describes the linear dependence of the density on the temperature. On the probe the heat density is set to a constant value $c_{\text{probe}} = 4125\,\text{J kg}^{-1}\,\text{K}^{-1}$.

Due to the vascular structure which is contained in the CT data, we model the cooling effect of the vessels as described in (3.7). The parameters for the modeling of the perfusion term Q_{perf} are $\nu_v = 0.01765\,\text{s}^{-1}$ and $\nu_c = 0.002\,\text{s}^{-1}$ for the vascular cooling and the capillary perfusion respectively, together with $\rho_{\text{blood}} = 1059\,\text{kg m}^{-3}$ and $c_{\text{blood}} = 3850\,\text{J kg}^{-1}\,\text{K}^{-1}$ for the density and the heat capacity. The values for the perfusion coefficients are set nearly arbitrarily, since the real values are not known exactly. The perfusion coefficient ν_c can be calculated as product of the density and the blood perfusion rate, which differs highly for different tissue types. In table 10-6 in the book of Stein [78] the blood perfusion rate for the liver is $1\,\text{cm}^3\text{g}^{-1}\text{min}^{-1}$ whereas the perfusion rate for tumorous liver tissue is given as $0.12\,\text{cm}^3\text{g}^{-1}\text{min}^{-1}$. Together with a density of approximately $\rho = 1050\,\text{kg m}^{-3}$ this leads to $\nu_c = 0.0175\,\text{s}^{-1}$ and $\nu_c = 0.0021\,\text{s}^{-1}$ for native liver tissue and tumorous liver tissue respectively. The values for the density and the heat capacity are taken from table 10-4 in [78].

The monopolar probe, i.e. the center of the electrode, is placed at the position $(21, 9.6, 11)$ with an orientation of $(0, 0, -1)$. For the identification of the parameters the probe has not to be placed in th emiddle of the tumor since the identification should work ideally for any position. The focus is the correct identification and not the destruction of the whole tumor. The thermal conductivity is set to a constant value $\lambda_{\text{probe}} = 0.589\,\text{W K}^{-1}\text{m}^{-1}$ and we use Dirichlet conditions for the temperature distribution on the probe to model a cooled RF-applicator. For the generator power we choose $P_{\text{set}} = 60\,\text{kg m}^2\,\text{s}^{-3}$ and set the inner resistance of the generator to $R_I = 80\,\Omega$.

The identification problem with respect to the thermal conductivity is solved by the SQP solver `WORHP`, described above. We use the provided methods for the calculations of the first and second derivatives, i.e. we calculate the first derivative with FD, with a

	liver	tumor	vessel
final $\lambda_{\mathrm{ref}}\,(\mathrm{W\,K^{-1}m^{-1}})$	0.4300000465	0.3799999865	0.3500007087
final α_λ	0.01599999681	0.01400000133	0.0139997962
optimal $\lambda_{\mathrm{ref}}\,(\mathrm{W\,K^{-1}m^{-1}})$	0.43	0.38	0.35
optimal α_λ	0.016	0.014	0.014

Table 6.2: The results for the optimization of the thermal conductivity after 35 iterations.
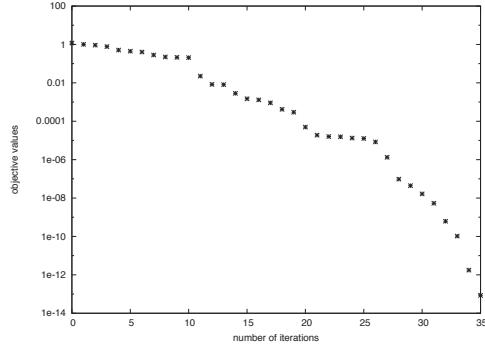
Figure 6.10: The progression of the objective values for the identification of a temperature and tissue dependent thermal conductivity.

stepsize of $\tau = 10^{-7}$ and use the BFGS update for the Hessian. The tolerance for the optimization is set to tol $= 10^{-9}$.

The objective is given by (cf. (5.16))

$$F(T, \lambda) = \frac{1}{2}\big\| T(t_{\mathrm{fin}}, x) - T_g(x) \big\|^2_{L^2(\Omega)}$$

at a final time t_{fin} and without any regularization, since we use an exact data set as input. The initial values are $\lambda_{\mathrm{ref}} = 0.5\,\mathrm{W\,K^{-1}\,m^{-1}}$ and $\alpha_\lambda = 0.01$ for all tissue types.

After 35 iterations the results depicted in table 6.2 are obtained. The final objective value was $F = 1.29451929919 \cdot 10^{-14}$ and the value for the KKT condition was $2.74484282 \cdot 10^{-11}$. The progression of the objective values during the optimization is displayed in figure 6.10. A remarkable effect during the optimization is the order in which the different values are optimized, the order correlates to the total mass of the tissue type in the computational domain. Accordingly the values at the native tissue are optimized first, followed by the values for the tumorous tissue. The values for the vascular structures are optimized at last. Therefore, if we choose a larger tolerance the values at the vascular structures will not fit the given values as good as they do with the small tolerance of 10^{-9}, the fitting of the other parameters will be almost the same as for the current setting. The progression of the parameter values at the different tissue types during the optimization is depicted in figure 6.11.
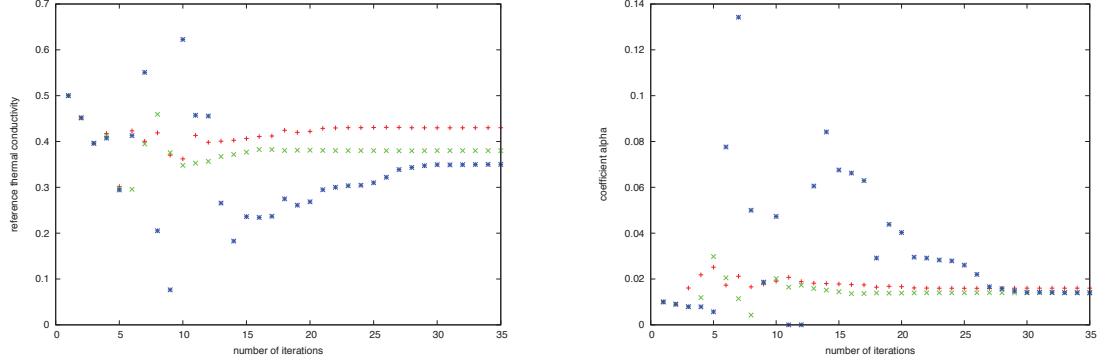
Figure 6.11: The progression of the parameter values for the different tissue types during the optimization process is depicted. On the left the values for λ_{ref} and on the right the values for α_λ. The values for the liver tissue are denoted with red plus, the values in the tumorous tissue with green crosses and the values in the vascular structures with blue asterisks.

6.1.4 Identification of both the thermal conductivity and the electrical conductivity (Problem B and Problem C)

At last in this section we will describe the identification of both, the thermal and the electrical conductivity for the artificial scenario with real CT data for the spatial domain. We will consider three distinct cases, the first one uses a temperature dependent but spatially constant thermal conductivity and a constant electrical conductivity. In the second case both parameters are linear temperature dependent, but spatially constant. In the third case both parameters are tissue dependent, with a linear temperature dependent thermal conductivity and a constant electrical conductivity, with respect to the temperature. That means we have at first a situation as in Problem C and in the third case a combination of Problem B and Problem C. For all problems the same objective functional is used (cf. (BIP))

$$F(T, \lambda, \sigma) = \frac{1}{2} \big\| T(t_{\mathrm{fin}}, x) - T_g(x) \big\|^2_{L^2(\Omega)},$$

without any regularization and with the pre-calculated temperature T_g at the final time t_{fin}.

6.1.4.1 Temperature dependent thermal conductivity and constant electrical conductivity (Problem C)

At first the identification of spatially constant parameters will be considered.
Again the optimization is done by the SQP solver WORHP. The setting is the same as in section 6.1.3, i.e. we have a grid of $39 \times 26 \times 26$ points as discretization of the computational domain and the monopolar probe is placed at the position $(21, 9.6, 11)$ with an orientation of $(0, 0, -1)$. The material parameters, beside the thermal conductivity and

position	$\lambda_{\text{ref}}\,(\text{W}\,\text{K}^{-1}\text{m}^{-1})$	α_λ	$\sigma\,(\text{S}\,\text{m}^{-1})$	F
(21, 9.6, 11)	0.4300453777	0.02099539395	0.5586274751	$1.99925 \cdot 10^{-11}$
(7.4, 4.5, 4.5)	0.4299996846	0.02100004323	0.5599979177	$9.33475 \cdot 10^{-16}$
given values	0.43	0.021	0.56	

Table 6.3: The results for the identification of the electrical conductivity and the thermal conductivity are presented for two different probe positions. The optimal values are displayed in the last row for comparative purposes and the objective values are depicted in the last column.
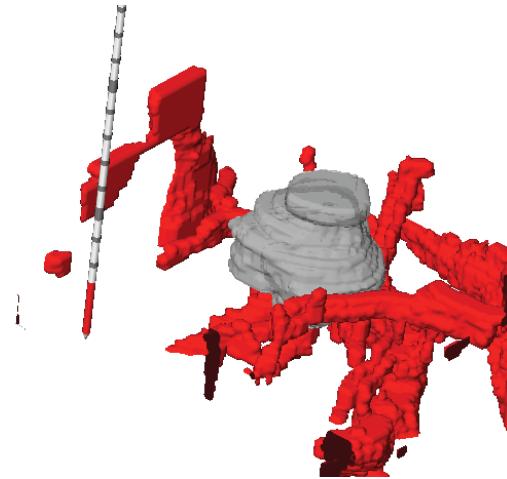

Figure 6.12: Another probe placement for the identification of the thermal conductivity and the electrical conductivity. This setting is only for test purposes and not reasonable for real applications.

the electrical conductivity, are set to the same values as before.

The intention is to identify the thermal conductivity λ and the electrical conductivity σ where we assume the latter one to be a constant scalar value. Whereas the thermal conductivity is assumed to be temperature dependent but constant for the different tissue types. For the pre-calculated temperature distribution the parameters are defined as $\sigma = 0.56\,\text{S}\,\text{m}^{-1}$ and $\lambda_{\text{ref}} = 0.43\,\text{W}\,\text{K}^{-1}\text{m}^{-1}$ and $\alpha_\lambda = 0.021$.

As before the FD method provided by the solver is used to calculate the derivatives. The step size is set to $\tau = 10^{-5}$ and the tolerance for the optimization algorithm is set to $\text{tol} = 10^{-14}$. For the results shown in table 6.3 the solver needs 49 iterations and as final value for the objective we obtain $F = 1.99924898698 \cdot 10^{-11}$ and the value for the KKT conditions is $1.01238750712 \cdot 10^{-15}$. The progression of the objective values during the optimization process is presented in figure 6.13. The final success of the optimization process does not only depend on the optimization parameters, e.g. the step size for FD, tolerance or initial starting point, it further depends on the whole setting. In figure 6.13 and table 6.3 also the results for the optimization with a slightly modified setting are
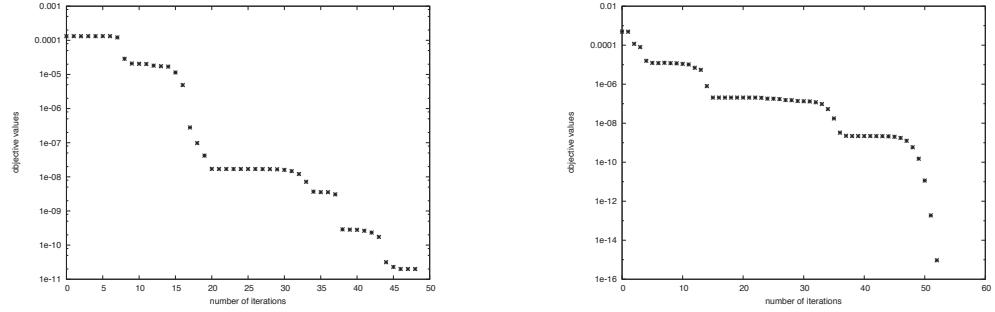
Figure 6.13: The progression of the objective for the identification of the thermal conductivity and the electrical conductivity for artificial data is displayed. For the description of the objective values a logarithmic scale is used. On the left the progression for the more centered probe position (21, 9.6, 11) is depicted and on the right the progression for the probe placed near the boundary of the computational domain.

presented. The setting is mainly the same as described before but we choose a different position for the probe, it is placed at (7.4, 4.5, 4.5) instead and a larger tolerance of $\text{tol} = 10^{-11}$ is used. This leads to marginally different results. The final objective value is smaller and the parameters fit to the given ones little better than with the previous setting. These differences may be caused by the fact that the second position is not only near the boundary but also in a nearly homogeneous tissue, cf. figure 6.12.

The influence of the tissue on the temperature distribution is restricted to the vicinity of the probe. Therefore at the second position the influence of cooling effects on the temperature distribution is small. In addition the position at the boundary implies modifications in the temperature distribution. However, considering further investigations and attempts to identify a tissue dependent electrical conductivity it seems to be apparent that the tissue has a significant influence on the temperature distribution and therewith also on the optimization. However, the differences in the results are marginal which means that the position is not that important for the identification of constant parameters but we should keep that in mind for further investigations. Beyond that, such positions of the probe are not relevant for real applications.

6.1.4.2 Linear temperature dependent conductivities (Problem C)

In this section we will consider the identification of a linear temperature dependent thermal conductivity $\lambda(T)$ and also a linear temperature dependent electrical conductivity $\sigma(T)$. The thermal conductivity is modeled as before, cf. (3.9), and the electrical conductivity is modeled as follows

$$\sigma = \sigma_0 + \sigma_1(T - T_{\text{ref}})/\text{K},$$
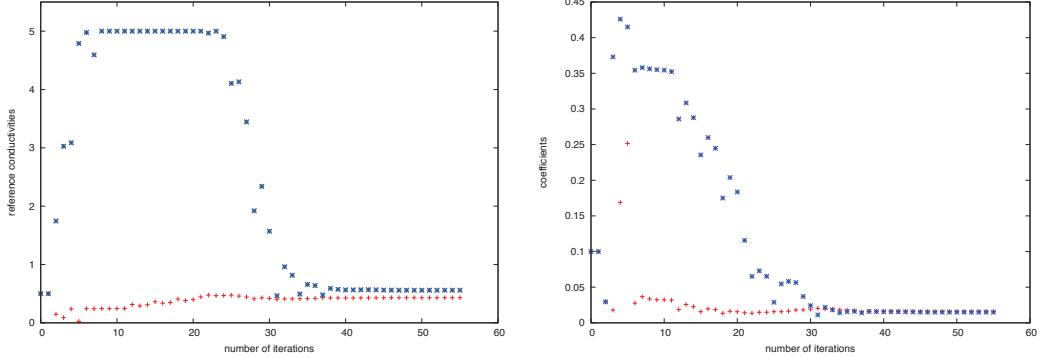
Figure 6.14: The progression of the parameter values for the optimization of linear temperature dependent conductivities. On the left the reference values $\lambda_{\mathrm{ref}}\,(\mathrm{W\,K^{-1}m^{-1}})$ (red plus) and $\sigma_0\,(\mathrm{S\,m^{-1}})$ (blue asterisks) are displayed and on the right the coefficient values α_λ (red plus) and $\sigma_1\,(\mathrm{S\,m^{-1}})$ (blue asterisks).

	$\lambda_{\mathrm{ref}}\,(\mathrm{W\,K^{-1}m^{-1}})$	α_λ	$\sigma_0\,(\mathrm{S\,m^{-1}})$	$\sigma_1\,(\mathrm{S\,m^{-1}})$
given values	0.43	0.016	0.56	0.015
calculated values	0.42999955	0.01600003	0.56000123	0.01500008

Table 6.4: The results for the identification of linear temperature dependent parameters after 55 iterations.

where $T_{\mathrm{ref}} = T_{\mathrm{body}} = 37\,^\circ\mathrm{C}\,(310.15\,\mathrm{K})$ in both cases and K denotes the SI units Kelvin.. The setting is the same as above for the identification of a temperature dependent thermal conductivity and a constant electrical conductivity. The given values for the parameters to calculate the given temperature T_g are set to $\lambda_{\mathrm{ref}} = 0.43\,\mathrm{W\,K^{-1}m^{-1}}$, $\alpha_\lambda = 0.016$, $\sigma_0 = 0.56\,\mathrm{S\,m^{-1}}$ and $\sigma_1 = 0.015\,\mathrm{S\,m^{-1}}$.

Again the optimization problem is solved by the SQP solver `WORHP` and the provided FD method is used with step size $\tau = 10^{-5}$. The tolerance for the algorithm is set to tol $= 10^{-12}$. The optimization needs 55 iterations and the results for the parameters are presented in table 6.4. The final objective value is $F = 3.09869172243 \cdot 10^{-13}$ and the corresponding KKT value $KKT = 4.97609082706 \cdot 10^{-14}$. The progression of the objective values is shown in figure 6.15. During the optimization process it is observed that the thermal conductivity is optimized prior to the electrical conductivity, i.e. the values for the thermal conductivity are near their optimum first. This is mainly based on the fact that the thermal conductivity influences the temperature distribution more than the electrical conductivity. The progression of the parameter values is depicted in figure 6.14.

Further investigations with a polynomial of higher degree for the modeling of the electrical conductivity, as in (3.10), did not lead to a successful optimization. The values for the thermal conductivity were optimized but the coefficients for the electrical con-
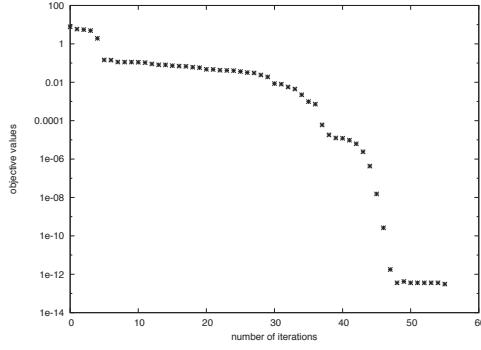
Figure 6.15: The progression of the objective function for the identification of linear temperature dependent parameters. For the objective values a logarithmic scale is used.
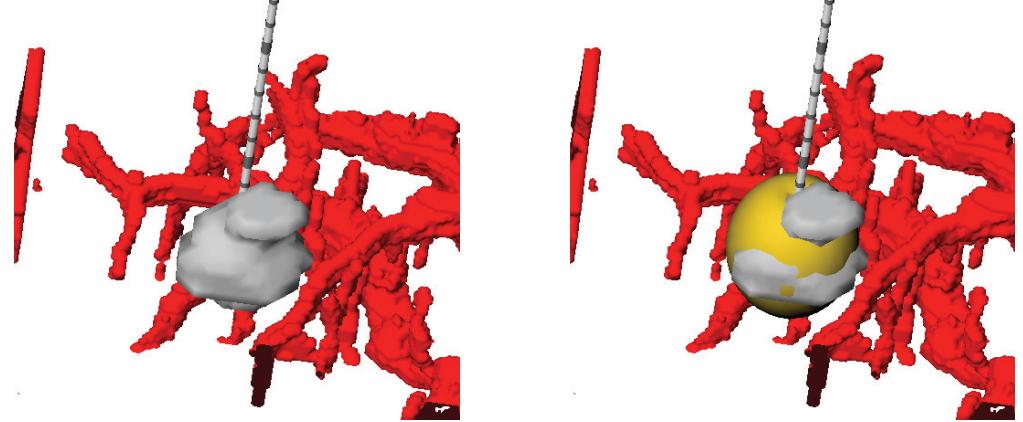

Figure 6.16: The probe placement for the identification of tissue dependent parameters. The vascular system is illustrated in red and the tumor in grey. The monopolar probe is placed in the tumor. On the right the 60 °C iso-surface of the final temperature is additionally displayed in yellow.

ductivity were not identified correctly. On the one hand this may be based on the minor influence of the electrical conductivity on the temperature, on the other hand this can also be founded in the modeling of the electrical conductivity itself. For a modeling with a polynomial of degree ≥ 2, the conductivity can not be assumed to be in L^2 any longer. However, since we do not know how the electrical conductivity is modeled correctly, it is questionable to use a polynomial of a certain degree. Therefore, it may be rather advisable to use a spatially distributed model for the electrical conductivity as described in Problem A1.2, if we want to reflect the real temperature dependence in a real problem.

6.1.4.3 Identification of tissue dependent parameters (Problem B and C)

For the identification of tissue dependent parameters where the thermal conductivity additionally depends linearly on the temperature, mainly the same setting as above is chosen. The distinction is in the placement of the monopolar probe, which is now placed at (22, 13, 11), and in the cooling term, since there is no vascular cooling or blood perfusion assumed during the ablation. The optimal values for the parameters are set as described in table 6.5.

The optimization algorithm differs slightly from above. For the tissue dependent parameters a successive optimization is implemented. Since the different tissue types has a diverse influence on the optimization process the optimization is split according to the tissue types. That means we optimize successively for the parameters on the different tissue types.

Therewith for each type 6 iterations are performed before the algorithm switches to the next type. The results shown in table 6.5 are obtained after 151 calls of the solver for the different tissue types (i.e. 151×6 iterations), for a tolerance of tol $= 10^{-14}$ and a step size $\tau = 10^{-5}$ for the FD. The final value for the KKT condition is $KKT = 1.46764142812 \cdot 10^{-13}$ and the final objective value is $F = 2.33327227709 \cdot 10^{-08}$.

The optimization of tissue dependent parameters depends significantly on the placement of the probe. Several test scenarios with different probe placements demonstrate that the tissue dependent parameters are identified only if the probe is placed at least in the vicinity of the corresponding tissue. For example for the setting visualized in figure 6.12 only the parameters for the liver tissue are optimized. The presented results in table 6.5 also illustrate that the values at the vascular system which is farthest from the probe, cf. figure 6.16, is optimized least and the values for the tumor, where the probe is placed in, are optimized best. Moreover the comparatively bad results for the electrical conductivity illustrates the difficulties in identifying the electrical conductivity from temperature distributions especially if they are spatially varying.

	tumor	liver	blood vessels
λ_{ref} (W K^{-1}m^{-1})	0.56070750969	0.47184559579	0.52168720638
α_λ	0.01500964204	0.01389826880	0.01478672026
σ (S m^{-1})	0.58073618812	0.52825129578	0.54203255957
optimal λ_{ref} (W K^{-1}m^{-1})	0.56	0.47	0.53
optimal α_λ	0.015	0.014	0.014
optimal σ (S m^{-1})	0.62	0.56	0.58

Table 6.5: The results for the identification of tissue dependent parameters. The optimal values are given in the last three rows.
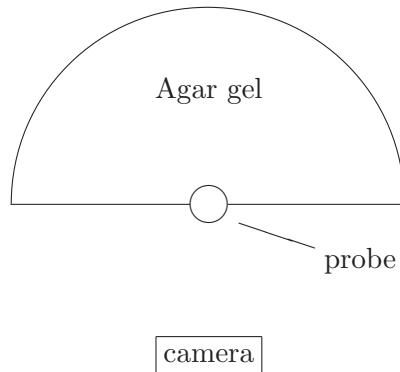
Figure 6.17: Schematic figure of the setting for the ablation in Agar gel and the position of the camera.
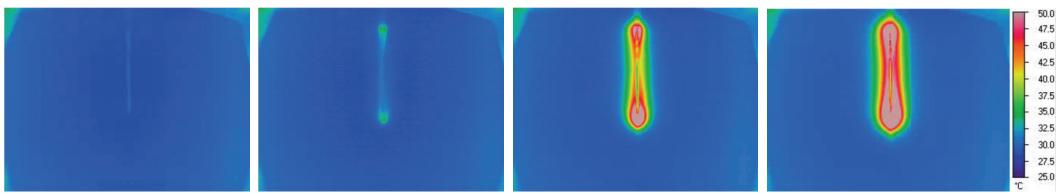
Figure 6.18: From left to right four pictures of the temperature distribution in agar gel during the ablation are depicted. On the right a scale for the temperature in °C is shown.

6.2 Data from Agar-model

In this section we will use temperature measurements from an RFA in Agar-gel to identify the material parameters. The temperature data are provided by Dieter Haemmerich from the Medical University of South Carolina, USA.

To apply the developed model to real data we need some modifications due to the kind of the available data. In the present case we have given measurements from an infrared camera of an RFA in an Agar model (Agar-gel with 5 % Agar and 5 % NaCl and 90 % water). The gel was arranged half cylindrical with a diameter of 15 cm. The probe with the electrode was placed in the middle of the plane side, see figure 6.17. The used probe is a non-cooled 17-gauge needle, i.e. it has a diameter of approximately 1.4 mm and accordingly a radius of 0.7 mm, with 3 cm active electrode. The data are taken with an infrared camera (Mikron M7500) from the side of the model where the electrode is placed. The pictures reflect the temperature at the surface only but with a pixel size of 0.2×0.2 mm and approximately three frames per second. A selection of four pictures at different time steps during the RFA is depicted in figure 6.18.

To apply the existing algorithms to the present problem in the Agar gel we need a three

dimensional temperature distribution. Since the Agar gel is a homogenous material and the probe is placed in the center we assume that the temperature is rotationally symmetric. Hence we can calculate a three dimensional temperature distribution by rotating the given data and fill the corners with values of body temperature to obtain a rectangular domain. For the following calculations we must have in mind that the rotation increases the data errors.

If we consider the optimal control problem with steady state heat equation as in (A1.1') we will get some troubles by adapting this to the given data due to different aspects. In (A1.1') we model a perfusion term $\nu(T - T_{\text{body}})$ in the heat equation which describes the cooling effect of the blood vessels and additionally the perfusion of the tissue by capillary vessels. In the Agar-model we do not have any effects like this thus we have to neglect this term. Furthermore we have a non-cooled RF probe which means we have to neglect also the boundary condition $T = T_{\text{body}}$ at the probe. We end up with a steady state heat equation with Neumann boundary conditions at the outer boundary and this problem can not be solved uniquely. We can evade this by choosing Dirichlet Conditions at the outer boundary and obtain the following problem

$$
\begin{aligned}
-\operatorname{div}(\lambda \nabla T) &= u && \text{in } \Omega \\
T &= T_{\text{body}} && \text{on } \partial\Omega,
\end{aligned}
\tag{6.3}
$$

where $\Omega \subset \mathbb{R}^N$ denotes the computational domain.
At the electrodes $\Gamma_+ \cup \Gamma_-$ it is additionally required that $u = 0$ and in the whole domain it is necessary to assume $u \geq 0$. This problem can be solved numerically with standard finite element methods but it involves another kind of difficulties or rather do not model the given situation in a correct manner. To understand the underlying problem let us consider the simplified one-dimensional model

$$
\begin{aligned}
-\Delta T &= u && \text{in } [a, b] \subset \mathbb{R} \\
T &= T_{\text{body}} && \text{for } x = a, x = b
\end{aligned}
\tag{6.4}
$$

with $u \geq 0$ everywhere and $u = 0$ on a small subinterval to form the electrode.
The given shape of the temperature and the above equation provides that the right hand side has to be negative for a left oriented curvature of the temperature and positive for a right oriented curvature. But due to the restriction $u \geq 0$ we force the right hand side to be positive everywhere beside the electrode where $u = 0$. These two conditions lead to high values near the electrodes and small values near zero everywhere else.
The results for an identification of the heat source with Dirichlet conditions for the temperature on the outer boundary is depicted in figure 6.19. The optimization has been interrupted after 1000 iterations but the results show arising problems near the electrode. Whereas the calculated temperature, also depicted in figure 6.19, illustrates the ill-posedness of the problems since the difference to the optimal temperature is not as severe as for the power density.
Hence we need some additional constraints or conditions for the model. There exist two
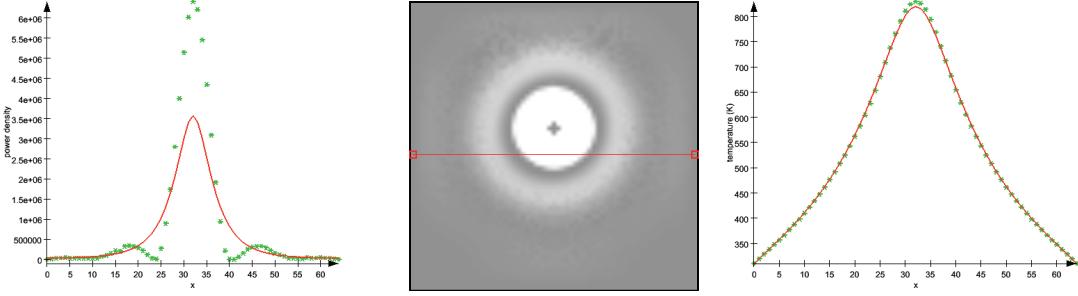
Figure 6.19: In the diagram on the left we depict the given heat source (red line) and the calculated heat source (green asterisks) after 1000 iterations at the spatial position, which is shown as red line in the picture in the middle, where the cross in the middle denotes the probe. On the right the given temperature (red line) is displayed vs the calculated one (green asterisks), at the same spatial position as the heat source.

options, either to use a time dependent model or to introduce a cooling term. Since there is no cooling in the presently used setting and we are interested in avoiding a time dependent problem, we consider only one discrete time step. Correspondingly, we obtain a Helmholtz-term in the bio-heat equation

$$\frac{\rho c}{\tau}(T - T_0) - \mathrm{div}(\lambda \nabla T) = u \quad \text{in } \Omega, \tag{6.5}$$

which gives us an appropriate model that is solvable for Dirichlet conditions as well as Neumann conditions at the outer boundaries.

The corresponding adjoint equation for the objective (A1.1') and the above heat equation (6.5) in the weak formulation is given by

$$\frac{\rho c}{\tau}\int_{\Omega} h\mu \, dx + \int_{\Omega} \lambda \nabla \mu \nabla h \, dx = \int_{\Omega} (T - T_g)h \, dx + \int_{\Omega} \nabla(T - T_g)\nabla h \, dx \quad \text{in } \Omega,$$

for all test functions $h \in H^1(\Omega)$, together with appropriate boundary conditions.

6.2.1 Identification of the heat source (Problem A1.1)

To identify the spatially distributed heat source the same method as for the artificial setting in section 6.1.2.1 is applied with small modifications in the optimization parameters. The objective functional is defined as follows

$$F(T, u) = \frac{1}{2}\big\|T(\tau, x) - T_g(x)\big\|^2_{H^1(\Omega)} + \frac{\gamma}{2}\big\|\nabla u\big\|^2_{L^2(\Omega)}.$$

After a discretization with FEM the optimization is performed with `QuocMesh` by the gradient method described on page 45. For the results presented in figure 6.21 the ther-
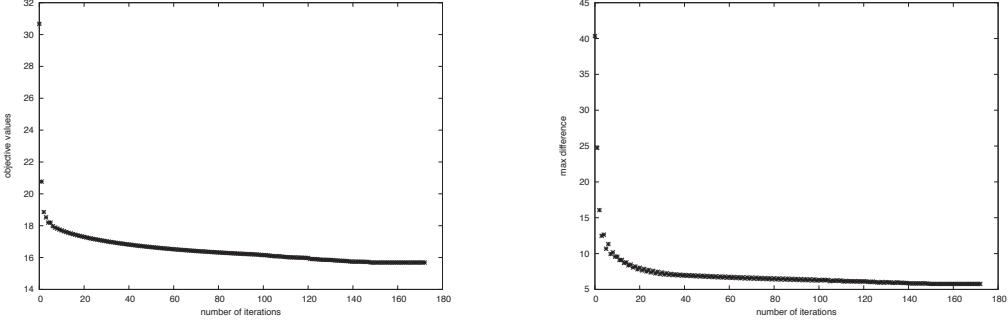
Figure 6.20: On the left the progression of the objective functional for the identification of the heat source from temperature measurements of RFA in an Agar model is depicted. On the right the maximal absolute difference between the calculated and the given temperature is shown.

mal conductivity is set to $\lambda = 0.6 \, \text{W} \, \text{K}^{-1} \text{m}^{-1}$, on the basis of the thermal conductivity of water. Due to the large values of the power density and especially due to the large differences in the gradient a regularization coefficient $\gamma = 10^{-20}$ is chosen. Typically, the regularization term without the coefficient $\frac{\gamma}{2}$ is in the range of 10^{13}. The initial step size is set to $s_0 = 10^5$. According to the setting for the RFA in the agar model the generator power is set to $P_{\text{set}} = 22 \, \text{W}$, whereas the inner resistance is chosen arbitrarily as $R_I = 70 \, \Omega$. Since we do not have any perfusion or vascular structures, the cooling term can be neglected, i.e. the coefficient ν is set to zero. The probe is placed at $(32, 28, 32)$ with an orientation of $(0, 1, 0)$ according to the given data set. For the results presented in figure 6.21 the heat capacity of the tissue is set to $c = 4181.3 \, \text{J} \, \text{kg}^{-1} \text{K}^{-1}$ and the density to $\rho = 997 \, \text{kg} \, \text{m}^{-3}$ according to the typical values of water. The tolerance for the termination criterion is set to $\text{tol} = 10^{-8}$. The progression of the objective functional is displayed in figure 6.20, together with the maximal difference between the calculated temperature and the given temperature.

The regularization parameter γ plays a major role in the optimization process. The parameter influences not only the quality of the result furthermore it influences the number of needed iterations. By replacing $\gamma = 10^{-20}$ with $\gamma = 10^{-22}$ the algorithm needs 380 iterations instead of 172 as needed in the present situation. Whereas the results improve only marginally. In figure 6.21 the results for the optimization, i.e. the identified heat source and the corresponding temperature distribution, are compared with the given temperature as well as the results for the optimization with a regularization parameter $\gamma = 10^{-16}$. The diagrams illustrate that the results for $\gamma = 10^{-20}$ are significantly better than for $\gamma = 10^{-16}$ and the number of iterations increases from 9 to 172. Another effect which can be detected in the diagram of the heat source is the smoothing of the data if the regularization parameter is increased.
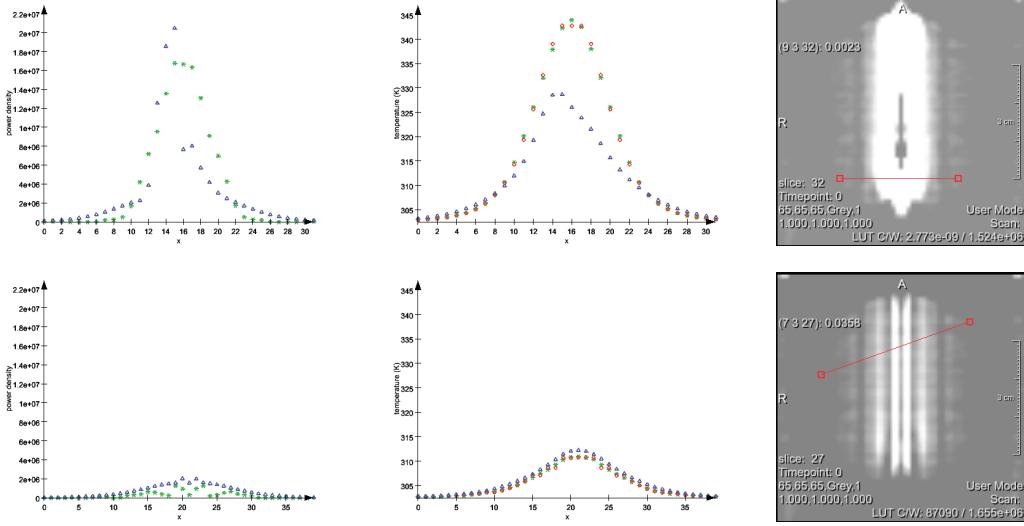
Figure 6.21: Results for the identification of the heat source from temperature measurements for RFA in Agar-gel. The calculated heat source for $\lambda_u = 10^{-20}$ (green asterisks) and for $\lambda_u = 10^{-16}$ (blue triangles) are plotted on the left along the position denoted as red line in the pictures of the heat source on the right. In the middle the calculated temperatures (green asterisks for $\lambda_u = 10^{-20}$, blue triangles for $\lambda_u = 10^{-16}$) are compared with the given temperature distribution (red circles).

6.2.2 Identification of the electrical conductivity (Problem A1.2)

Since the aim of the present work is the identification of the material parameters we will consider the following: as described previously in section 6.1.2 we will use the identified heat source for the determination of the spatially distributed electrical conductivity as described in problem A1.2. For the optimization the gradient method is applied to the objective functional (cf. (A1.2'))

$$F(\phi, \sigma) = \frac{1}{2} \| \mathcal{S} \left(p\,\sigma |\nabla\phi|^2 - u_g \right) \|_{L^2(\Omega)}^2 + \frac{\beta}{2} \|\nabla\sigma\|_{L^2(\Omega)}^2.$$

For the results presented in figure 6.22 the previously identified heat source is used as measurement data u_g for the optimal control problem described in 5.2.2.3. The initial value is chosen as above as $\sigma_0 = 3.0\,\mathrm{S\,m^{-1}}$ with a scaling factor $p = 350$. Since the used generator power is much lower than in the example above, the scaling factor has to be smaller. With a tolerance of tol $= 10^{-8}$ and a regularization parameter $\beta = 10^{-8}$ the optimization with the gradient method needs 7 iterations for the presented results. The progression of the objective values is presented in figure 6.23.

The electrical conductivity is identified only accurate to a multiplication factor, which is set to one at the presented plot. Even if the conductivity does not match the given
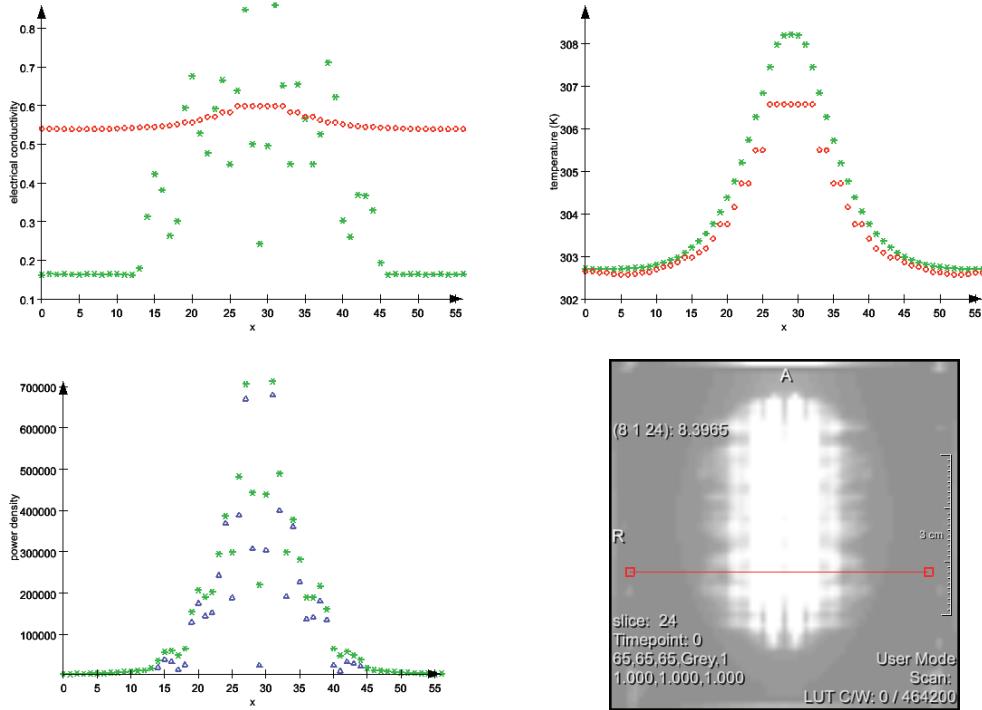
Figure 6.22: At the top left the calculated electrical conductivity (green asterisks) in comparison with the assumed conductivity (red circles) with 1.5% temperature dependency is displayed. At the top right the corresponding temperatures are depicted. The corresponding power density (green asterisks) is shown at the bottom left, compared with the previously identified power density (blue triangles). All displayed values are taken along the red line, depicted in the picture of the calculated power density at the bottom right.
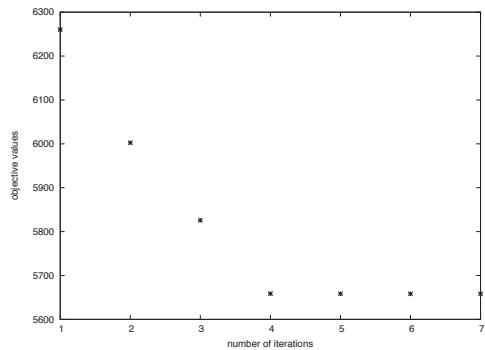
Figure 6.23: The progression of the objective values for the identification of the electrical conductivity from temperature measurements of an RFA in Agar-gel via a previously identified heat source.

$\sigma(T) = 0.56 + 0.015(T - T_{\text{body}})/\text{K}$, the tendency is visible. Moreover the correct electrical conductivity is not known and the used approximation with a linear temperature dependent conductivity is only an estimation [32]. Since the heat source u_g used in the objective functional is an approximation as well the results may be not as good as in the artificial setting. However, even for the artificial setting with the previously identified heat source the exact identification of the electrical conductivity was impossible at the tissue types which differ from the main liver tissue. Moreover, the initial temperature distribution is not the best data base since by rotating the two dimensional data additional artifacts will appear and debase the identification.

In the figures 6.24 and 6.25 the identified electrical conductivity for a modified setting is presented. Instead of using $c = 4181.3 \, \text{J} \, \text{kg}^{-1} \, \text{K}^{-1}$ for the heat capacity, comparable with the heat capacity of water, we use the same capacity as in the artificial setting $c = 3455 \, \text{J} \, \text{kg}^{-1} \, \text{K}^{-1}$. The same for the density, which is no longer adapted to the density of water but to the human tissue $\rho = 1080 \, \text{kg} \, \text{m}^{-3}$. The scaling factor is set to $p = 700$. The presented results are from two different settings. The first one is the identification of the electrical conductivity from a previously identified heat source u_g. The second one is slightly modified such that the heat source u_g is additionally smoothed. That means the heat source is convolved with a Gaussian function with mean $\kappa = 0$ and a standard deviation $\varsigma = 1.5$. For the first setting a regularization parameter of $\beta = 2 \cdot 10^{-8}$ is used whereas in the second case the regularization parameter is set to $\beta = 10^{-8}$. The resulting identified electrical conductivity for the second setting is considerably smoother than the one from the first setting without smoothed input data. These results illustrate that if the input data, i.e. u_g, are smooth the resulting electrical conductivity will be smoother too and the calculated power density will fit the given one in a better way.

Further, the quality of the results depends on the spatial position in the three dimensional data setting. Especially the results for the non-smoothed input data are spatially varying a lot. Comparing the results for the temperature in figure 6.24 with those in figure 6.25 it is noticeable that the match of the temperature to the given one depends on the spatial distribution. In figure 6.25 the temperature calculated from the identified electrical conductivity fits the given values much better than the temperature calculated corresponding to the electrical conductivity identified from the smoothed right heat source. On the other hand in figure 6.24 it is vice versa. This points out that a previously smoothing of the input data simplifies the identification of the electrical conductivity which additionally becomes smoother. However, if we do not know how smooth the original conductivity was, this may lead to more errors than an identification without smoothing. Furthermore even if the whole output is smoother the non-smooth output may fit in a better way to the given data, at least partially as seen above.

Since the scaling term $\frac{P_{\text{eff}}}{P_\Omega}$ is replaced by a scalar $p = 700$ (or $p = 350$ in the first setting) the identified values reflect the conductivity except a multiplication factor that is not known and cannot be calculated. However the calculated power density and the resulting temperature distribution are not affected by this unknown factor. The only limitation is that we cannot really compare the values with the electrical conductivity we assume to

be a good approximation. The results in figure 6.26 illustrate that we have to be careful in choosing the scaling factor due to the spatial position where we compare the results. In the figure the results are multiplied with 0.8 and 1.2, which are chosen arbitrarily. The displayed diagrams suggest a multiplication factor larger than 1 will be a good choice for the present problem. However, the choice of the multiplication factors will always pose a challenge in real applications since the exact parameters are not known and even the approximations are not that good, otherwise we would not need an identification of the parameters. On the other hand the temperature distribution according to the identified parameters will be the same whatever is chosen as multiplication factor.

However, even if the presented results for the identification of the electrical conductivity from the measurements have not been proved satisfactory, the results are an improvement compared to the assumption of a constant value. In figure 6.27 temperature distributions calculated under different assumptions are compared. The original given temperature as well as the temperature corresponding to the identified heat source, the temperature according to the identified electrical conductivity and the temperature calculated with a constant electrical conductivity of $\sigma = 0.56\,\mathrm{Sm}^{-1}$ are displayed at different positions in the three dimensional object. The figures illustrate that the identified electrical conductivity accounts more for diverse spatial informations. Comparing the corresponding temperature distributions for the identified electrical conductivity and the constant conductivity, the results approve that the temperature for the identified conductivity fits better to the original data. Whereas for some spatial positions the temperature for a constant conductivity is superior.

6.2.3 Identification of the thermal conductivity (Problem C)

The identification of the thermal conductivity from the temperature data of the RFA in Agar-gel is really difficult. Since an appropriate scaling for the parameters to enable an identification with a spatially distributed conductivity has not yet been found, the temperature dependent modeling and the optimization problem with the SQP solver `WORHP` is used. For the identification different approaches have been pursued but with minor success. One approach was to use the previously identified heat source as heat source for the present problem to avoid the calculation of the power density with an estimated electrical conductivity. But the results were non-satisfying, we could have chosen arbitrary values as well. Potentially the SQP algorithm needs further modifications according to the problem.
The second approach is to use only the temperature measurements as input data and calculate the power density by choosing a constant value for the electrical conductivity. But also for this approach the results were non-satisfying. A problem for the optimization is founded in the given temperature measurements. The duration time of the RFA is comparatively small. At the beginning of the heating the temperature diffusion in the tissue is mainly generated by the heat source. Not until a certain time the thermal conductivity influences the temperature distribution. Therefore, the provided data are inadequate most likely for the identification of the thermal conductivity.
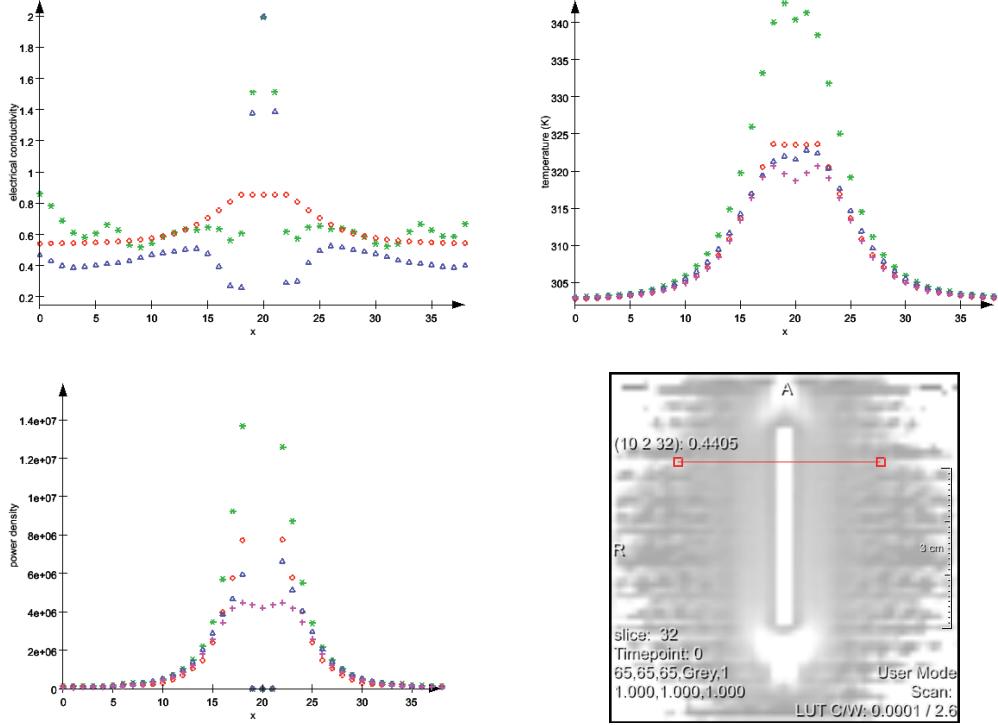
Figure 6.24: At the top left the calculated electrical conductivity for the non-smoothed input (green asterisks) and for the smoothed power (blue triangles) is compared with the conductivity $\sigma(T) = 0.56 + 0.015(T - T_{\mathrm{body}})/\mathrm{K}$ (red circles). The resulting temperature distributions and power densities are displayed at the top right and the bottom left, respectively. Additionally the temperature for the smoothed power is depicted with magenta plus and the previously identified power is depicted as red circles, since we do not know the original power. The spatial position of all values is visualized as red line in the data at the bottom right.
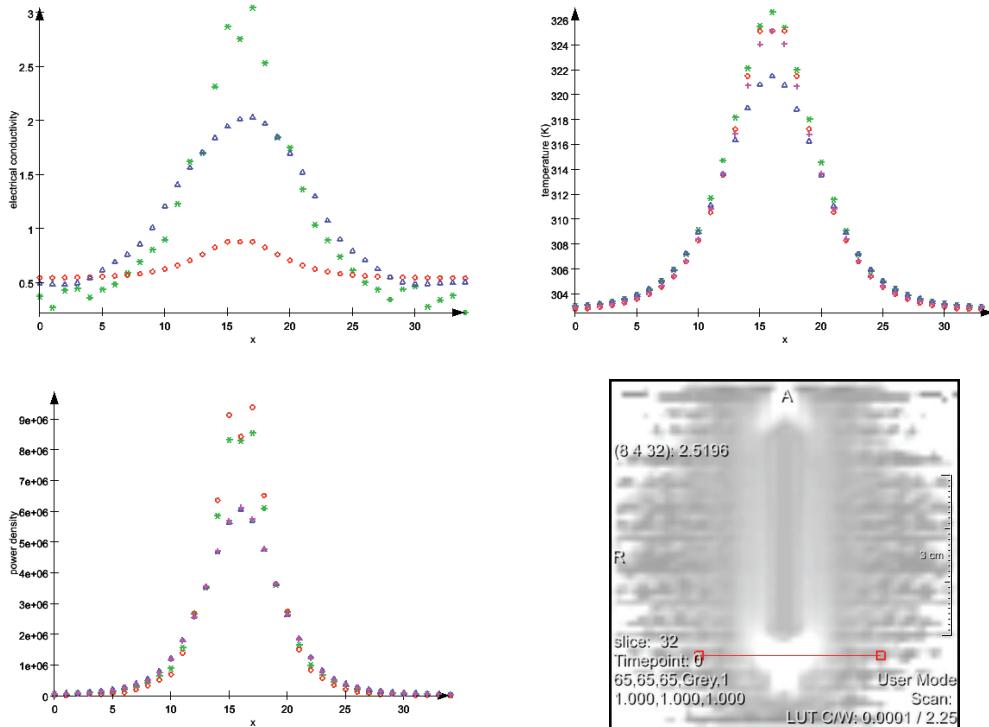
Figure 6.25: The same as in figure 6.24 at a different spatial position.
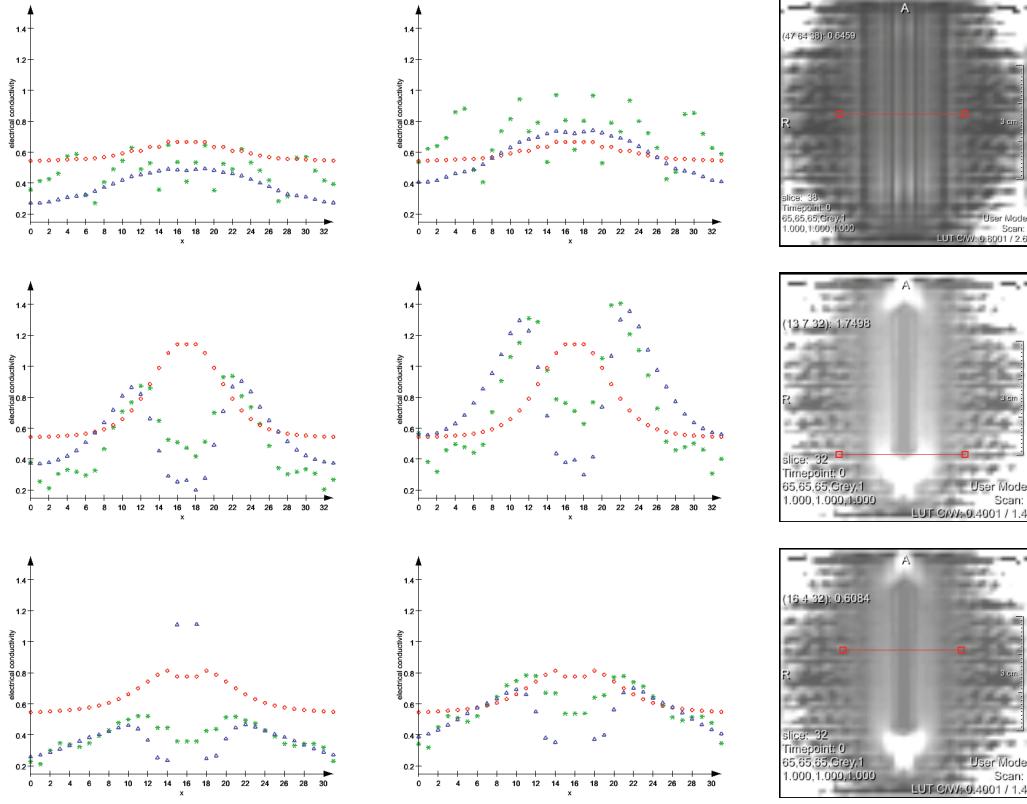
Figure 6.26: Comparison of the electrical conductivity multiplied with different factors. At the left column the identified conductivity for the non-smoothed power (green asterisks) and the identified conductivity for the smoothed power (blue triangles) are multiplied with 0.8 and compared with the values for $\sigma(T) = 0.56 + 0.015(T - T_{\text{body}})/\text{K}$ (red circles). In the centered column the values are multiplied with 1.2. The right column displays the spatial position as red line in the three dimensional object.
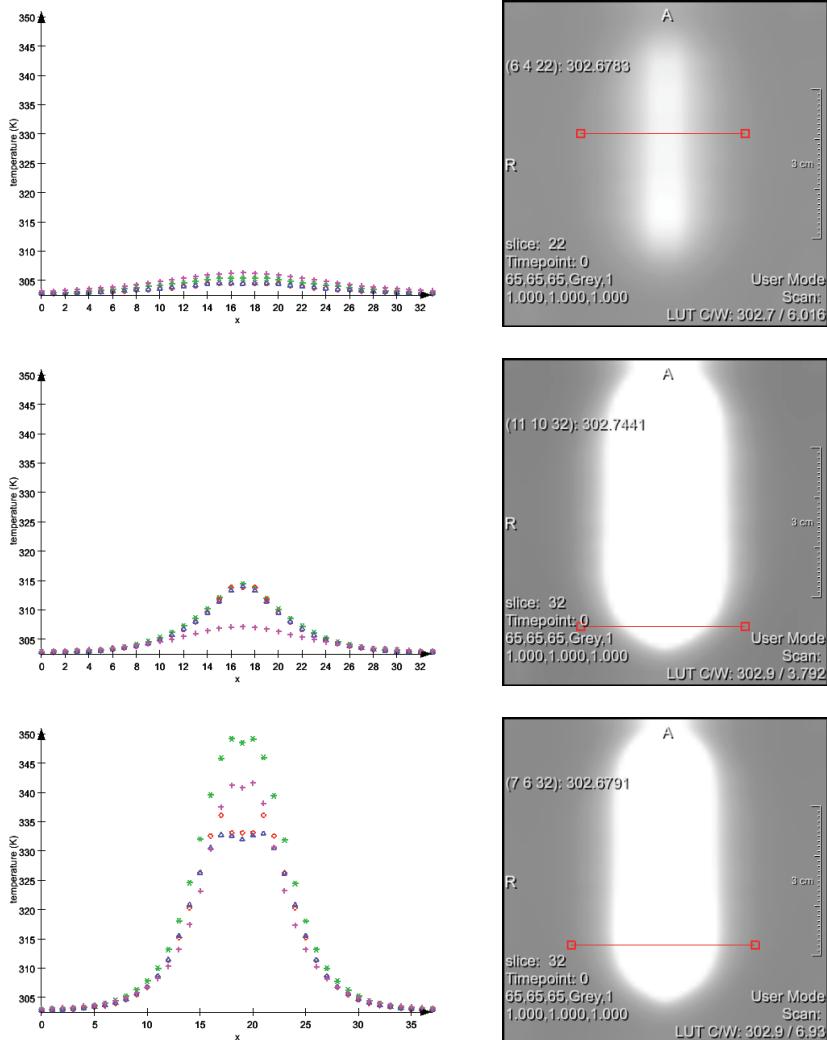
Figure 6.27: A comparison of the original temperature distribution (red circles) with the temperatures calculated corresponding to the identified heat source (blue triangles), the identified electrical conductivity (green asterisks) and a constant electrical conductivity $\sigma = 0.56\,\mathrm{S\,m}^{-1}$ (magenta plus). The values are depicted for different spatial positions, displayed as red line in the pictures in the right column.

7 Outlook

In this chapter an outlook to further investigations is given. At first the identification of an additional parameter is described. Second the extension to another thermal treatment, the high-intensity focused ultrasound therapy, is investigated and first results are presented.

7.1 Identification of the specific heat capacity and the density

Beside the thermal conductivity λ and the electrical conductivity σ the specific heat capacity c and the density ρ of the tissue influence the temperature distribution in the human body during the RFA. In the following an outlook to the additional identification of the specific heat capacity c and the density ρ is given.

7.1.1 The model

The heat capacity describes the relation of the supplied heat and the change in the temperature of the substance. The specific heat capacity c denotes the relation between the heat capacity and the substance's mass. The SI units for the specific heat capacity are $\mathrm{J\,kg^{-1}\,K^{-1}}$. Water at $20\,°\mathrm{C}$ has a specific heat capacity of $c = 4182\,\mathrm{J\,kg^{-1}\,K^{-1}}$. In comparison olive oil has a specific heat capacity of $c = 1970\,\mathrm{J\,kg^{-1}\,K^{-1}}$ [54]. Actually, the specific heat capacity depends on the temperature but for temperatures between $0\,°\mathrm{C}$ and $100\,°\mathrm{C}$ it can be assumed to be constant.

The density ρ describes the relation between the mass of a substance and its volume. The SI units are $\mathrm{kg\,m^{-3}}$. The density of liquids and solids is temperature dependent whereas the density of gases is additionally influenced by the pressure [54]. Moreover, Stein [78] models the density in dependence of the coagulation state, the temperature and the state of vaporization. The density of water at $37\,°\mathrm{C}$ is $\rho = 993.331\,\mathrm{kg\,m^{-3}}$ and for $100\,°\mathrm{C}$ we have $\rho = 958.35\,\mathrm{kg\,m^{-3}}$ [54].

Both parameters are needed for the calculations of the temperature distribution during the RFA, since they are used as parameters in the bio-heat transport equation (3.8) derived in chapter 3

$$\rho c \partial_t T(t,x) - \mathrm{div}\,(\lambda \nabla T(t,x)) = Q_{\mathrm{rf}}(t,x) + Q_{\mathrm{perf}}(t,x) \qquad \text{in } \mathbb{R}^+ \times \Omega \setminus \Omega_{\mathrm{pr}}, \tag{7.1a}$$

$$\begin{aligned}
T(0,x) &= T_{\mathrm{body}} && \text{in } \Omega, \\
T(t,x) &= T_{\mathrm{body}} && \text{on } \mathbb{R}^+ \times \Omega_{\mathrm{pr}}, \\
\nabla T(t,x) \cdot n &= 0 && \text{on } \mathbb{R}^+ \times \partial\Omega.
\end{aligned} \tag{7.1b}$$

In the following we will consider an identification problem for the product of the specific heat capacity c and the density ρ of the tissue. That means we want to identify a temperature dependent parameter $q := c\rho$. To account for the temperature dependency we assume a spatially and temporally distributed parameter $q \in L^\infty(Q)$. The objective functional is given by

$$\min_{T,q} F(T,q) := \frac{1}{2}\|T(t_{\text{fin}}, x) - T_g(x)\|^2_{H^1(\Omega)} + \frac{\theta}{2}\|\nabla q\|^2_{L^2(\Omega)} \tag{7.2}$$

with the regularization parameter $\theta \in \mathbb{R}$. The constraints are given by the bio-heat transport equation depicted above (7.1). That means we have an optimal control problem similar to Problem A2.

To derive the optimality system we use the Lagrangian technique. The Lagrange functional $\mathcal{L}(T,q,\mu) : L^2(0,t_{\text{fin}}; H^1(\Omega)) \times L^\infty(Q) \times L^2(0,t_{\text{fin}}; H^1(\Omega)) \to \mathbb{R}$ with Lagrange multiplier $\mu \in L^2(0,t_{\text{fin}}; H^1(\Omega))$, $Q := [0,t_{\text{fin}}] \times \Omega$ and constraints $h(T,q)$ as above is given by the following equation

$$\begin{aligned}
\mathcal{L}(T,q,\mu) =& F(T,q) - (h(T,q), \mu)_{L^2(Q)} \\
=& \frac{1}{2}\int_\Omega (T - T_g)^2 \, dx + \frac{1}{2}\int_\Omega (\nabla(T - T_{\text{body}}))^2 \, dx + \frac{\theta}{2}\int_\Omega (\nabla q)^2 \, dx \\
& - \int_0^\tau\!\!\int_\Omega q\partial_t T \, dx - \int_0^\tau\!\!\int_\Omega \lambda\nabla T\nabla\mu \, dx - \int_\Omega \nu(T - T_{\text{body}})\mu \, dx.
\end{aligned}$$

The corresponding adjoint system is derived by differentiating the Lagrangian functional and similar to the adjoint equation described in (5.13). If we use a linearization in time, i.e. the time derivative $\partial_t T$ is replaced by a Helmholtz term $\frac{1}{\tau}(T - T_0)$, we obtain the following adjoint system

$$\begin{aligned}
\frac{q}{\tau}\mu - \text{div}(\lambda\nabla\mu) + \nu\mu =& (T - T_g) - \text{div}\left(\nabla(T - T_g)\right) && \text{in } \Omega, \\
\mu =& 0 && \text{on } \Omega_{\text{pr}}, \\
\nabla\mu \cdot n =& 0 && \text{on } \partial\Omega.
\end{aligned}$$

The corresponding variational inequality is given by

$$D_q\mathcal{L}(T,q,\mu)(v - q) = \int_\Omega \alpha\nabla q\nabla(v - q) \, dx - \int_\Omega (T - T_{\text{body}})\mu(v - q) \, dx \geq 0, \quad \forall v \in U^q_{\text{ad}},$$

with $U^q_{\text{ad}} := \{q \in L^\infty(\Omega)\,|\, 0 < q_a \leq q(x) \leq q_b\}$.

The existence of an optimal control can be shown similar to the problems described in chapter 5. After a linearization in time by replacing the time derivative $\partial_t T$ with a Helmholtz-term, we obtain from the Lemma of Lax-Milgram the existence of a unique solution $T \in H^1(\Omega)$ for every $q \in U^q_{\text{ad}}$ for the linearized version of (7.1). Therewith we have a control-to-state operator $S : L^\infty(\Omega) \to H^1(\Omega)$ and can proceed as for Problem
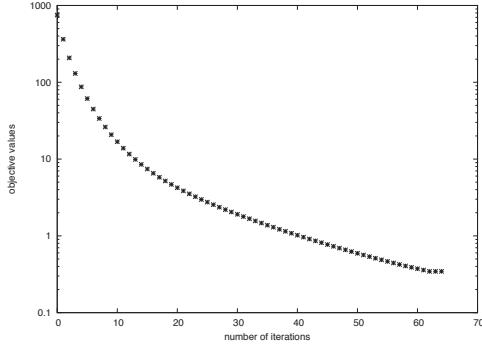
Figure 7.1: The progression of the objective values for the optimization of the specific heat capacity and the density. The optimized parameter is spatially distributed. A logarithmic scale is used for the objective values.

A1 and Problem A2 (see chapter 5).

7.1.2 First numerical results

The problem described above is implemented for two different cases, which are both discretized with FEM. The first case works with a spatially distributed parameter q and is implemented in `QuocMesh`. The used algorithm is the gradient descent method described in Algorithm 2 on page 45. The same setting as in 6.1.2 is used. That means the same data are used and the position of the probe is the same as well as the body temperature and the boundary conditions for the potential and the heat equation. The electrical conductivity is set to $\bar{\sigma} = \{0.48, 0.42, 0.48\}\,\mathrm{S\,m^{-1}}$ and the thermal conductivity is chosen as $\bar{\lambda} = \{0.45, 0.53, 0.45\}\,\mathrm{S\,m^{-1}}$ for native liver tissue, tumorous tissue and the vascular system respectively. The optimal values for the product of the specific heat capacity c and the density ρ is set to $q = \rho c = 3.74 \cdot 10^6\,\mathrm{J\,K^{-1}m^{-3}}$ in the native liver tissue and the vascular system and to $q = \rho c = 3.75 \cdot 10^6\,\mathrm{J\,K^{-1}m^{-3}}$ in tumorous tissue. As initial guess we choose $q_0 = 50000\,\mathrm{J\,K^{-1}m^{-3}}$. The regularization term is neglected since an exactly known data set is used. The progression of the objective functional values is displayed in figure 7.1. First results are depicted in figure 7.2. The calculated parameter is depicted as well as the corresponding temperature. Both are compared with the given values.

The second test case is formulated as optimization problem and uses the same setting as described in section 6.1.3. That means the same data are used and the same conditions for the potential and the heat equation. The probe is placed at (22, 13, 11) in the grid with an orientation of (0, 0, -1). The optimal values for the tissue dependent electrical conductivity are $\bar{\sigma} = \{0.56, 0.62, 0.58\}\,\mathrm{S\,m^{-1}}$ for liver tissue, tumorous tissue and the vascular structures. The thermal conductivity is additionally temperature dependent and set as follows: $\bar{\lambda}_{\mathrm{ref}} = \{0.47, 0.56, 0.53\}$ and $\bar{\alpha}_\lambda = \{0.014, 0.105, 0.014\}\,\mathrm{S\,m^{-1}}$. The regularization parameter θ is equal zero since we do not use any regularization due to
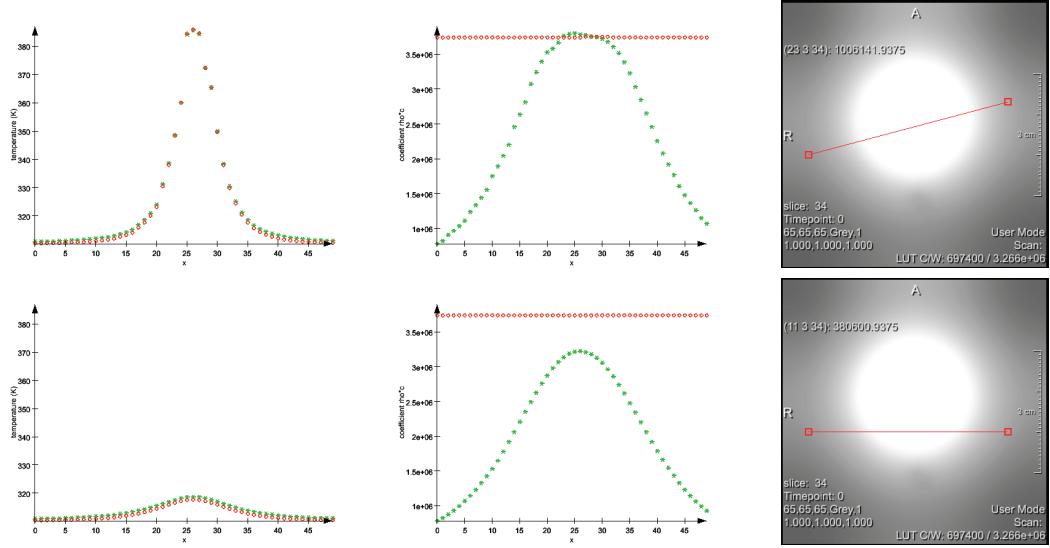
Figure 7.2: The results for the identification of a spatially distributed parameter $q = \rho c$. From left to right: the temperature, the identified parameter and the spatial position of the displayed values depicted as red line in the picture of the identified parameter. The calculated values (green asterisks) are compared with the optimal values (red circles).

the exact input data. The optimization is performed with the SQP solver `WORHP`. We assume a constant parameter $q = \rho c$ and model the problem without any constraints. The heat equation is incorporated in the calculations of the objective and the gradient is calculated by the FD method provided by the solver. The step size for the FD method is defined as $\tau = 10^{-5}$. As initial value $q = \rho c = 10000\,\mathrm{J\,K^{-1}m^{-3}}$ is chosen and the tolerance for the solver is set to tol $= 10^{-17}$. Additionally the objective is multiplied with a scaling factor $\xi = 10^7$. In figure 7.3 the progression of the objective values during the optimization is displayed.

Beside the objective functional described in (7.2) also the following objective functional is considered, where the H^1-norm in the main part is replaced by the L^2-norm as described for Problem C

$$\min_{q} F(T, q) := \frac{1}{2}\|T(t_{\mathrm{fin}}, x) - T_g(x)\|^2_{L^2(\Omega)} + \frac{\theta}{2}\|\nabla q\|^2_{L^2(\Omega)}.$$

The results for both optimization problems, i.e. H^1-norm and L^2-norm with a constant parameter $q = \rho c \in \mathbb{R}$, are displayed in table 7.1. In figure 7.4 the temperature calculated according to the optimized parameter q is compared with the given temperature. Therewith, the temperature for the results from the objective functional with L^2-norm and with H^1-norm are displayed.

The presented results for both cases, the spatially distributed parameter and the con-
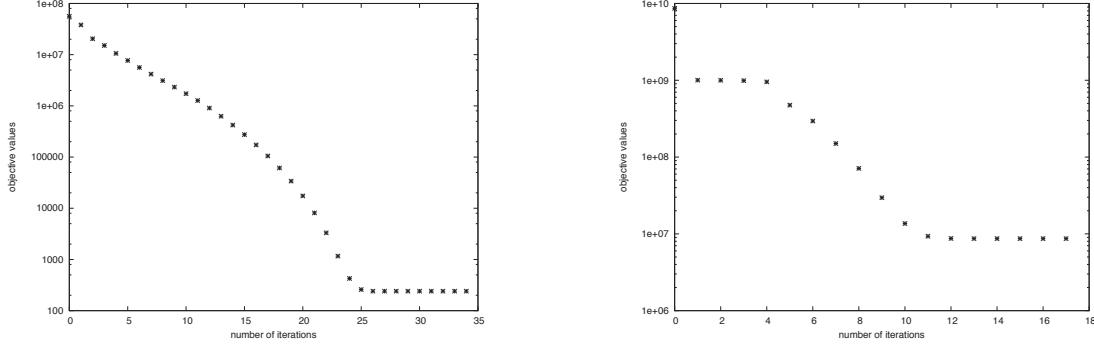
Figure 7.3: The progression of the objective values for the optimization of the heat capacity and the density. On the left the objective values for the L^2-norm in the objective functional are displayed. On the right the objective values for the H^1-norm in the objective functional are shown. The optimized coefficient is assumed to be a constant value.

objective	$\bar{q}$ $(\mathrm{J\,K^{-1}m^{-3}})$	q $(\mathrm{J\,K^{-1}m^{-3}})$	F	KKT
$L^2(\Omega)$	$3.4 \cdot 10^6$	3735451.32095	240.452	$2.381 \cdot 10^{-19}$
$H^1(\Omega)$	$3.4 \cdot 10^6$	3819166.02542	8682497.24	$1.962 \cdot 10^{-20}$

Table 7.1: The results for the identification of the constant parameter $q = \rho c$. From left to right: the norm in the objective functional, the given parameter $\bar{q}$, the calculated parameter q, the final objective value F and the final KKT value.

stant parameter, illustrate that this problem need to be investigated further. For the spatially distributed parameter the calculated values fit the given ones in the vicinity of the probe. However, distant to the probe the values do not match. This is founded by the local impact of the temperature distribution. As in the problems describe before, an additional scaling may improve the results a lot. Further, a separated optimization for the density and the heat capacity are possible. Due to the only small temperature dependency of the heat capacity the identification should improve for this parameter. The results for the optimization of the constant parameter $q = \rho c$ are similar. According to the non-matching parameters, described in table 7.1, the temperature distributions, depicted in figure 7.4, do not fit to the optimal temperature. Since we assume a constant value for the whole domain the mismatch can not only be based on the impact of the temperature distribution, there must be other effects which has to be explored further. Presumable another scaling for the objective will change something. First investigations with different scalings led to distinct results. However, a better solution has not been found to date.
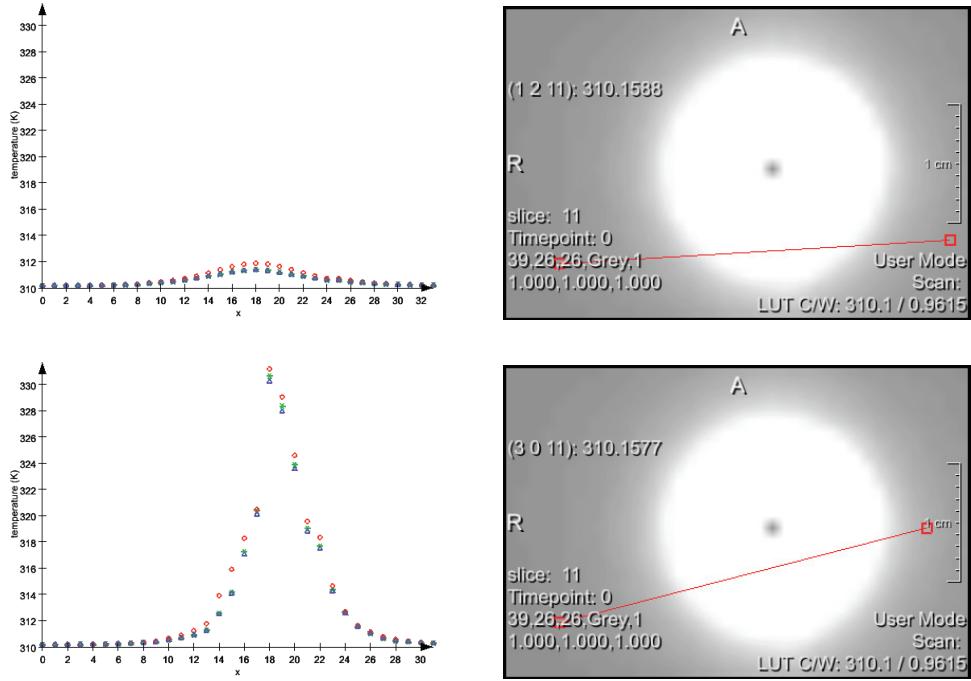
Figure 7.4: The results for the identification of a constant parameter $q = \rho c$. The temperature for the result from the objective with L^2-norm is depicted as green asterisks. The temperature for the H^1 objective with blue triangles. The given values are given as red circles. At the right the position of the depicted values is shown as red line in the picture of the temperature.

7.2 Extension to the method of high-intensity focused ultrasound

In this section a brief outlook is given on how the identification can be extended to other thermal treatments as the method of high-intensity focused ultrasound.

7.2.1 High-intensity focused ultrasound

Another promising ablation technique beside the RFA is the method of high-intensity focused ultrasound (HIFU). HIFU is a non-invasive therapy where focused ultrasound waves lead to a heating of the tissue. HIFU is a therapeutic modality which is applicable for tumor ablation as well as hemostasis, thrombolysis or targeted drug delivery. An overview of the method is given e.g. in the review of Kim et al. [48]. The different modalities and applications are also described in the paper of Ter Haar [86].

For tumor ablation, e.g. benign prostatic hyperplasia, the idea of HIFU therapy is the same as for RFA. By conducting energy to the tissue the tumorous cells will be heated

and therewith destroyed due to the coagulation of the proteins. The main difference is the way how the energy is inflicted. For the method of RFA a probe has to be placed in the tumorous tissue whereas by the method of HIFU the transducer is placed outside the tissue. The arising pressure of the applied ultrasound leads to a heating of the tissue. The ultrasound beams are focused at that point where the tissue shall be destroyed whereas the surrounding tissue is almost unaffected. The generated lesions are much smaller than for RFA but the exposure time is even less (in the range of seconds) such that several exposures are placed side by side to achieve a larger affected area.

For the simulation of the temperature distribution generated by HIFU the bio-heat transport equation will be used as for the simulation of the RFA. But due to the different energy conduction the term which describes the heat source has to be replaced, instead of the squared potential the squared pressure is used. The resulting steady state bio-heat transport equation is given by

$$-\mathrm{div}\,(\lambda \nabla T) + \nu(T - T_{\mathrm{body}}) = \frac{\omega}{\rho_p c_p} p p^T \quad \text{in } \Omega, \tag{7.3}$$

where Ω is the computational domain and p denotes the pressure and p^T its transpose. The attenuation coefficient for a certain ultrasound frequency is denoted by ω and the values ρ_p and c_p denote the density of sound and the speed of sound respectively. The cooling effect of the vascular system and the blood perfusion are taken into account via the perfusion term $\nu(T - T_{\mathrm{body}})$ as described in section 3.2 for the RFA. Altogether, equation (7.3) is the same as (3.8) with steady state and beside the heat source. The pressure p can be calculated in different ways as e.g. described in the paper of Zeng and McGough [93]. In the following we will consider the identification of the pressure as heat source for the temperature distribution given by MR thermometry. Since the heat equations are similar for the RFA and HIFU we can use the same algorithm as before.

7.2.2 MR thermometry

In this section the method of MR thermometry is briefly explained.

MRI is not only an imaging method, it offers more functional modalities, as e.g. the temperature measurements, the so called MR thermometry. The method of MRI is based on electromagnetic fields and their influence on the water protons in the body. With the help of a powerful magnetic field the water protons are aligned and afterwards this alignment is systematically altered by a radio-frequency field. The realignment of the protons can be measured by the scanner. Since the protons in the diverse tissue types need different times to realign to their equilibrium state, an image of the diverse tissue types can be constructed.

For the MR thermometry the sensitivity of the proton resonance frequency (PRF) to the temperature is used. Further information to the temperature sensitivity of the PRF can be found in [45]. To calculate the temperature we use changes in the phase images which depend on the changes in the resonance frequency [68]. That means we calculate the temperature from the difference between two phase images. The changing of the
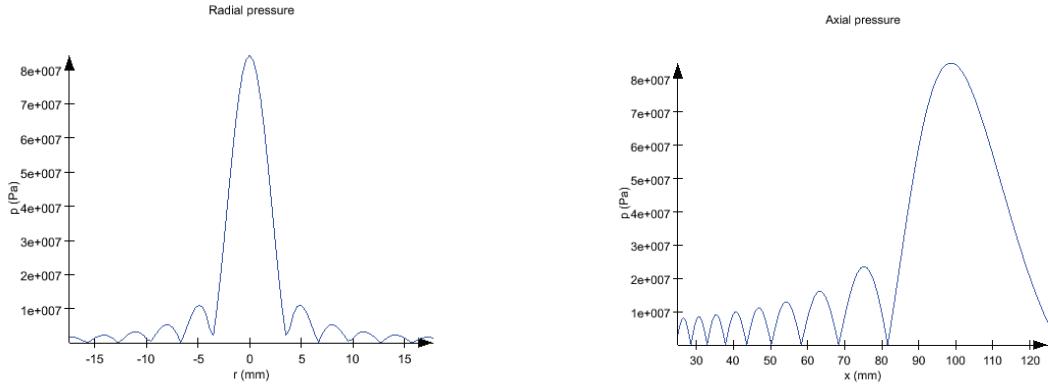
Figure 7.5: The radial and axial view of the pressure for HIFU are displayed. The used frequency is $f = 0.5\,\mathrm{MHz}$ and the depth of the focus is $10\,\mathrm{cm}$. The data are provided by S. Meier from Fraunhofer MEVIS, Germany.

temperature ΔT can be calculated with the following formula

$$\Delta T = \frac{\Psi(T) - \Psi(T_0)}{\varrho \theta B_0 TE},$$

where $\Psi(T)$ denotes the current image and $\Psi(T_0)$ the reference phase image at a known temperature. The further parameters denote the gyromagnetic ratio ϱ, the PRF change coefficient θ, the magnetic field strength B_0 and the echo time TE. There exists different software for the calculation and illustration of the temperature, as e.g. TAM [59]. The data which are used in the following are provided by D. Haemmerich[1].

7.2.3 Identification of the pressure

The measurements which are used in the following are generated by MR thermometry during an HIFU ablation in an Agar-gel. The used gel is the same as in the example above. Due to the different method for the temperature measurement the obtained data distinguish from that above. The size of the pixels is with $2.5 \times 2.5\,\mathrm{mm}$ larger than those taken by the infrared camera but the number of pixels is larger, we have 160×160 pixels in each time frame. Between the recorded data frames there is a slot of approximately $2.9\,\mathrm{s}$. The duration of the ablation was about $30\,\mathrm{s}$ followed by $90\,\mathrm{s}$ cooling afterwards. In figure 7.5 typical pressures in an axial and radial view are displayed.

For the identification of the spatially distributed pressure the given data is at first rotated to obtain a three dimensional object and afterwards they are resampled to a size of $128 \times 128 \times 128$ pixel. As in the case of the RFA in the Agar-gel we assume that the data is rotationally symmetric with a horizontal rotation axis. The tissue parameters density ρ and heat capacity c are set to the typical values of water as above,

---

[1]Medical University of South Carolina, USA.

i.e. $\rho = 997 \, \mathrm{kg \, m^{-3}}$ and $c = 4181.3 \, \mathrm{J \, kg^{-1} \, K^{-1}}$. The body temperature is set to $35.142 \, \mathrm{^{\circ}C}$ according to the measured data. As initial value the pressure is set to $u_0 = 100$. The optimization is done as described before for the heat source in Problem A1.1, performed by the gradient method described in Algorithm 2 on page 45, implemented in `QuocMesh`. After 22 iterations the optimization stops due to the termination criterion as described before in (5.20). The progression of the objective values is depicted in figure 7.6. The results shown in figures 7.7 and 7.8 illustrates that the main shape of the pressure is reflected, compared with the artificial examples in figure 7.5, but the temperature values are larger than the given ones. This may be caused by different effects and needs further investigations. One reason can be the parameters in the optimization algorithm, as termination condition, step size or regularization parameter. But further the mismatch can also be based on the given data. Further information how these data are generated may improve the results as well as the usage of a finer grid. Moreover, there are some parts in the domain where the measured temperature is below the assumed body temperature. This might be also a reason for the calculated temperature being a little bit too large at the boundary and partly in the center. However, the calculated pressure reflects the typical shape and these first results are promising that with further investigations an identification of the pressure will be possible.
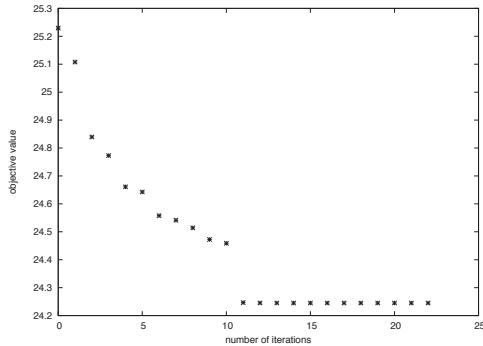
Figure 7.6: The progression of the objective values for the identification of the pressure in HIFU.
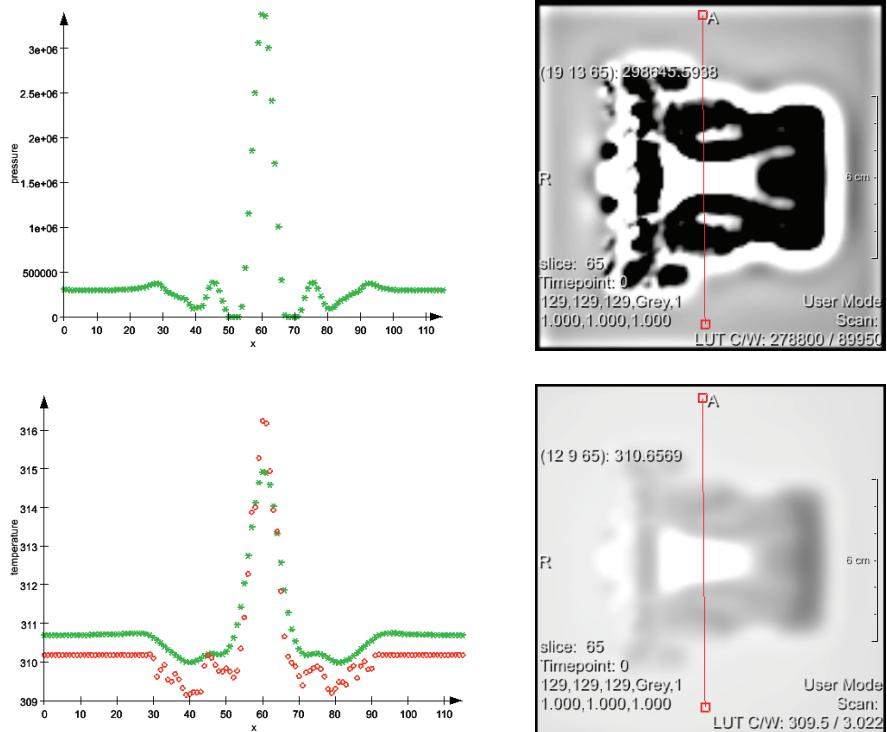
Figure 7.7: The results for the identification of the pressure from MR thermometry measurements for the HIFU ablation in Agar-gel. The calculated pressure (top left) and the resulting temperature (bottom left) are denoted by green asterisks, whereas the given temperature is displayed with red circles. The results show a radial view through the center of the data, displayed as red line in the right column.
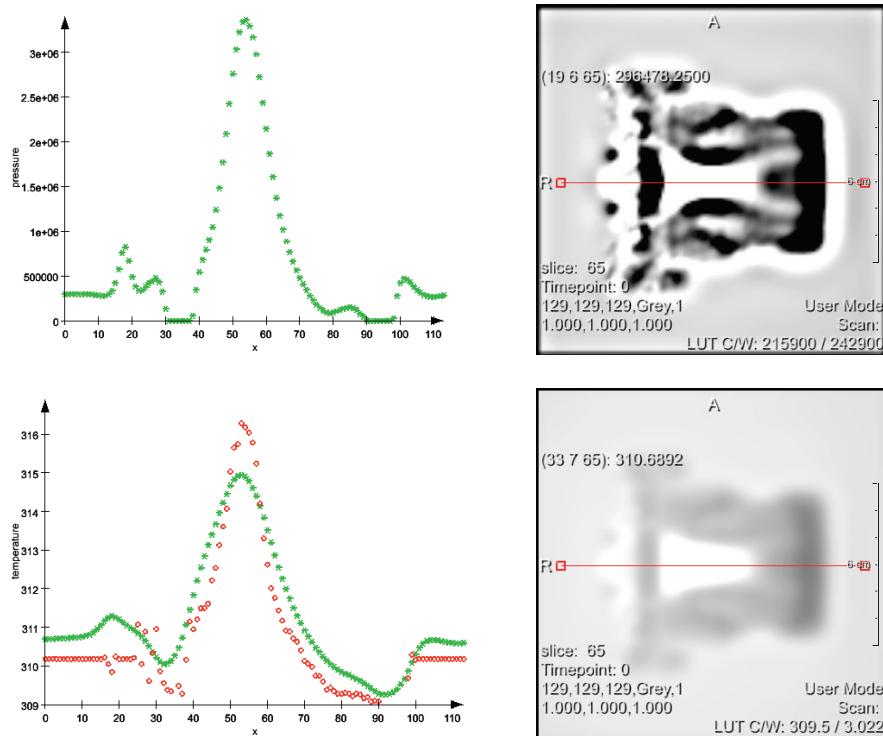
Figure 7.8: The results for the identification of the pressure from MR thermometry measurements for the HIFU ablation in Agar-gel. The calculated pressure (top left) and the resulting temperature (bottom left) are denoted by green asterisks, whereas the given temperature is displayed with red circles. The results show an axial view through the center of the data, displayed as red line in the right column.

8 Conclusions

In this thesis the parameter identification from temperature measurements during the RFA has been discussed.

For a realistic prediction of the outcome of an RFA we need a mathematical model that describes the physical effects as good as possible. Due to the lacking knowledge of the exact material parameters and the patient individual differences we addressed in this work to the patient individual identification of the material parameters during the RFA. To simulate the result of the RFA the temperature distribution during the treatment is modeled by a system of two coupled PDEs, the bio-heat transport equation and the potential equation. Both equations are significantly influenced by the material parameters. Therefore a parameter identification problem was formulated by fitting the temperature to a given temperature distribution. This states a minimization problem with tracking type functional. Since different parameters were considered which influence the whole system in distinct ways the identification was split into two main parts. For the identification of the thermal conductivity the minimization problem was defined as the minimization of the difference between the calculated and the given temperature distribution. For the identification of the electrical conductivity a modified approach was needed. The electrical conductivity influences the temperature distribution only via the heat source, i.e. the right hand side of the heat equation. Due to the only local impact of the heat source on the temperature distribution the identification of a spatially varying electrical conductivity is nearly impossible. Therefore, a second minimization problem was considered where at first the heat source was identified from the temperature distribution. Afterwards this identified heat source was used for the identification of the electrical conductivity. For both approaches the optimality systems were formulated and in a general form investigated concerning the existence of solutions.

To apply the above minimization problems different aspects needed to be considered. The first question was the modeling of the parameters. In this work different models were investigated, constant, tissue dependent, temperature dependent and spatially distributed parameters. All formulations have advantages and drawbacks. The local impact of the heat source suggests to choose a modeling which includes information from the whole domain, as e.g. the temperature. That means the parameters should be defined in dependency of the temperature. For the thermal conductivity this worked well since it is known from different measurements that the thermal conductivity depends linearly on the temperature. However, for the electrical conductivity this is not the case. As the measurements from porcine liver have shown the electrical conductivity does not depend linearly on the temperature. Therefore a more complex model would be needed. But a description with a polynomial of higher degree will lead to a more complex optimization particularly if we do not know the type of temperature dependency. Hence

an identification problem with a spatially distributed electrical conductivity was formulated. This increases the number of optimization variables significantly and therewith demands another kind of optimization method. For the constant or temperature dependent parameters the SQP solver *WORHP* was used whereas for the spatially distributed parameters a gradient method was implemented in *QuocMesh*, an FEM toolbox.

The spatially distributed parameters rose a new challenge since the advantages of the temperature dependent parameters had been lost. The local influence of the heat source and the temperature on the system precluded a direct identification of the parameters. An additional scaling of the parameters or the objective functional was necessary. However for the original system stated by the system of given PDEs for the modeling of the RFA an appropriate scaling has not been found yet. Nevertheless, for the identification of the electrical conductivity a solution was possible by approximating the scaling term $\frac{P_{\text{eff}}}{P_{\Omega}}$ for the heat source by a scalar value. Additionally the objective was scaled with the piecewise reciprocal of the squared gradient of the potential. The scaling factor is introduced in the model since for the potential an arbitrarily chosen value of $+1$ and -1 at the electrodes is assumed which does not correspond to the reality. Furthermore the effect of the impedance matching is modeled by this scaling term. The problem for the optimization caused by this term is that the term $\frac{P_{\text{eff}}}{P_{\Omega}}$ depends nonlinear on the electrical conductivity and the potential, which in turn depends on the conductivity. Therefore the gradient, which is already problematic with a constant scaling factor, became even worse. Due to the local influence of the heat source the gradient is almost flat in most parts of the domain. Only near the probe it is really steep which causes the main problems in the optimization process. For the scaling factor depending on the conductivity this effect is aggravated. For a spatially distributed thermal conductivity a similar effect was observed which made an identification without scaling impossible.

The presented results show the identification of constant parameters, tissue dependent parameters, temperature dependent parameters and spatially distributed electrical conductivity. The methods were applied to artificial data mainly to illustrate the advantages and drawbacks of the approaches. Finally, they were partially applied to real data from temperature measurements of the RFA in an Agar-gel as well as MR thermometry data of a HIFU therapy in Agar-gel. The quality of the results depended highly on the quality of the input data. For example for a generated and well known heat source it was possible to identify the electrical conductivity nearly exactly whereas for the real data the results were less accurate. Moreover the quality of the results also depends on the setting. In the artificial setting it was observed that the optimization of tissue dependent parameters only worked if the probe were placed in the vicinity of the according tissue types. This is originated by the local impact of the power density. However the results indicate that an identification of the parameters improve the model for the RFA as well as the ameliorated knowledge of the behavior of the heat source. This improvements will also influence the simulation in a positive way. It will enhance the simulation and lead to a corrected prediction of the outcome of the RFA.

The basic idea of the present thesis was the patient individual improvement of the simulation of the RFA. The aim was to identify the patient individual parameters from

temperature measurements during the RFA and to update the values for the simulation accordingly. The predicted results from the corrected simulation of the RFA could be used to adapt the current setting, e.g. the probe's position, and therewith improve the success of the ablation.

However, the long-term goal, the identification of the parameters during the RFA, has not been reached yet, since the calculations are too time consuming and the identification is limited by different problems. Nevertheless, the identification works well for artificial data and also with measured data, if we restrict the problem to the identification of the heat source. The problems concerning the identification of the spatially distributed parameters from measured temperature distributions are based on the problem modeling, namely the ill-posedness of the bio-heat transport equation, as well as on the insufficient quality of the temperature data. An approach to improve the identification is to modify the measured data, e.g. to smooth the data with an additional scaling. This will need further investigations since an additional smoothing always leads to attenuation of spatial information. But as already seen in this work a smoothing can also be advantageous since the optimization ease. The loss of information and the benefit for the optimization must be weighed.

To improve the identification itself, different approaches are imaginable. The model can be improved as well as the algorithm. However, the main benefit will be obtained by an appropriate scaling of the parameters or the objective functional. That means if we want to apply the developed methods successfully to measured data we have to include an additional scaling term, as has been used for the identification of the electrical conductivity in a first attempt. This scaling together with the approximation of the scaling term $\frac{P_{\text{eff}}}{P_\Omega}$ with a constant value $p \in \mathbb{R}$ made the identification of a spatially distributed electrical conductivity σ possible, except for the factorization. That means we can determine only the product $p\sigma$ and not the conductivity σ itself. However, for the temperature calculations the exact factorization is not needed. An appropriate scaling will provide the identification of spatially distributed parameters.

Furthermore we may think of an improvement of the algorithms by using an SQP method for the spatially distributed parameters or combine the tissue and temperature dependent parameter modeling in the optimization problem with a higher spatial diversity of the coefficients. That means we would use a higher spatial resolution for the parameters instead of only three different tissue types.

Regarding the problem with the computational time, even if we are not able to speed up the calculations to identify the parameters during the RFA we can use the results from different temperature measurements to get an impression of the temperature dependence and the typical values of the parameters. Even if this is not a patient individual improvement it is still an improvement of the model and the simulation if we rely no longer on the experimental data from porcine liver or ex vivo measurements.

Beside an improvement of the model we may also think of another application of the parameter identification. As the results in the outlook have shown, the application of the identification of the heat source is transferable to other thermal ablation methods as high focused ultrasound. This first results suggests that an identification of the heat

source and probably also the material parameters is possible also from HIFU temperature measurements. The advantage from HIFU is that in many cases MRI is used for imaging as well as for thermometry measurements whereas RFA is often performed with X-ray computed tomography since for the ablation in MRI there are special probes needed. Therefore in practice the method of HIFU is a promising scope of application.

Bibliography

[1] MeVisLab. *http://www.mevislab.de*, 07.06.2011.

[2] Quocmesh. *http://numod.ins.uni-bonn.de/teaching/ss10/numsim/doc/html/main.html*, 07.06.2011.

[3] R. A. Adams and J. J. F. Fournier. *Sobolev Spaces*. Academic Pres, Elsevier Ltd, Amsterdam, 2003.

[4] H. W. Alt. *Lineare Funktionalanalysis*. Springer-Verlag, Berlin Heidelberg, 2006.

[5] I. Altrogge. *Optimization of the Probe Placement for Radiofrequency Ablation*. PhD thesis, University of Bremen, 2009.

[6] S. N. Antontsev and M. Chipot. The thermistor problem: Existence, smoothness, uniqueness, blowup. *SIAM J. Math. Anal.*, 25:1128–1156, 1994.

[7] H. Arkin, L. X. Xu, and K. R. Holmes. Recent developments in modeling heat transfer in blood perfused tissues. *IEEE Transactions on Biomedical Engineering*, 41(2):97–107, 1994.

[8] S. Arrhenius. Über die Reaktionsgeschwindigkeit bei der Inversion von Rohrzucker durch Säuren. *Z Phys Chem*, 4:226–248, 1887.

[9] U. Aßmann and A. Rösch. Identification of an unknown parameter function in the main part of an elliptic partial differential equation. *submitted*, 2011.

[10] E. J. Berjano. Theoretical modeling for radiofrequency ablation: state-of-the-art and challenges for the future. *Biomed Eng Online*, 5(24), 2006.

[11] J. F. Bonnans, J. C. Gilbert, C. Lemaréchal, and c. A. Sagastizábal. *Numerical Optimization: Theoretical and Practical Aspects*. Springer-Verlag, Berlin Heidelberg, 2006.

[12] H. F. Bowman. Heat transfer and thermal dosimetry. *J Microwave Power*, 16(2):121–133, 1981.

[13] H. F. Bowman, E. G. Cravalho, and M. Woods. Theory, measurement, and application of thermal properties of biomaterials. *Ann. Rev. Biophys. Bioeng.*, 4:43–80, 1975.

[14] D. Braess. *Finite Elemente. Theorie, schnelle Löser und Anwendungen in der Elastizitätstheorie*. Springer-Verlag, Berlin Heidelberg, 2003.

Bibliography

[15] I. Chang. Finite element analysis of hepatic radiofrequency ablation probes using temperature-dependent electrical conductivity. *BioMedical Engineering OnLine*, 2, 2003.

[16] Ch.-Ch. R. Chen and M. I. Miga. Optimizing electrode placement using finite-element models in radiofrequency ablation treatment planning. *IEEE Transactions on Biomedical Engineering*, 56:237–245, 2009.

[17] H. W. Engl and J. Zou. A new approach to convergence rate analysis of tikhonov regularization for parameter identification in heat conductivity. *Inverse Problems*, 16:1907–1923, 2000.

[18] E. C. Feliberti and L. D. Wagman. Radiofrequency ablation of liver metastases from colorectal carcinoma. *Cancer control*, 13(1):48–51, 2006.

[19] J. Ferlay, D. M. Parkin, and E. Steliarova-Foucher. Estimates of cancer incidence and mortality in europe in 2008. *European Journal of Cancer control*, 46(4):765–781, 2010.

[20] C. Gabriel, S. Gabriel, and E. Corthout. The dielectric properties of biological tissues: I. literature survey. *Phys. Med. Biol.*, 41:2231–2249, 1996.

[21] T. Gänzler, S. Volkwein, and M. Weiser. SQP methods for parameter identification problems arising in hyperthermia. *Optimization Methods and Software*, 21:869–887, 2006.

[22] C. Geiger and C. Kanzow. *Theorie und Numerik restringierter Optimierungsaufgaben*. Springer-Verlag, Berlin Heidelberg, 2002.

[23] M. Gerdts. Optimization. *http://www.unibw.de/lrt1/gerdts/lehre/optimierung.pdf (02.07.2009)*, 2006.

[24] D. Gilbarg and N. S. Trudinger. *Elliptic Partial Differential Equations of Second Order*. Springer-Verlag, Berlin, Heidelberg, 2001.

[25] P. E. Gill, W. Murray, and M. H. Wright. *Practical Optimization*. Elsevier Academic Press, London, 2004.

[26] D. Givoli. Use of the kirchhoff transformation in finite element analysis. *Int. J. Num. Meth. Heat Fluid Flow*, 3:473–479, 1993.

[27] R. Griesse. Lecture notes: Infinite-dimensional optimization, 2006.

[28] C. Grossmann, H.-G. Roos, and M. Stynes. *Numerical Treatment of Partial Differential Equations*. Springer-Verlag, Berlin, Heidelberg, 2007.

[29] C. Großmann and J. Terno. *Numerik der Optimierung*. B. G. Teubner, Stuttgart, 1993.

[30] W. A. Gruver and E. W. Sachs. *Algorithmic methods in optimal control.* Pitman, London, 1980.

[31] S. Gutman. Identification of discontinous parameters in flow equations. *SIAM J. Control and Optimization*, 28:1049–1060, 1990.

[32] D. Haemmerich. Medical University of South Carolina, USA. *Personal communication*, Mai 2011.

[33] D. Haemmerich, S. T. Staelin, J. Z. Tsai, S. Tungjitkusolmun, D. M. Mahvi, and J. G. Webster. In vivo electrical conductivity of hepatic tumours. *Physiol. Meas.*, 24:251–260, 2003.

[34] S. P. Han. A globally convergent method for nonlinear programming. *Journal Of Optimization Theory And Applications*, 22(3):297–309, 1977. printed.

[35] P. C. Hansen. The l-curve and its use in the numerical treatment of inverse problems. *http://www.sintef.no/project/eVITAmeeting/2005/Lcurve.pdf (18.04.2011)*, 2005.

[36] L. Hermann. Über eine Wirkung galvanischer Ströme auf Muskeln und Nerven. *Pflügers Archiv Gesamte Physiol. Menschen und Tiere*, 5:223 ff, 1872.

[37] B. Hofmann. *Mathematik inverser Probleme.* B. G.Teubner Stuttgart Leipzig, 1999.

[38] D. Hömberg, C. Meyer, J. Rehberg, and W. Ring. Optimal control of the thermistor problem. *SIAM Journal Control Optim.*, to appear, 2009.

[39] S. Humphries, K. R. Rick, D. A. Schechter, and N. Goldberg. Three-dimensional finite-element code for electrosurgery and thermal ablation simulations. (Patent: US 2006/0257836 A1), Nov. 16, 2006.

[40] A. D. Ioffe and V. M. Tihomirov. *Therory of extremal problems.* North-Holland Publishing Company, 1979.

[41] C. Johnson. *Numerical solution of partial differential equations by the finite element method.* Cambridge U. Pr., Cambridge, 1988.

[42] P. C. Johnson and G. M. Saidel. Thermal model for fast simulation during magnetic resonance imaging guidance of radio frequency tumor ablation. *Annals of Biomedical Engineering*, 30:1152–1161, 2002.

[43] J. Kačur. Method of rothe in evolution equations. *Lecture Notes in Mathematics*, 1192:23–34, 1986.

[44] Y. L. Keung and J. Zou. Numerical identifications of parameters in parabolic systems. *Inverse Problems*, 14:83–100, 1998.

[45] A. Kickhefel. Untersuchung zur laserinduzierten thermotherapie. Master's thesis, Ernst-Moritz-Arndt-Univeristät Greifswald, 2007.

Bibliography

[46] S. Kim. A simple direct estimation of temperature-dependent thermal conductivity with kirchhoff transformation. *Int. Comm. Heat Mass Transfer*, 28(4):537–544, 2001.

[47] S. Kim, B.-J. Chung, M. C. Kim, and K. Y. Kim. A note on the direct estimation of thermal properties in a transient nonlinear heat conduction medium. *Int. Comm. Heat Mass Transfer*, 29(6):787–795, 2002.

[48] Y. Kim, H. Rhim, M. J. Choi, H. K. Lim, and D. Choi. High-intensity focused ultrasound therapy: an overview for radiologists. *Korean J Radiol*, 9(4):291–302, 2008.

[49] I. Knowles. Parameter identification for elliptic problems. *Journal of Computational and Applied Mathematics*, 131:175–194, 2001.

[50] T. Kröger. CeVis, University of Bremen. *Personal communication*, 2010.

[51] T. Kröger, T. Pätz, I. Altrogge, A. Schenk, K. Lehmann, B. Frericks, J. P. Ritz, H. O. Peitgen, and T. Preusser. Fast estimation of the vascular cooling in RFA based on numerical simulation. *The Open Biomed. Eng. J.*, 4:16–26, 2010.

[52] T. Kröger and T. Preusser. Therapy planning with numerical mathematics. *Lecture at the University of Bremen, Germany*, summer term, 2007.

[53] L. Kubisz and E. Marzec. Studies on the temperature dependence of electrical conductivity of solid-state proteins. *Journal of Non-Crystalline Solids*, 305:322–327, 2002.

[54] H. Kuchling. *Taschenbuch der Physik*. Fachbuchverlag Leipzig im Carl Hanser Verlag, München, Wien, 2004.

[55] S. Kurcyusz. On the existence and nonexistence of lagrange multipliers in banach spaces. *Journal of optimization theory and applications*, 20:81–110, 1976.

[56] S. Laufer, A. Ivorra, V. E. Reuter, B. Rubinsky, and S. B. Solomon. Electrical impedance characterization of normal and cancerous human hepatic tissue. *Physiol. Meas.*, 31:995–1009, 2010.

[57] A. K. Louis. *Inverse und schlecht gestellte Probleme*. Teubner Studienbücher: Mathematik, Stuttgart, 1989.

[58] R. Luce and S. Perez. Parameter identification for an elliptic partial differential equation with distributed noisy data. *Inverse problems*, 15:291–307, 1999.

[59] F. Maier, A. Krafft, J. Jenne, W. Semmler, and M. Bock. Tam a thermal ablation monitoring tool: In vivo evaluation. In *IFMBE Proceedings*, volume 25/6, pages 247–250, 2009.

[60] H. Maurer and J. Zowe. First and second order necessary and sufficient optimality conditions for infinite-dimensional programming problems. *Mathematical Programming*, 16:98–110, 1979.

[61] S. Mulier, Y. i, J. Jamart, L. Michel, G. Marchal, and T. Ruers. Radiofrequency ablation versus resection for resectable colorectal liver metastases: Time for a randomized trial? *Annals of Surgical Oncology*, 15:144–157, 2007.

[62] T. Nikolayzik, C. Büskens, and M. Gerdts. Nonlinear large-scale optimization with WORHP. *Berichte aus der Technomathematik, University of Bremen*, report 10-08, 2010.

[63] E. Paulet, C. Aubé, P. Pessaux, J. Lebigot, E. Lhermitte, F. Oberti, A. Ponthieux, P. Calès, C. Riderau-Zins, and P. L. Pereira. Factors limiting complete tumor ablation by radiofrequency ablation. *Cardiovasc Intervent Radiol*, 31:107–115, 2008.

[64] H. H. Pennes. Analysis of tissue and arterial blood temperatures in a resting forearm. *J. Appl. Physiol.*, 1:93–122, 1948.

[65] P. L. Pereira. Actual role of radiofrequency ablation of liver metastases. *European radiology*, 17(8):2062–2070, 2007.

[66] M. Pop, A. Molckovsky, L. Chin, M. C. Kolios, M. A. S. Jewett, and M. D. Sherar. Changes in dielectric properties at 460 khz of kidney and fat during heating: importance for radio-frequency thermal therapy. *Physics in medicine and Biologie*, 48:2509–2525, 2003.

[67] T. Preusser and H.-O. Peitgen. Patient-specific planning for radio-frequency ablation of tumors in the presence of uncertainty. *it-technology*, 52:256–271, 2010.

[68] V. Rieke and K. B. Pauly. Mr thermometry. *Journal of magnetic resonance imaging*, 27:376–390, 2008.

[69] M. N. O. Sadiku and C. N. Obiozor. A simple introduction to the method of lines. *International Journal of Electrical Engineering Education*, 37(3):282–295, 2000.

[70] W. E. Schiesser. *The numerical methods of lines: integration of partial differential equations.* Academic Press, San Diego, 1991.

[71] C. Schumann, J. Bieberstein, C. Trumm, D. Schidt, P. Bruners, M. Niethammer, R. T. Hoffmann, A. H. Mahnken, P. L. Pereira, and H.-O. Peitgen. Fast automatic path proposal computation for hepatic needle placement. *Proceedings of SPIE*, 7625:76251J–1–76251J–10, 2010.

[72] C. Schumann, C. Rieder, J. Bieberstein, A. Weihusen, S. Zidowitz, J. H. Moltz, and T. Preusser. State of the art in computer-assisted planning, intervention and assessment of liver tumor ablation. *Critical Reviews in Biomedical Engineering (Special Issue on Thermal Tumor Ablation)*, 38:31–52, 2010.

Bibliography

[73] H. P. Schwan and K. R. Foster. Rf-field interactions with biological systems: Electrical properties and biophysical mechanisms. *Proceedings of the IEEE*, 68(1):104–113, 1980.

[74] H. P. Schwan and C. F. Kay. The conductivity of living tissues. *Annals New York Academy of Sciences*, 65:1007–1013, 1957.

[75] A. Seitel, M. Engel, C. M. Sommer, B. A. Radeleff, C. Essert-Villard, C. Baegert, M. Fangerau, K. H. Fritzsche, K. Yung, H. P. Meinzer, and L. Maier-Hein. Computer-assisted trajectory planning for percutaneous needle insertions. *Medical Physics*, 38(6):3246–3260, 2011.

[76] R. E. Showalter. *Monotone Operators in Banach Space and Nonlinear Partial Differential Equations*. American Mathematicl Society, 1997.

[77] S. A. Solazzo, Z. Liu, S. M. Lobo, M. Ahmed, A. U. Hines-Peralta, R. E. Lenkinski, and S. N. Goldberg. Radiofrequency ablation: Importance of background tissue electrical conductivity - an agar phantom and computer modeling study. *Radiology*, 236:495–502, 2005.

[78] T. Stein. *Untersuchungen zur Dosimetrie der hochfrequenzstrominduzierten interstitiellen Thermotherapie in bipolarer Technik*, volume 22 of *Fortschritte in der Lasermedizin*. ecomed verlagsgesellschaft AG & Co. KG, Landsberg, 2000.

[79] J. Stoer and R. Bulirsch. *Numerische Mathematik 2*. Springer-Verlag Berlin Heidelberg, 2005.

[80] A. Stogryn. Equations for calculating the dielectric constant of saline water. *IEEE Transactions on Microwave Theory and Techniques*, 19:733–736, 1971.

[81] C. Sumi and J. Kuwabara. Determination of thermal conductivity distribution from internal temperature distribution measurements. *Review of Scientific Instruments*, 77, 2006.

[82] C. Sumi, A. Suzuki, and K. Nakayama. Determination of the spatial distribution of a physical parameter from the distribution of another physical variable a differential inverse problem. *J. Appl. Phys.*, 80:1–7, 1996.

[83] C. Sumi and H. Yanagimura. Reconstruction of thermal property distributions of tissue phantoms from temperature measurements - thermal conductivity, thermal capacity and thermal diffusivity. *Physics in Medicine and Biology*, 52:2845–2863, 2007.

[84] A. Suppiah, T. J. White, S. H. Roy-Choudhury, D. J. Breen, J. Cast, A. Maraveyas, J. E. Hartley, and J. R. T. Monson. Long-term resutls of percuamteous readiofreqeuncy ablation of unresectable colorectal hepatic metastases: final outcomes. *Digestive Surgery*, 24:358–360, 2007.

140

[85] A. Surowiec, S. S. Stuchly, and A. Swarup. Radiofrequency dielectric properties of animal tissues as a function of time following death. *Phys.Med.Biol.*, 30:1131–1141, 1985.

[86] G. ter Haar. Therapeutic applications of ultrasound. *Progress in Biophysics and Molecular Biology*, 93:111–129, 2007.

[87] F. Tröltzsch. On the lagrange-newton-sqp method for the optimal control of semilinear parabolic equations. *SIAM Journal on Control and Optimization*, 38:294–312, 1999.

[88] F. Tröltzsch. *Optimale Steuerung partieller Differentialgleichungen*. Vieweg, Wiesbaden, 2005.

[89] S. Tungjitkusolmun, S. T. Staelin, D. Haemmerich, J.-Z. Tsai, H. Cao, J. G. Webster, Jr. F. T. Lee, D. M. Mahvi, and V. R. Vorperian. Three-dimensional finite-element analyses for radio-frequency hepatic tumor ablation. *IEEE Transactions on Biomedical Engineering*, 49, 2002.

[90] J. W. Valvano, J. R. Cochran, and K. R. Diller. Thermal conductivity and diffusivity of biomaterials measured with self-heated thermistors. *International Journal of Thermophysics*, 6:301–311, 1985.

[91] C. Villard, L. Soler, and A. Gangi. Radiofrequency ablation of hepatic tumors: simulation, planning, and contribution of virtual reality and haptics. *Journal of Computer Methods in Biomechanics and Biomedical Engineering*, 8:215–227, 2005.

[92] H. Watanabe, N. Yamazaki, Y. Kobayashi, T. Miyashita, M. Hashizume, and M. Fujie. Temperature dependence of thermal conductivity of liver based on various experiments and a numerical simulation for rf ablation. *32nd Annual International Conference of the IEEE EMBS*, pages 3222–3228, 2010.

[93] X. Zeng and R. J. McGough. Optimal solutions of ultrasonic fields produced by large thermal therapy arrays using the angular spectrum approach. *Journal of Acoustical Society of America*, 125(5):2967–2977, 2009.

[94] J. Zowe and S. Kurcyusz. Regularity and stability for the mathematical programming problem in banach spaces. *Applied Mathematics and Optimization*, 5:49–62, 1979.

[95] U. Zurbuchen, C. Holmer, K. S. Lehmann, T. Stein, A. Roggan, C. Seifarth, H. J. Buhr, and J. P. Ritz. Determination of the temperature-dependent electric conductivity of liver tissue ex vivo and in vivo: Importance for therapy planning for the radiofrequency ablation of liver tumours. *Int J Hyperthermia*, 26:26–33, 2010.